EVALUATION OF NOVEL RUTHENIUM-BASED ANTI-CANCER METALLODRUGS IN THE ZEBRAFISH MODEL

By

BRITTANY FAYE KARAS

A dissertation submitted to

School of Graduate Studies

Rutgers, The State University of New Jersey

In partial fulfillment of the requirements

For the degree of

Doctor of Philosophy

Graduate Program in Toxicology

Written under the direction of

Brian T. Buckley & Keith R. Cooper

and approved by

_____

_____

_____

_____

_____

New Brunswick, New Jersey

October 2020

ABSTRACT OF THE DISSERTATION

Evaluation of novel ruthenium-based anti-cancer metallodrugs in the zebrafish model

By BRITTANY FAYE KARAS

Dissertation Directors:
Brian T. Buckley and Keith R. Cooper

Cancer progression into metastasis is an incredibly complex, multistep process that is the major cause of cancer-related deaths. Although new potentially therapeutic metallodrugs are being synthesized at high rates, there is currently no robust method for evaluation of toxicity or efficacy in mice or other model organisms. In fact, New Anti-Tumor Metastasis Inhibitor (NAMI-A), a ruthenium (Ru)-based complex, showed excellent anti-metastatic properties *in vitro* and in the nude mouse model (the current model systems), but failed clinical trials. As such, there is a substantial need for an alternative method of evaluating therapeutic efficacy, to prioritize the most promising of candidate compounds.

In order to evaluate zebrafish as a potential model for metallodrug evaluation, cisplatin, a widely used platinum (Pt)-based chemotherapeutic drug, was utilized as a proof-of-principle compound. We coupled a modified OECD FET (Organisation for Economic Cooperation and Development Fish Embry Acute Toxicity) protocol with lesion identification, morphological endpoints and metallodrug up-take quantification by Inductively Coupled Plasma Mass

Spectrometry (ICPMS). By coupling these experiments with ICPMS analysis of waterborne solutions and larval tissue we were able to determine drug uptake associated with dose-dependent endpoints with cisplatin as well as two novel ruthenium-based metallodrugs: PMC79 and LCR134. This provided a method to overcome a common limitation of the zebrafish model: waterborne dose delivery and identify doses for future experiments. Lowest observed adverse effect levels (LOAELs): 3.75 mg/L, 3.1 mg/L and 17.4 mg/L for cisplatin, PMC79, and LCR134, respectively.

These compounds were then evaluated for their anti-proliferation and angiogenic capabilities. Gene expression of Vascular Endothelial Growth Factors *(vegfa* and *c*), Wingless/Integrated signaling (*wnt 3a* and *8a*) and Hypoxia-inducible factor 1-alpha (*hif1-α*) were evaluated. Significant inhibition of mRNA expression of all genes with the exception of wnt3a was associated with PMC79 metallodrug exposure. However, LCR134 exposure did not cause significant changes in gene expression. In addition to PMC79 exposure significantly decreasing gene expression, the sub-intestinal blood vessels showed significantly less branching which indicates inhibition of angiogenesis. LCR134 did deviate from control branching. Lastly, PMC79, LCR134 and cisplatin were utilized in a tail fin regeneration assay conducted concurrently with whole mount immunofluorescence using proliferating cell nuclear antigen (PCNA), a marker of proliferation. Our findings demonstrated similar inhibition profiles with cisplatin. This was a marked finding as cisplatin was used at levels with a higher propensity for toxicity than either Ru metallodrugs.

Furthermore, we were able to recapitulate the *in vitro* mechanisms of LCR134 and PMC79 in the teleost model. These metallodrugs were previously investigated in several cancer cells lines; LCR134 was found to significantly inhibit P-glycoprotein (Pgp) efflux pump also known as multidrug resistance protein 1; mdr1. This protein is often found to be correlated with increased drug resistance. PMC79 has been found to initiate an apoptotic cascade through disrupting cytoskeleton (F-actin) in the plasma membrane. Gene expression of *b-actin* after PMC79 exposure was significantly down-regulated; however, gene expression of *mdr1* after LCR134 was not affected. *In vivo* Pgp inhibition showed significant retention of the Pgp-specific fluorescent substrate Rhodamine 123 (Rh123) after treatment with LCR134 and a clinically-relevant inhibitor, cyclosporine A. PMC79 *in vivo* assessment of membrane cytoskeletal impact demonstrated a significant decrease in the presence of cytoskeletal structures. These experiments provided insight to the retention of mechanistic activity in whole organism models.

The objective of this project was to assess the specific modes of action for novel metallodrugs in a higher through-put, alternative animal model. The culmination of this work has shown the zebrafish model as a powerful platform for the evaluation of novel Ru metallodrugs as well as their promising candidacy for evaluation in higher organisms.

ACKNOWLEDGMENTS

I would first like to thank my thesis advisors Drs. Brian Buckley and Keith Cooper. Without their collaboration, I would have never been able to incorporate my passion for analytical chemistry with toxicology. Their mentorship, guidance, and training these past years have honed my scientific acumen and provided me with a truly interesting project. Dr. Buckley's pride in my work and myself was always obvious in his countless letters of recommendation, and discussions of what he believed was a truly promising future for me. His confidence in me was often contagious and gave me the drive to push onwards. I cannot say enough kind things about Dr. Cooper: to do so would result in a document as long as this dissertation. Although his patience and wisdom were certainly developed over years of experience, his kindness is a genuine part of who he is. His advice and direction were invaluable and I will be forever grateful.

Secondly, I need to thank and express my appreciation for the other members of my doctoral committee: Dr. Lori White, Dr. Kyle Murphy, and Dr. Phoebe Stapleton. I would like to thank Dr. White and Dr. Murphy for allowing me constant use of their lab, for letting me barge in on them at any given moment for all types of advice, and thank them for listening to me during both times of struggle and success. Dr. Stapleton, thank you for rounding out dissertation committee. Your feedback was especially thought-provoking, and added much needed perspective. Thank all of you for our round-table discussions which were always fruitful. You helped provide me with direction and focus. Your time and constructive criticism has made me a better scientist, and my dissertation stronger.

I have immense appreciation for the past and present lab members of Dr. Buckley and Dr. Cooper. Drs. Elizabeth McCandlish and Cathleen Doherty are superb analytical chemists. Dr. McCandlish's witty euphemisms and guidance helped me understand the basics of the analytical process of ICPMS, and Dr. Doherty's direction and intuition helped me troubleshoot and optimize my methods. I am very grateful they were willing to share their wisdom and advice. I'm also sincerely thankful to Dr. Victoria DiBona for teaching me the science behind confocal microscopy. She has demonstrated countless times the level of thinking that differentiates a post-doc and a graduate student. Dr. DiBona is exactly what I envision a good leader to be. She has provided guidance, direction and feedback on countless experiments, projects, and management styles. I truly try to emulate her in my interaction with students, science, and professional life. I also want to thank Gina Moreno who is an endless source of wisdom and experience. Gina was the first to teach me how to use the zebrafish model and we have worked closely together for five years; she has been an ally and a great friend.

A huge thank you goes to Drs. Andreia Valente and Dr. Leonor Côrte-Real for the use of their compounds and preliminary data. Dr. Côrte-Real, is one of the most driven scientists I have ever worked with. Our fruitful collaboration of just six months resulted in three publications. I am so thankful I had the chance to work alongside and learn from her.

I would also like the thank the Joint Graduate Program in Toxicology (JGPT). This outstanding program has provided the foundation for my success. Our program director, Dr. Aleksunes, has been exemplary. She has dedicated a

considerable amount her time and energy into optimizing the program, classes, interdisciplinary relationships and professional development. I am also grateful our outstanding faculty for their wisdom and support. The administrative staff of both the toxicology program as well as Lipman Hall require appreciation for all that they do for the department; especially Jessie Maguire and Liz Rossi who I endlessly barraged with questions.

I also need to thank the Department of Biochemistry and Microbiology. Lipman Hall has housed my research and much of my funding opportunity and academic awards these past five years. I was able to teach alongside some truly outstanding professors including Dr. Sharron Crane and Dr. Natalya Voloshchuk. They taught me how to lecture, how to design courses, and how to provide beneficial feedback to students. Additionally, I need to thank Dr. Peter Kahn for his worldly and scientific advice. I always appreciated how much he cared about his teaching assistants and our efforts.

I had the privilege to mentor many undergraduates during my dissertation. I would like to thank them for their dedication, their thought-provoking ideas and novelty, as well as their positivity and the joy they brought to the lab. I am especially thankful to Jordan Hotz, Kristin Terez, Shorbon Mowla, Dylan Fitzgerald, and Brian Gural. These outstanding young scientists helped troubleshoot and execute experiments. It has been an honor to have been their mentor and I am very proud of the scientists they have become.

Last, but not least, I want to thank all of my friends for their love and support, especially Kurt Roman who helped me study and challenged me to do better and

be confident as well as Kyle Robbins who has always believed in me and is the reason I applied to the graduate program in the first place, when I firmly believed I was not qualified. I want to thank my loving and caring in-laws, Coleen and David Tyler, as well as my parents, Peter and Lisa Karas, and Pete Mancini for their encouragement and pride in my efforts. My father, Peter, has been the root of my curiosity in science and physiology. To this day we still have great scientific discussions on the human body and health care. My mother, Lisa, has always believed in me. She has always pushed me towards betterment. I would like to one day be as great as the person she believes I already am. Finally, I want to thank my husband, Ed Tyler. Ed has been endlessly supportive and motivational. He is without a doubt my biggest advocate. This accomplishment could not have been done without all of you.

The content of Chapter 2 has been published. The citation for this publication is: Karas, B. F., Côrte-Real, L., Doherty, C. L., Valente, A., Cooper, K. R., & Buckley, B. T. (2019). A novel screening method for transition metal-based anticancer compounds using zebrafish embryo-larval assay and inductively coupled plasma-mass spectrometry analysis. Journal of Applied Toxicology, 39(8), 1173-1180. doi:10.1002/jat.3802. Additionally, partial content of published data was used in Chapters 3 and 4. The citation for this data is: Corte-Real, L., Karas, B., Girio, P., Moreno, A., Avecilla, F., Marques, F., . . . Valente, A. (2019). Unprecedented inhibition of P-gp activity by a novel ruthenium-cyclopentadienyl compound bearing a bipyridine-biotin ligand. European Journal Medicinal Chemistry, 163, 853-863. doi:10.1016/j.ejmech.2018.12.022

TABLE OF CONTENTS

DATA FIGURES

CHAPTER 4

CHAPTER 1. INTRODUCTION

Cancer is a ubiquitous disease with almost 1.7 million new cases diagnosed in the United States alone (NCI, 2018). It comes as no surprise that this major disease is a large focus for medicinal therapy. Unfortunately, chemotherapeutic treatment and remission can be limited by serious off-target toxicity and acquired or spontaneous solid tumor resistance. This is especially true for one of the most prevalent chemotherapeutics cisplatin, which was approved by the FDA in 1978. As such, improvement in metal-based chemotherapies has become a very active center of research. Although these compounds are being synthesized at high rates, there is currently no robust method for evaluation of toxicity or efficacy. In fact, New Anti-Tumor Metastasis Inhibitor (NAMI-A), a ruthenium (Ru)-based complex, showed excellent anti-metastatic properties *in vitro* and in the nude mouse model, but failed clinical trials (Leijen et al., 2015). There is a substantial need for a high throughput and robust method of toxicity and therapeutic efficacy. The zebrafish (*Danio rerio*) model has been used to assess a myriad of human diseases and for approximately 40 years, has been a valuable vertebrate model for development, genetics, behavior and toxicology (Leonard & Randall, 2005; Meyers, 2018). Due to some very powerful attributes of the model, such as high fecundity and gene conservation, the zebrafish model has begun to be incorporated into the drug development process. This vertebrate model may provide an accelerated means of evaluating novel metallodrugs.

1.1 Overview of Cisplatin as a Chemotherapeutic

The fortuitous discovery of the platinum-based (Pt) chemotherapeutic cisplatin precipitated advancement within the field of medicinal metal complexes, or metallodrugs, due to highly successful anti-neoplastic properties. It is so successful, in fact, that the World Health Organization (WHO) regards cisplatin as one of the world's essential drugs (WHO, 2016). Cisplatin also known as *cis*-diamminedichloroplatinum(II) (CAS No. 15663-27-1; Formula: $PtCl_2H_6N_2$) has a molecular weight of 301.1 gm/mol and is a square planar molecule comprised of a single platinum (Pt) scaffold, two chlorine atoms and two ammonia groups in a cis configuration (Figure 1). This compound was originally an inadvertent byproduct of an electrolysis experiment conducted with Pt electrodes by Rosenberg et al, 1965 . This group of researchers at Michigan State University observed that the Pt complexes caused filamentous growth of Escherichia coli, or growth without cell division. Because they inhibited proliferation, these Pt-based compounds were subsequently tested for their anti-neoplastic activity. Indeed, several of these compounds were found to be both potent and effective across a wide spectrum of solid tumors (Rosenberg & VanCamp, 1970) Currently, cisplatin is used to treat testicular, ovarian, bladder, head and neck, cervical, non-small cell lung, small cell lung, esophageal, biliary, and brain cancers among others. Cisplatin has additionally been used in combination therapies for anti-solid tumor effects and anti-metastatic therapies (BMS, 2002; Medical Letter, 2003; NCI, 2014; Rosenberg, 1977). Notably, since the use of cisplatin in testicular cancer treatments, cure rates have exceeded 90% (NCI, 2014). Subsequent Pt-based

chemotherapeutics (or platins), carboplatin and oxaliplatin, were created with strategic and rational drug design and have also been accepted to market as alternatives to cisplatin. Today, approximately 50% of chemotherapy regiments include a platin (Wheate et al., 2010). However, although these platins highly used in chemotherapeutic treatment, most alternative platins have failed clinical trials. As such, platin development has shifted from small molecule design and manipulation of spectator ligands, or ligands that do not participate in the chemical reactions of the complex, to improving drug delivery and nanotechology (Michael et al., 2015).

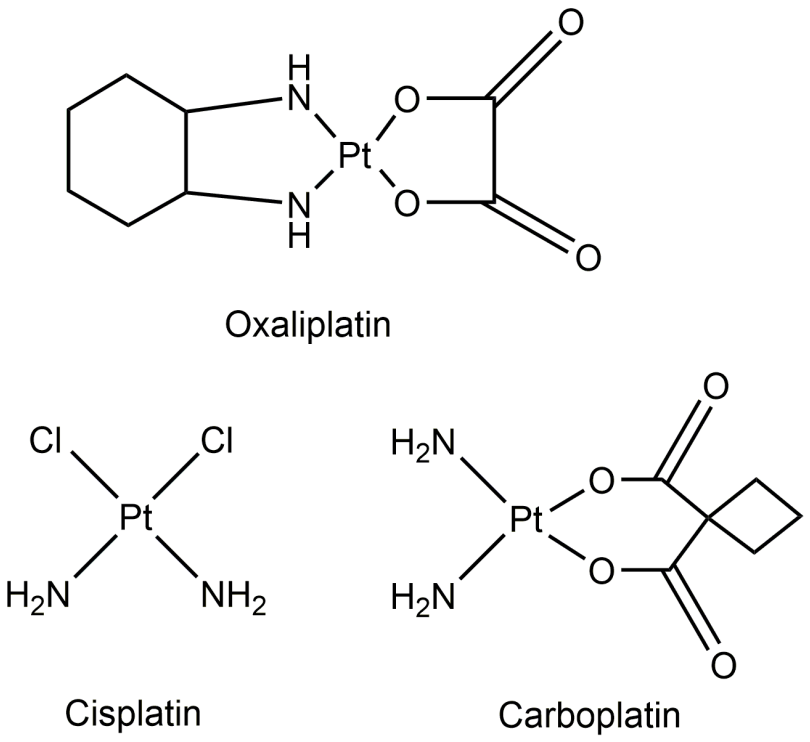

Figure 1. Chemical Structures of Oxaliplatin, Cisplatin, and Carboplatin – These metallodrugs have a Pt (II) core and exhibit square planar molecular geometry.

Mechanism of Action

Cisplatin entry into the cells has been shown to be carried out by facilitated transport systems (Eljack et al., 2014). Due to high levels of chloride in the blood, cisplatin can remain neutral and enter the cell by passive diffusion. An alternative mode of entry into cancer cells is the copper transporter CTR1; the absence of which has demonstrated significant cellular resistance, while its presence has shown significantly increased sensitivity to cisplatin, carboplatin and oxaliplatin (Holzer et al., 2006; Larson et al., 2009). Overall, it is suspected that the drug may enter the cell as multiple chemical species albeit through different pathways resulting in different cellular kinetics (Hambly, 1997).

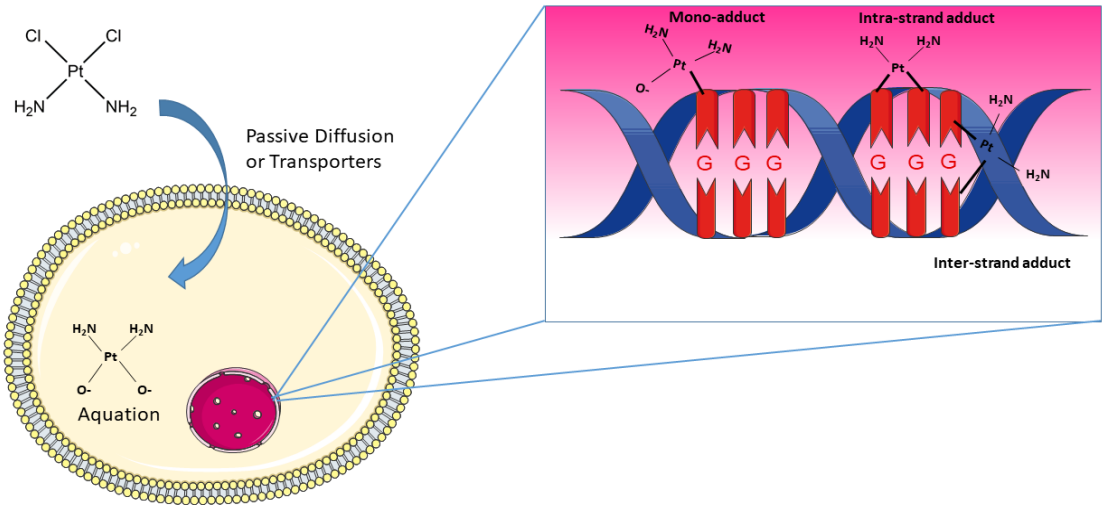

Figure 2. Cisplatin Mechanism of Action – When cisplatin enters the low chloride environment of the cytoplasm the chlorine ligands are exchanged to hydroxyl groups. These highly reactive hydroxyl groups create a potent electrophile which can react with nucleophiles such as the nucleic acids of DNA. This causes adduct formation which results in an apoptotic cascade. This figure was created using Servier Medical Art templates, which are licensed under a Creative Commons Attribution 3.0 Unported License; https://smart.servier.com.

Mechanistically, cisplatin remains inactivated until the first aquation step, which takes place within the cytoplasm (Davies et al., 2000). The aquation of cisplatin is due to the low chloride concentration within the cell where a chloride leaving group is exchanged for water, resulting in a positively charged species. This species is then hydrolyzed and yields a neutral chlorohydroxo complex, which is either mono- or di-aquated. Alternatively, carboplatin and oxaliplatin are activated by the exchange of a carboxylate or oxalate group, respectively (Harrington & Taylor, 2015). The aquated species is reactive and forms DNA adducts. Specifically, the reactive species binds to the N7 of guanine and or adenine within DNA, the majority of which form bifunctional adducts including intrastrand-crosslinks of nucleotides and DNA-protein crosslinks (Eastman, 1987; Hall et al., 2008a). These adducts initiate a cascade of events through damage recognition proteins resulting in cellular apoptosis (Bellon et al., 1991).

Drug/Cross Resistance by Reduced Cellular Accumulation

Drug resistance is a major impediment of platin cancer treatment. Although the process by which cancer cells develop resistance to cisplatin is considered to be due to multiple pathways (cell detoxification by glutathione, enhanced DNA repair mechanisms, subsequent reduced apoptosis), the primary means appears to be reduced cellular accumulation (Corte-Rodríguez et al., 2015; Godwin et al., 1992; Hall et al., 2008b; Kelland et al., 1995). It is speculated that cisplatin drug-resistance results by up and down-regulation of various facilitated transport systems and transport proteins. Significantly decreased influx and/or increased

efflux transporters were found in resistance cells lines; additionally, cells treated with influx or efflux inhibitors reduced resistant cells by half (Andrews et al., 1991; Andrews et al., 1988). It appears that influx resistance may be due to multiple transporters including CTR1 or hCTR1 ([human] copper transporter 1, *SLC31A1;*), a conserved copper importer, found to mediate resistance in yeast and mouse knockout strains (Ishida et al., 2002).However, it is speculated that transport by CTR1 does not keep the structure necessary for DNA adduction due to increased accumulation via hCTR1 not necessarily resulting in increased cytotoxicity (Holzer et al., 2004). The solute carrier (SLC) gene series may play a role as well, specifically the organic cation transporters (OCTs) due to their high expression in the proximal tubules of the kidney and the nephrotoxic effects of cisplatin. However, the influx transporter substrate specificity for platins appears to be structure dependent (Briz et al., 2002; Pan et al., 1999; Yonezawa et al., 2006). Copper efflux transporters ATP7A and B were implicated in cisplatin resistant cells lines (Katano et al., 2002). Although other transporters have been investigated, the ATP7A and B were supported by clinical evidence relating negative prognosis to increased expression in carcinomas (Nakayama et al., 2004; Nakayama et al., 2001). There is still scientific debate regarding the relative importance of various transport pathways and potential pleiotropic resistance. The multifaceted regulation of transporter-based drug resistance also causes the additional clinical issue of cross resistance to a diverse range of alternative chemotherapies (Safaei et al., 2004) (Hamaguchi et al., 1993; Stordal et al., 2012). As such, focus on circumventing transporter mediated resistance has gained interest, including

simultaneous treatments with transport inhibitors, or alternative drugs that cause less inducible resistance.

Nephrotoxicity

One of the primary dose-limiting adverse effects of Pt-based chemotherapeutics is nephrotoxicity, characterized by necrosis of the renal tubular cells and resulting in acute kidney injury (de Jongh et al., 2003; Lieberthal et al., 1996). Pt-based compounds are primarily excreted by the OCT2 transport proteins of the kidneys which mediates the basolateral to apical transfer of cations (Safirstein et al., 1984). Studies have shown that upon uptake, cisplatin is transformed into a toxic glutathione-conjugate metabolite and ultimately a reactive thiol (Townsend et al., 2003). Additionally, cisplatin has been shown to cause damage by reactive oxygen species (ROS), lipid peroxidation, and mitochondrial disfunction (Brady et al., 1993). Clinically, this is a major limitation for cancer treatment. Nephrotoxicity is rarely reversible and as such is minimized to every extent possible. The onset of renal failure due to cisplatin is slow and has shown to occur approximately 3–5 days after dosing in about one third of patients (Miller et al., 2010). Carboplatin and oxaliplatin were designed to have less nephrotoxic effects, but they have also shown to either be less effective or induce greater alternative side effects, like neurotoxicity (Hotta et al., 2004; Huang et al., 2016; Jiang et al., 2007). Due to these significant drawbacks of platins, research has been geared to find alternative transition metal-based chemotherapies.

1.2 Overview of Ruthenium-Based Metallodrugs

Organometallics are a subset of metal-based complexes containing at least one covalent metal-carbon bond. They primarily consist of a transition metal core with a wide range of feasible ligands and variability in molecular coordination (Figure 2). These characteristics produce a broad class of molecules that have been exploited in medicinal chemistry. Organometallics, depending on the transition metal core, can have enhanced opportunity for manipulation including ligand kinetics, charge distribution, lipophilicity, and oxidation state (Gianferrara et al., 2009; Guo & Sadler, 1999). As such, these compounds can be designed for specific modes of action. Perhaps the most versatile and well-studied transition metal has been ruthenium (Ru) (Clarke et al., 1999).

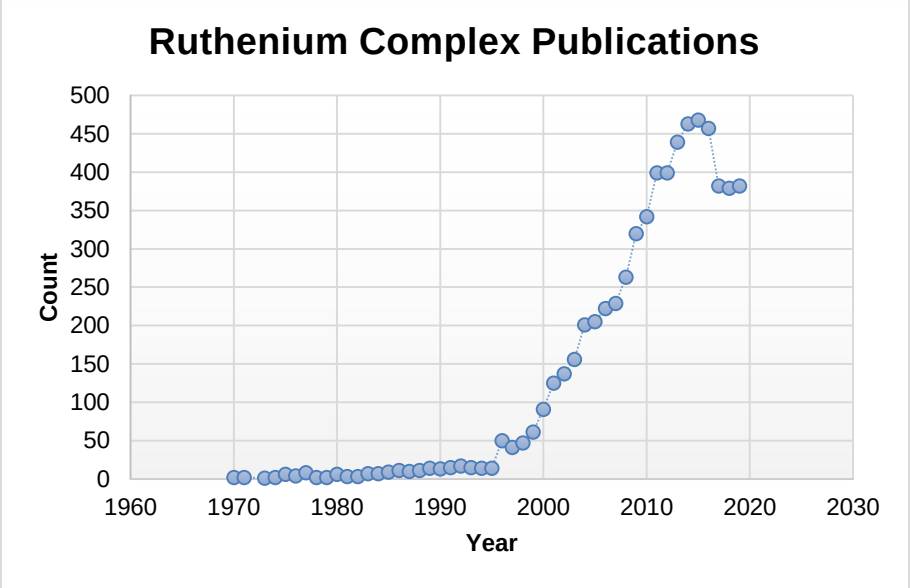

Figure 3. Number of Ruthenium Complex Publications – Ruthenium complex related publications have been on the rise over the course of approximately 50 years.

Ru is an attractive candidate in medicinal organometallics due to its octahedral stereochemistry, and, as a 5d-block element, is characterized by its stability in multiple oxidation states (predominately Ru^{II} and Ru^{III}; Ru^{IV} is possible but less stable). In contrast, most Pt compounds are limited by their square-planar coordination, and reduction of Pt results in a change in both coordination and interatomic bond distances (Melnik & Holloway, 2006). These chemical properties have stimulated a great deal of interest in this class of Ru metallodrugs.

Reduced Toxicity and Drug/Cross Resistance

Ru-based complexes have ligand kinetics similar to Pt derivatives, however, they offer clinical advantages including reduced toxicity and drug/cross resistance (Aird et al., 2002). The multiple oxidative states of Ru are one means of lowering toxicity. Ru^{III} are relatively more inert regarding ligand exchange than its Ru^{II} counterpart. Therefore, Ru^{III} compounds can be designed to exploit the distinct nutritional and metabolic environments of tumors. Often, solid tumors lack adequate vascularization and are subsequently deficient in oxygen in non-vascularized areas. Furthermore, tumor environments are generally acidic due to the well documented Warburg Effect, i.e. relatively high aerobic glycolysis rates and subsequent lactic acid production in addition to increased rates of ATP hydrolysis under hypoxic conditions (Tannock & Rotin, 1989; Vander Heiden et al., 2009). This acidic, hypoxic environment favors reduction to the more active Ru^{II} form. As such, Ru^{III} compounds are similar to prodrugs, in which they are pharmacologically inactive until further metabolism or derivatization. Due to this activation-by-

reduction activity these compounds result in higher selectivity with the potential for lower adverse effects. In addition, a portion of the reduced toxicity is believed to be due to Ru and iron (Fe) physiochemical homology. Ru and Fe have similar kinetic binding to transferrin (Tf) and human serum albumin (HSA) reducing the amount of unbound drug (Frasca et al., 2001; Kratz et al., 1994). Additionally, Ru homology to Fe allegedly increases effectiveness of Ru-based compounds as cancer cells can express increased levels Tf receptors and mistakenly accumulate Ru, instead of the highly coveted Fe, into the cell (Daniels et al., 2012; Prior et al., 1990). However, this proposed reason for reduced toxicity is currently controversial. Alessio (2017) suggested that the mechanism behind the inherently low Ru metallodrug toxicity is not based on the physiochemical similarities to Fe, but likely the increased specificity of the overall molecules (Alessio, 2016). Both mechanisms may be at play in reducing off target toxicity and specificity.

Modes of Action

Initially, Ru-based compounds were anticipated to behave similarly to cisplatin in which DNA-crosslinking induces apoptosis, but due to their large structural diversity a wide range of intra- and extracellular targets are responsible for their anti-cancer efficacy (Figure 2). Although Ru-based compounds can bind to DNA, the manner of binding appears to be different than cisplatin. The large heterocyclic Ru bulky adducts bind primarily at guanine bases that can affect the conformation of DNA (Malina et al., 2001).

Table 1: Examples Of Proteins And Enzymes Known To Form Adducts Or Be Inhibited By Ru-Based Compounds

Protein/Enzyme	Functionality	References
MST1	Proapoptic cytosolic kinase with role in oxidative stress	Anand et al., 2009
GSK-3	GSK-3 inhibition has been found to be a potent activator of tumor protein p53, which induces apoptosis	Bregman et al., 2004
Cathepsin B	Lysosomal enzyme responsible for degrading the ECM; potentially involved in migration and invasion	Casini et al., 2008
Thioredoxin Reductase	Responsible for maintaining the cellular redox state and central functions of the cell	Casini et al., 2008
MutS	Ru^{II} Arene complex bound DNA inhibits ability of this mismatch repair (MMR) protein from identifying Ru-DNA adducts	Castellano-Castillo et al., 2008
TPMET	Increased glycolytic rates of cancer cells are dependent on TPMET. Ru glycolytic inhibitors target cell metabolism.	Corte-Real et al., 2014
Glutathione	Antioxidant used for detoxification of the cell	Fuyi et al., 2005
CA II	Overexpressed in certain forms of cancer	Monnard et al., 2011
PTP-1B	Tyrosine phosphatase found to be associated with cancer	Ong et al., 2012
A3AR	Adenosine receptor found to be associated with cancer	Paira et al., 2013
Pim-1	Potent and selective inhibitor at nanomolar concentrations of protein kinases	Smalley et al. 2007
CspC	Cold-shock protein which adapts cells to unfavorable conditions thereby reducing damage	Will et al., 2007
ppiD, osmY, SucC	Stress response proteins which adapts cells to unfavorable conditions thereby reducing damage	Will et al., 2007
Helicase dinG	Induced by DNA damage and involves recombinational DNA repair and replication after DNA damage	Will et al., 2007
BRAF	Kinase found in humans cancers	Xie et al., 2009

Additionally, research has shown certain Ru-based compounds bind proteins with greater affinity than DNA and thus may cause toxicity through a different mechanism. It appears that both nitrogen in proteins and nucleic acids as well as sulfur ligands can bind readily to Ru (Egger et al., 2005; Wang et al., 2002). Within Table 1 are examples of proteins and enzymes reported to have altered function after Ru complex exposure. Ru complexes have also been shown to accumulate to a higher extent in alternative organelles such as the mitochondria, endoplasmic reticulum and lysosomes than the nuclei (Groessl et al., 2011; Puckett & Barton, 2007).

Ru M-Arene Complexes

It is apparent that each compound's structure can influence the mechanisms that are involved in targeting tumor cells (toxicodynamic) and their toxicokinetic effect. Ru M-Arene complexes, also known as half-sandwich or piano-stool complexes (Figure 2) are defined by the Ru metal core bound to an arene. The arenes are typically benzene or cyclopentadiene. Benzene, designated as (η6-arene), is considered a neutral ligand where the six signifies the electrons donated. The six electrons are considered to take up three coordination sites at a metal, but can also become (η4-arene) allowing a substitution without ligand loss. Alternatively, cyclopentadienes are mildly acidic and are deprotonated to form a cation. These cyclic polyene ligands are designated as (η^5-C_5H_5-) or η^5 cyclopentyldienyl and are considered a six-electron donor. They are noted for their relatively high stability and are the archetype arene for these M-arenes. An additional advantage is their

ability to undergo Friedel-Crafts acylation which can either add steric bulk or (potentially medicinal) ligands to the arene (Gasser et al., 2011).

The mechanism of action of most Ru M-Arene complexes involve a similar initial activation as observed with cisplatin drugs, in which the chloride bonds are stable until transported into the chlorine-dilute cytoplasm. The low chloride environment of the cell causes the Ru-Cl bond to undergoes hydrolysis generating an activated aquated species. The activated aquated species binds with affinity to the N7 position of guanine bases forming monofunctional adducts, unlike cisplatin which mainly forms bifunctional adducts and DNA cross-links (Hall et al., 2008b; Novakova et al., 2003; Wang et al., 2002). Additionally, larger inert Ru-based compounds with bulky and rigid aromatic rings have been shown to have similar cytotoxicity to cisplatin, although they appear to involve cell membrane function modification and/or disrupt cell adhesion as opposed to DNA intercalation (Schatzschneider et al., 2008). Instead of direct cytotoxicity, two fields merged from these compounds: anti-metastasis and metal-drug synergism. Several RAPTA (Ru arene 1,3,5-triaza-7-phosphaadamantane) derivatives were not toxic to cancerous or healthy cells, but inhibited lung metastases in CBA mice bearing the MCa mammary carcinoma (Scolaro et al., 2005). In addition, NAMI-A (discussed below), has shown anti-metastatic capabilities, and is thought to inhibit mechanisms of tumor angiogenesis and invasion. This is particularly noteworthy as treatment options for metastases are limited compared to the relatively success rates available for primary tumors.

Ru half-sandwich complexes have been explored as scaffolds for the design of enzyme inhibitors due to their stability in air, water, and buffer systems (Meggers, 2009). As scaffolds, the metal ion has a structural role in determining the unique three dimensional shape of the metal coordination sphere and have high affinity for the receptor space of endogenous compounds. These complexes are intended to remain unchanged in vivo, and bind non-covalently (Gasser et al., 2011). For example, several compounds were created in order to mimic the hydrogen binding pattern of staurosporine, a naturally-occurring kinase inhibitor. The synthesized derivatives bind with both glycogen synthase kinase 3 (GSK-3) and proto-oncogene serine/threonine-protein kinase (Pim-1), two primary receptors of staurosporine (Atilla-Gokcumen et al., 2006; Bregman et al., 2004).

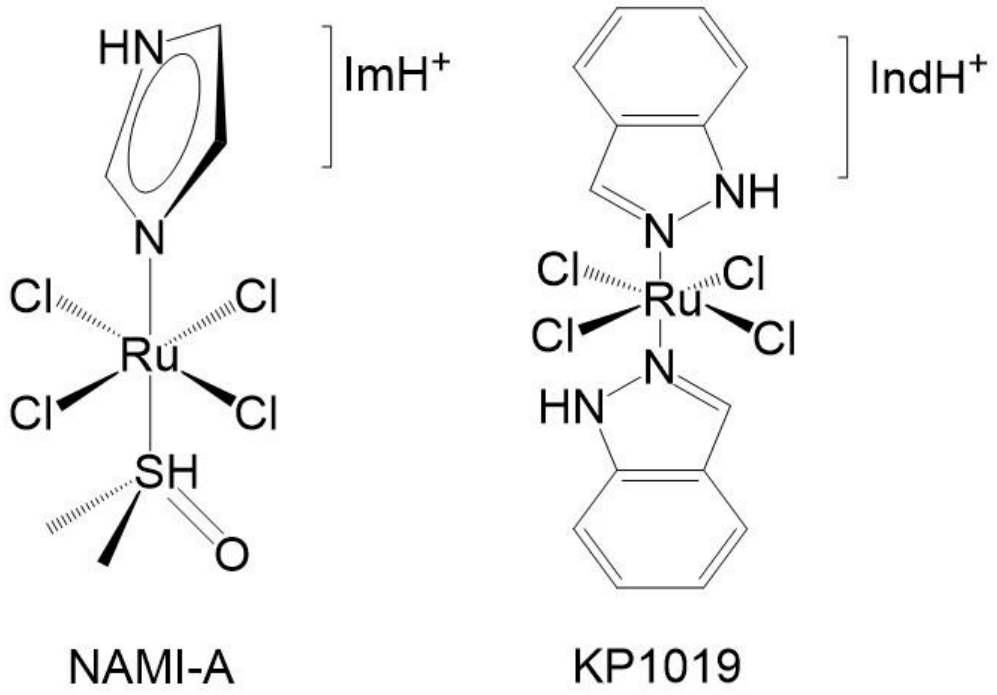

Figure 5. Chemical Structures of Clinically Trialed Ru Metallodrugs – NAMI (Na+) and NAMI-A (imidazole) as well as KP1339 (Na+) and KP1019 (indazole) were two iconic Ru metallodrugs that had undergone clinical trial.

Clinical Trials for Ru Metallodrugs: NAMI-A and KP1019

Two of the most prominant Ru-based metallodrugs are NAMI-A (New Anti-cancer Metastasis Inhibitor) and KP1019; ((ImH)[*trans*-$RuCl_4$(dmso-S)(Im)], Im = imidazole) and Na[*trans*-$RuCl_4(Ind)_2$]), Ind = indole, respectively. NAMI-A, a sulfoxide-ruthenium complexes with nitrogen-donor ligands has exhibited effects on metastasis growth and increased resistance to the formation of metastasis. Anti-metastatic growth has been demonstrated in metastasizing cancers including Lewis lung carcinoma, B16 melanoma, TS/A adenocarcinoma and MCa mammary carcinoma (Bergamo et al., 1999; Gagliardi et al., 1994; Sava et al., 1995; Zorzet et al., 2001); Although the mechanism is still unknown, it is believed that NAMI-A reduction results in activation. The sulfur bound DMSO ligand provides a pi-accepting effect resulting in an increased reduction potential (Ni Dhubhghaill et al., 1994). Although low cytotoxicity was initially perceived as a poor anti-cancer characteristic, it has been shown that this does not correlate with NAMI type compounds to inhibit metastasis; furthermore, this attribute is favorable to limit adverse effects of combination treatment and long-term dosing for prevention of metastasis after tumor removal. Unlike cisplatin, a lack of *in vivo* host toxicity was observed in non-target tissues including lung, liver and kidney, as well as additionally susceptible tissue such as muscle, splenocytes, and bone marrow (Gagliardi et al., 1994). NAMI-type compound administration exhibited low blood concentrations which are attributed to rapid renal clearance. This is in contrast to cisplatin in which blood concentrations can increase and indicate nephrotoxicity (Sava et al., 1999b).

Because NAMI-A reduces metastatic growth as opposed to reduction of the primary tumor; it would appear that the mechanism of action on the tumor are very different than cisplatin. Several mechanisms for NAMI-A have been suggested and investigated including a) inhibited invasion either by matrix metalloproteinase-2 (MMP-2), involved in the breakdown of the extracellular matrix either directly and/or its inhibitor TIMP-2, or increase protective capsule around the tumor by increase collagen production (Sava et al., 1999a; Zorzet et al., 2000) b) limiting migrating adhesion and cell motility by actin and integrin β1 interference, (Bergamo & Sava, 2007; Sava et al., 2004), and c) with anti-angiogenic effects including inhibition of vascular endothelial growth factor (VEGF) (Vacca et al., 2002).

These characteristics precipitated Phase I and Phase II clinical studies with NAMI-A. The Phase I monotherapy clinical study conducted at the Netherlands Cancer Institute involved NAMI-A administered by infusion 12 dose levels ranging from 2.4-500 mg/m^2/day, for patients with solid tumors including colorectal cancer, non-small cell lung cancer (NSCLC), melanoma, ovarian cancer, pancreatic cancer and mesothelioma (Leijen et al., 2015). The major adverse events listed in this study included extreme nausea, vomiting, and diarrhea, phlebitis and painful blistering on the hands fingers and toes, although it was noted that no part of the formal common toxicity criteria (CTC) was dose-limiting. As a stand-alone treatment, 79% of patients showed disease progression and, as such, monotherapy NAMI-A was determined as unsuccessful. Optimistic results of clinical combination with gemcitabine and Pt-based compounds, the results of

which showed enhanced activity against metastatic growth as well as increased life expectancy, inspired preclinical trials of NAMI-A and gemcitabine (Bergamo et al., 1999; Leijen et al., 2015; Sava et al., 1998).

The results of a Phase I/ II clinical trials of a total of 32 patients were conducted and documented by Leijen, et al (2015). These trials were meant to establish the optimal doses, pharmacokinetic profiles, anti-tumor activity, and dose limiting toxicity or maximum tolerated doses. Initial dose escalation was performed with NAMI-A administered at 300 mg/m^2 at days 1, 8 and 15 in rotation with gemcitabine at 1,000 mg/m^2 at day 2, 9, and 16. A subsequent dose escalation with a 21 day schedule and an initial dose of 450 mg/m^2 was performed as well.. At the end of the study, a single patient was in unconfirmed partial remission of lung lesions, but had increased brain metastases. The combination treatment resulted in various adverse effects that were relatively high for CTC criteria. Overall, the treatment was found to be “insufficiently effective”, and even had a lower efficacy than predicted for monotherapy gemcitabine. Interestingly, Alessio (2017), who was actively involved in the development of NAMI-A, has pointed out that the anti-metastatic properties of NAMI-A were repeatedly observed in *in vitro*, *in vivo* and clinical trials independently of dose, and well below cytotoxic levels; often at the lowest administered dose. This observation showed that NAMI-A was anti-metastatic and that further studies examing other related structures or lower dose exposures might indicate a viable target for future studies examining related chemical structures.

KP1019

A second Ru-based compound that entered clinical trial was KP1019 (also known as FFC14A). This Ru^{III} compound is characterized by an octahedral Ru core with four chloride bonds and two indazole ligands and an indazolium counter ion (Figure 3). KP1019 has many parallels to the aforementioned M-Arene compounds: relative stability, reduction-activation, chloride ligand-hydroxo group exchange (Küng et al., 2001), binding to biological plasma transport molecules HSA and Tf, and primarily accumulation via transferrin receptors (Hartinger et al., 2005). Mechanistically, it is believed that KP1019 undergoes activation-by-reduction with redox potential and enacts its cytotoxicity by damage of the mitochondrial membrane by ROS generation as demonstrated in SW480 and HT29 cell lines (Kapitza et al., 2005). The ROS generation implies induction of apoptosis through the mitochondrial pathway (Kapitza et al., 2005; Smith et al., 1996). Preclinical studies evaluated KP10190 on autochthonous colorectal tumors in rats in which cisplatin was found to be inactive. Findings demonstrated that a twice weekly dose at 13 mg/kg significantly reduced tumor volume with limited adverse side effects (Berger et al., 1989; Seelig et al., 1992). A Phase I clinical trial was designed for patients with advanced solid tumors and no further therapeutic options. Eight patients received intravenous doses for solid tumors including: colon and rectum adenocarcinoma, liver, endometrium, and tongue carcinomas, melanoma of the choroidea and bladder cancer. At the maximum dose of 600 mg/kg, no dose-limiting toxicities were observed and KP1019 appeared to be well tolerated. Five of the patients had stabilized for several weeks which did not seem dose-

dependent (Hartinger et al., 2008). In order to overcome solubility issues, NKP-1339 was established which has the same structure as KP1019 with a sodium ion instead of an indazolium counter ion. This compound, also known as IT-139 was tested for safety and activity in a phase I study with expansion cohort (Burris et al., 2016). The study included 46 patients and demonstrated manageable adverse effects, although moderate anti-tumor activity. Phase I/II studies plan to further explore this compound in combination therapies with other chemotherapeutics or immunotherapy.

Passive and Actively Targeted Anti-Tumor Drug Delivery

Reducing off-target effects by improving drug delivery and selectivity is of large concern to medicinal chemists. The overarching term enhanced permeation and retention (EPR) encompasses the differences in the characteristics of tumor and normal tissue that may allow for macromolecular accumulation including leaky blood capillaries and impaired lymphatic drainage. These differences include increased permeability factors such as nitric oxide and bradykinin (Maeda et al., 1994; Wu et al., 1998); hypervascularity and increased vascular permeability. It is well established that tumors increase production of vascular growth factors such as vascular endothelial growth factor (VEGF) in order to maintain their high metabolic demands by increasing blood vessel formation. However, these blood vessels have shown to have poor architecture including wide fenestrations between endothelial cells allowing for macromolecule infiltration (Yamasaki et al., 2012). Additionally, clearance rates of lymphatics from tumors are much lower for

higher molecular weight drugs (>40K), as tumors lack abundant functional lymphatic vessels (Hoshida et al., 2006; Noguchi et al., 1998). In fact, higher MW compound tissue/blood ratios can be 100-fold higher depending on molecular size and tumor clearance (Maeda et al., 2009; Seymour et al., 1995). As such, the EPR phenomenon has become a means for investigation for improved drug delivery. Although EPR can serve as a selective passive targeting tool, this has been coupled with Ru coordination chemistry and rationally designed polymer conjugation to overcome the limitations of previous Ru compounds NAMI-A and KP1019. The next generation of Ru metallodrugs are including polymer-metal complexes (PMC) that have the potential to improve aqueous solubility, *in vivo* stability, pharmacokinetics, targeting and perform controlled release of conjugated high performing drugs like oxaliplatin (Cabral et al., 2005). The conjugation of poly(lactic acid) (PLA) nanoparticles with Tween 90 showed increased activity of KP1019 approximately 20 fold (Fischer et al., 2014); while NAMI-A conjugations showed increased cytotoxicity and anti-metastatic potential (Blunden et al., 2014). Studies are currently ongoing to further improve Ru-derived drugs for better tumor specific targeting, metastasis, and attempting to reduce undesirable side effects.

In conclusion, several characteristics of Ru-based compounds are of particular interest. a) The mechanism of action regarding cytotoxicity is structurally-dependent, several studies have shown that based on ligand kinetics and design, Ru-based compounds can be synthesized to preferentially bind to DNA or proteins b) Ru^{III} complexes can act like pro-drugs in which the reducing environment of a tumor c) Ru-complexes can be synthesized to be inert and mimic the structure and

binding of naturally occurring compounds d) Clinical trials indicate that efficacy may be independent of dose. Taken together, first generation molecules must be improved upon and specific endpoints be investigated in terms of dose. As such, conventional screening methods may need to be supplanted by additional *in vivo* mechanisms and inexpensive high-throughput *in vivo* models.

1.3 Overview of Zebrafish as Model Organism

Zebrafish (*Danio rerio)* are a freshwater teleost indigenous to South Asian countries and belong to the family Cyprinidae. They are relatively hardy fish that inhabit moderately flowing to stagnant water (Engeszer et al., 2007). The use of the zebrafish model was sparse until George Steisinger optimized means of husbandry and generated interest in genetic screens (Meyers, 2018). The sequencing of the zebrafish genome initiated at the Wellcome Trust Sanger Institute (carried out from 2001- 2013) greatly increased the prospects of the model (Howe et al., 2013) by illustrating a 70% functional homology with human genes and 84% association of disease-causing genes (Howe et al., 2013).

Aside from a variety of applicable genetic tools, this model offers several other advantages. Zebrafish are relatively small (approximately 4-5 cm) and prefer to shoal in larger groups. This makes the space required to house them relatively smaller and overall maintenance cheaper than most mammalian models (Veinotte et al., 2014).

Increased statistical power due to high fecundity contributes to the robustness of studies carried out with zebrafish. One breeding set can produce upwards of 300 eggs every 10 days. In addition, the transparent eggs are fertilized outside of the mother, which allows relatively easy monitoring of development and genetic manipulation. Statistical power can also be improved with the accelerated rate of experimentation. Zebrafish development into a free-swimming organism within three days and reach adulthood by approximately three months (Kimmel et al., 1995).

These inherent characteristics of zebrafish have inspired whole organism high-throughput screening (HTS) of chemicals using zebrafish embryos in which thousands of compounds are used for organism exposure. One such system called Complex Object Parametric Analysis System (COPAS) developed by Union Biometrica can automatically sort embryos on size and fluorescence and the Vertebrate Automated Screening Technology (VAST) BioImager, although not as high-throughput can conducted relatively fast imaging of 2-7 day old zebrafish larvae, avoiding the manual laborious positioning (Union Biometrica, 2016).

Zebrafish show great promise as an asset to pharmacology and toxicology. This model allows for examining adverse outcome pathways from biochemical to whole organism endpoints, in which cell culture lacks the complexity and in rodent model are cost-limiting. Large screening for drug activity and toxicity have already been conducted in zebrafish and have successfully identified compounds tested in clinical trials (Leonard & Randall, 2005; Santoriello & Zon, 2012; Tan & Zon, 2011). These studies have included the identification of compounds which modulate hematopeietic stem cells (HSC), neural crest transcriptional events and complimented *in vitro* and *in vivo* murine models (North et al., 2007; White et al., 2011). Zebrafish would do well to complement the drug development paradigm in which aspects like lead discovery, modes of action, target identification, and toxicological studies. As such, they could play an important role in identifying promising contenders for metallodrugs evaluation.

CHAPTER 2. NOVEL SCREENING METHOD OF TRANSITION METAL-BASED ANTICANCER COMPOUNDS USING ZEBRAFISH EMBRYO LARVAL ASSAY AND ICPMS ANALYSIS

2.1 BACKGROUND

The discovery of platinum (Pt)-based anti-proliferative compounds has resulted in their widespread use as chemotherapeutics. Originally identified in 1965, cisplatin, a square planar molecule comprised of a single platinum scaffold is currently considered by the World Health Organization (WHO) as an essential drug for treating the ten most common cancers and other tumors (Rosenberg et al., 1965; WHO, 2016) The broad-spectrum cytotoxicity of cisplatin is due to its electrophilic reactivity upon entering the cell. The reactive molecule has been shown to bind proteins as well as cellular DNA. The DNA binding and subsequent adduct formation result in an apoptotic cascade and cancer cell death (Harrington et al., 2010; Ming et al., 2017).

Cisplatin's success stimulated the synthesis and investigation of additional metal-based chemotherapeutics. Furthermore, drug resistance to Pt-based molecules has accentuated the need for alternative transition metal scaffolds (Corte-Rodriguez et al., 2015; Hall et al., 2008b). Ruthenium (Ru) is an attractive candidate due to the structural diversity that can be achieved; not only many Ru compounds are stable in multiple oxidation states relevant under physiological conditions, but the preferable octahedral geometry adopted by most of Ru compounds allows the fine tuning of electronic and steric properties (Gasser et al., 2011; Zhang & Sadler, 2017).

These characteristics led to the prolific production of Ru-based molecules, some of which like KP1019 and NAMI-A, have promising anticancer capabilities and entered clinical trials (Hartinger et al., 2006; Leijen et al., 2015).

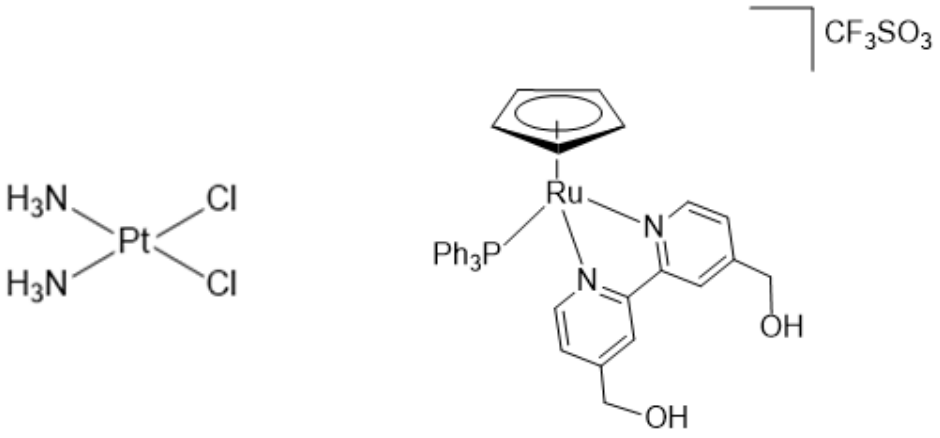

Figure 1. Cisplatin and PMC79 - Chemical structure comparison of platinum-based, square planar molecule, cisplatin (300.01 molar mass; left) and the ruthenium-based, piano stool molecule, PMC79 (793.76 molar mass; right).

Unfortunately, the rate of development for these compounds does not appear to have matched the rate of potency or efficacy assessment. The zebrafish model has gained popularity for toxicity assessment of drug candidate efficacy because it examines adverse outcome pathways (AOPs) from biochemical to whole organism endpoints, unlike cell culture and cost-limiting using rodent models. However, the zebrafish model has been limited due to determination of dose delivery through waterborne treatments, which would allow for comparison across higher and lower vertebrates delivered dosages. We propose using the zebrafish model (OECD, 2013) coupled with inductively coupled plasma mass spectrometry (ICPMS). This may allow for expedited bioanalytical screening of

critical toxicological endpoints including LC_{50} and EC_{50} values, (lethal and effective concentrations for 50% of the population) and the NOAEL and LOAEL, no or lowest observed adverse effect level. In order to refine the method, cisplatin the mechanism of which has been elucidated, and a novel Ru compound, PMC79, were evaluated (Figure 1) (Corte-Real et al., 2019; Moreira et al., 2019). PMC79 was found to be more cytotoxic than cisplatin in ovarian (A2780) and breast (MCF-7 and MDA-MB-231) human cancer cells. Both compounds induce cell death by apoptosis, however their targets are different. While DNA is the main target for cisplatin, in the case of PMC79, a proteomic study indicated that the proteins that regulate the actin dynamics are the main target for this compound. As such, we hypothesize the observed lesions will be similar although the potencies will be different due to their distinct modes of action. We report in this paper that the ICPMS method can be successfully used to track metal-based anticancer drugs, and that PMC79 was more potent than cisplatin and that very different lesions were observed in the developing zebrafish.

2.2 MATERIALS AND METHODS

Zebrafish Husbandry

AB strain zebrafish (*Danio rerio*), obtained from the Zebrafish International Resource Center, were bred and maintained in a recirculating aquatic habitat system on a 14-h light:10-h dark cycle. Fish system water, obtained by carbon/sand filtration of municipal tap water, was maintained at 28°C, < 0.05 ppm nitrite, < 0.2 ppm ammonia, and pH between 7.2 and 7.7. Zebrafish are fed a diet

of hatched Artemia cysts, brine shrimp (PentairAES) and a 1:4 ratio of Aquatox Fish Diet flake food (Zeigler Bros, Inc.) and Tetramin (Tetra)**.** The AB strain fish were used for all experiments, and the husbandry protocol (#08-025) was approved by the Rutgers University Animal Care and Facilities Committee.

Experimental Design

A modified version of Organization Economic Cooperation and Development (OECD) Fish Embryo Toxicity Test (FET) Test Number 236 (July 26, 2013) was incorporated in this study (OECD, 2013). AB strain zebrafish male and female were placed in groups for breeding. Fertilized eggs were collected, and randomly sorted into individual glass 3-dram glass vials beginning at 3 hours post fertilization (512-cell stage) (Kimmel et al., 1995). Zebrafish embryos were grown in with 500 µl of aerated egg water (60 µg/ml Instant Ocean in DI water) dosed with nominal concentrations of cisplatin (Cas No. 15663-27-1), *cis*-Diamineplatinum(II) dichloride, $Pt(NH_3)_2Cl_2$ (≥99.9% trace metals basis purchased from Sigma-Aldrich) or PMC79 ($[Ru(\eta^5\text{-}Cp)(PPh_3)(2,2'\text{-bipy-}4,4'\text{-}CH_2OH)]^+$, synthesized by us and previously reported (Corte-Real et al., 2019) (Figure 1). Embryos were observed daily and incubated in darkness at 26°C. Endpoints examined for both cisplatin and PMC79 included delayed hatching, pericardial sac edema, yolk sac edema, as well as embryo death. The dose response studies for cisplatin and PMC79 were repeated twice with 20 embryos per dose. LC_{50} and confidence interval (CI) values were calculated based on the Litchfield and Wilcoxon method (Litchfield & Wilcoxon, 1949).

Dose Administration

The cisplatin experiments were conducted as static renewal (every 24 hours) due to limited physical and chemical stability of cisplatin in solution over 24 hours, at concentrations of 0, 3.75, 7.5, 15, 30, or 60 mg/L. PMC79 was dissolved in pure dimethyl sulfoxide (DMSO) which was diluted to a maximum of 0.5% DMSO per dose. Nominal zebrafish dose response concentrations for PMC79: 0, 3.1, 6.2, 9.2, 12.4 mg/L were determined using derivatives of an IC_{50} value (3.1 mg/L) established following A2780 human ovarian cancer cells after 72 hours. The exposure vials were continuously rocked on shaker platforms at 26°C for the duration of the study to insure constant egg exposure. PMC79 experiments were conducted as static non-renewal.

Solution and Tissue Preparation for ICPMS Analysis

Cisplatin exposed embryos at 5-day post-fertilization (dpf) were euthanized by placement in -20 ºC for 30 minutes. Either upon lethality during the study, or at 5 dpf upon completion of the study, organisms were rinsed 3 times within the vial and subsequently collected and rinsed together with 50 mL of Milli-Q (EMD Millipore) to ensure removal of excess compound. Four embryos (still within chorion) or larvae (free swimming without chorions) were collected at random, to form composite samples, for a total of three composite samples, per dose, for analysis. Only viable PMC79 larvae (without chorions) were selected at 5 dpf for analysis and followed the same preparation protocol as cisplatin. All composite samples were drained of any remaining rinse water and digested in a CEM MARS

X microwave digester (Matthews, NC) using 0.25 mL of Nitric Acid, 67-70%, OmniTrace Ultra, until all organic matter was visibly oxidized (Table 1). The solutions were then diluted to 3.5% nitric acid using MilliQ water. In addition, PMC79 solutions were collected from at least 4 vials per dose to form the composite sample for analysis to confirm exposure dose. Because cisplatin dissolved well into solution and the stability kinetics are well known, ICPMS analysis for Pt equivalents of nominal cisplatin concentrations were not conducted (Karbownik et al., 2012) (Sewell, 2010).

Evaluation of chorionic accumulation

Fertilized embryos were randomly selected at 3 hpf and grouped in four sets of 10 to 15 for exposure to 7.5 mg/L and 15 mg/L cisplatin dissolved in egg water in 10 mL of solution in glass vials. These concentrations were selected due to the high rate of delayed hatching and low rate of perceived mortality. At 5 dpf, the embryos were drained of solution rinsed within the vial three times with 5 mL of Milli-Q water and subsequently collected and rinsed in with 50 mL of Milli-Q water to remove any excess remaining solution. The embryos were manually dechorionated under a dissecting scope using needles. The chorions and the larvae were collected separately per treatment in composite samples of four or more and the remaining water was drained. A Thermo Scientific CL2 Centrifuge was used to pellet the chorions. Samples were prepared for analysis as described above, however, an additional step was included for difficult to dissolve chorions in which 30% trace metal grade hydrogen peroxide was added to achieve a final concentration of 3.5%

nitric acid. The chorionic accumulation experiment was repeated twice and T-tests were performed between the larvae and chorion Pt concentrations.

ICPMS Analysis

Metal content in the samples was quantified via high resolution inductively coupled plasma mass spectrometry (HR-ICP-MS) [Nu Instruments Attom®, UK]. Data was recorded by the Attom software (Attolab v.1) and analyzed with NuQuant by using a seven-point calibration curve of either Ru or Pt. Samples were introduced using an ASX-510 Autosampler [CETAC Technologies]. Several isotopes of Pt and Ru were analyzed in order to minimize isobaric interferences and are listed in the Table 1 below. The limit of detection for tissue and solution ranged from 0.005 to 0.05 parts per billion (ppb), and remained a minimum of one order of magnitude below the treated samples per analytical run. Matrix matched samples (egg water, or digested larvae or chorions) were spiked with 1 ppb of standard and included every 10 samples to monitor for instrument drift. Additional ICPMS operating parameters are listed in Table 2 below. It should be noted that ^{100}Ru has isobaric interferences with strontium oxides, which are formed from the strontium salts contained in the egg water solutions. ^{192}Pt and ^{99}Ru were used for qualitative analysis. The instrument performed 3 technical replicates per sample. Outliers determined to exceed two standard deviations from the mean were removed from analysis.

2.3 RESULTS

Analytical Evaluation

Nominal waterborne concentrations of 0, 3.75, 7.5, 15, 30 and 60 mg/L cisplatin were compared to Pt accumulation in organism (larvae with or without chorion) tissue determined by ICPMS analysis. The nominal waterborne concentrations delivered respective doses of 0.05, 8.7, 23.5, 59.9, 193.2, and 461.9 ng (Pt) per organism with the average embryo mass at approximately 100 µg. The two highest cisplatin doses have larger variability than observed in lower dosages. This may be due to inclusion of viable and nonviable organisms or the delayed hatching phenomenon, as the entire organism was digested with no dechorionation. This was especially relevant in higher doses where higher percentages of delayed hatching were observed. Chorions were included as part of whole organism analysis.

Nominal waterborne concentrations of 0, 3.1, 6.2, 9.2, 12.4 mg/L of PMC79 were analytically determined to contain 0, 0.17, 0.44, 0.66, and 0.76 mg/L of Ru. The delivered tissue doses of these concentrations were only determined for viable larvae and thus were applicable for the first three lowest concentrations of PMC79. Because delayed hatching was not observed, chorions were not included in organism analysis. The respective tissue doses were 0.19, 0.41, and 68 ng (Ru) per larvae. The vehicle control for both the exposure medium and the tissue was below the detection limit (DL) of 0.005 ppb.

The relationship between exposure medium (cisplatin or PMC79) and metal equivalent (Pt or Ru) per organism is depicted in Figure 2.

Dose Response

Dose response studies were conducted with the aforementioned nominal waterborne concentrations of cisplatin. Lethality and a delayed hatching endpoint were analytically evaluated (Figure 3). The lethal concentration for 50% or half the group of test animal (LC_{50}) value was determined to be 31 (95% CI: 21-34) mg/L cisplatin (158.9, [95% CI 105-174] µM) and the corresponding delivered tissue dose was 193.2 (+/- 130) ng (Pt) per organism. The effective concentration for half the population regarding the delayed hatching endpoint (EC_{50}) was determined to be 5 mg/L (25.6 µM). Delayed hatching was observed at all concentrations and thus no NOAEL was able to be determined. However, the LOAEL value was observed at a nominal concentration of 3.75 mg/L (19.2 µM) and at a delivered dose of 8.7 Pt (ng) per organism (44 pmoles). The lethality curve appeared to have a threshold effect between 60 and 195 Pt (ng) per organism, which was not observed in the delayed hatching endpoint. Concentrations beyond this threshold appeared to have much greater variability than treatments below. Several lesions were observed including pericardial hemorrhaging, and spinal curvature (Figure 5).

Additionally, dose response studies were conducted with the ICPMS measured waterborne concentrations of PMC79. Lethality was evaluated, compared to the solution concentrations and delivered tissue dose (Figure 4). The LC_{50} was determined to be 0.79 (95% CI 0.43-1.20) mg/L Ru (7.8, [95% CI 4.2-11.8] µM). The NOAEL was not determined due to adverse lesions observed at the lowest treated dose. The lesions included hemorrhaging along the caudal vein

and tail artery, spinal curvature, and yolk sac edema (Figure 5). The LOAEL was 0.17 mg/L (1.7 µM).

In order to further investigate whether cisplatin levels in the chorion or larvae could be correlated with delayed hatching, embryos that exhibited delayed hatching at 5 dpf were dechorionated and both the chorion and larvae were analyzed. Contrary to the discarded chorions of the control larvae, the chorions for the cisplatin treated embryos were intact and rigid. This effect was not observed in PMC79 exposed embryos. The dechorionation results demonstrate that cisplatin preferentially bound to the chorion and much less to the developing organism (Figure 6). Doses of 7.5 mg/L resulted in 1.5 Pt (ng) per larvae (7.7 pmoles, 4% of total delivered dose [TDD]) and 37.3 Pt (ng) per the chorion (191 pmoles, 96% TDD). The higher dose of 15 mg/L resulted in 3.4 Pt (ng) per larvae (17.4 pmoles, 7% TDD) and 47.9 Pt (ng) per the chorion (245.6 pmoles, 93% TDD). Once removed from the chorion, the majority of the larvae exposed to 15 mg/L or higher of cisplatin did not respond to tactile stimuli. The embryos hearts were beating and no additional visible lesions were observed.

2.4 DISCUSSION

We developed an ICPMS technique that has the sensitivity necessary to detect Pt and Ru in zebrafish embryo, larval or chorionic tissue. Although metals have been detected in trace samples this study is unique in that it has used metal surrogates to detect the dose delivery of metallodrugs. This technique determined the tissue dose for the developing zebrafish which can allow for comparisons with dose

determined in other model systems. Additionally, dose quantification allows for determination of toxic potencies on a tissue basis for comparison across anti-cancer drugs (Table 3). This bioanalytical assessment used for evaluation and comparison of both cisplatin and PMC79 and is applicable to other metal-based compounds. With this assay we determined the individual LC_{50} and EC_{50} values, and NOAEL or LOAEL. Not only were the potencies of the compounds different, (Cisplatin LC_{50}: 31 mg/L (158.9 µM), PMC79: 0.79 mg/L (7.8 µM)), but the observed adverse effects of each compound manifested as disparate lesions. Although we hypothesized similar lesions with distinct potencies, both the lesions and potencies were distinct which provides further evidence that the different modes of action, although apoptotic, result in very different whole organism toxicity.

PMC79 treated larvae had yolk sac edema and no adverse effects on the pericardium were observed. The contrary was observed for cisplatin; no adverse effects were observed on the yolk sac size, but pericardial sac hemorrhaging was present. The organ related alterations indicate different chemical specific organ system toxicity by the two anti-cancer drugs. Additionally, the delayed hatching and intact chorions were not observed with exposure to the Ru-based compound. Control and PMC79 exposed chorions were completely disintegrated post-hatching. The rigid chorions following cisplatin exposure may be explained by cisplatin electrophilic cross-linking of the chorionic proteins, although this needs to be further investigated (Li et al., 2011). Preliminary studies demonstrated that proteases were less effective in breaking down the cisplatin treated chorions. This

cross-linking between proteins would cause rigidity and resistance to protease degradation. Delayed hatching and protease chorion breakdown may be able to be exploited as a biomarker for compounds that rely on a cross-linking mechanism of action.

Additionally, the evaluation of cisplatin distribution between the chorion and the larvae indicated that the majority of the cisplatin (92-96% TDD) was bound to the chorion reducing the amount of drug available to reach the embryo (Figure 6). This is in contrast with PMC79, in which the chorions were digested and unable to be collected for analytical evaluation. This stymied delivery to the larvae may explain the different in toxicities. However, it is still unclear whether the chorionic accumulation of cisplatin contributes to alternative lesions including the immobility which may be explained by either the potential alteration of the physiochemical properties of the chorion (diminished nutrient and oxygen exchange), or extended confinement. Finally, given the immobility of the dechorionated embryos, one must consider the criteria for considering an organism viable. Regardless, these questions must be taken into consideration regarding the toxicological and efficacy evaluation of future metal-based compounds using zebrafish embryo larval assays.

Coupling ICPMS with the zebrafish embryo larval model brought unforeseen insight into the toxicological evaluation of these compounds and we believe this model could be a promising asset to high throughput evaluation of metal-based anticancer compounds. This model differentiates tissue effects and allows for direct comparison of a series of Ru anticancer drugs using the zebrafish.

Additionally, it is important to determine the actual dose and not rely on nominal concentrations. The use of zebrafish may help elucidate the mechanism of action of the drug and potential non-targeted tissues or biochemical pathways.

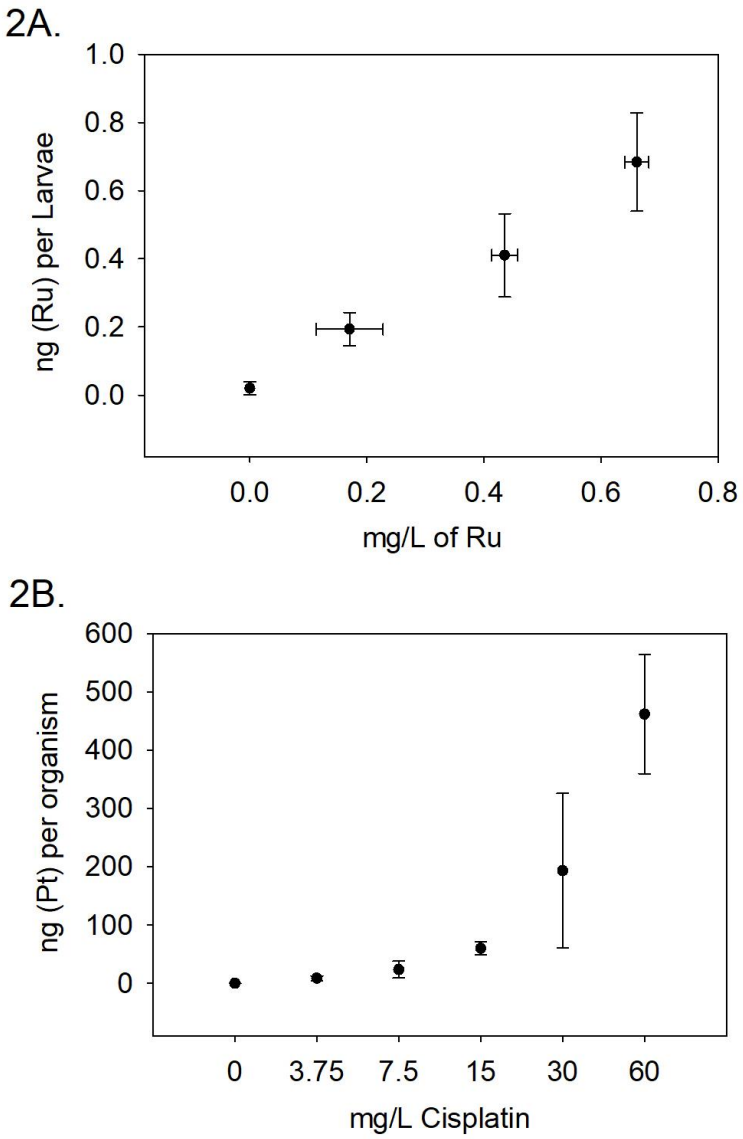

Figure 2. Analytical Dose Response - ICPMS analytical determination of Pt (A) and Ru (B) concentrations in digested tissue samples relative to nominal and analytically determined concentrations of anticancer Cisplatin and PMC79 compound, respectively. N = 4-6 composite samples per dose, 2 experimental replicates.

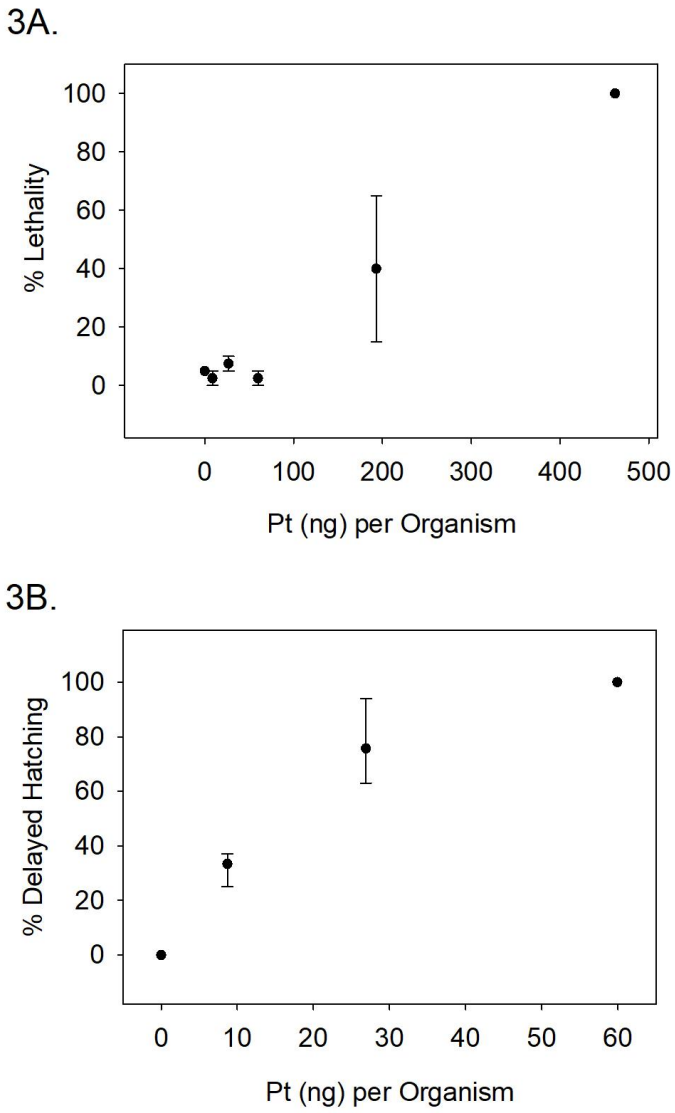

Figure 3. Cisplatin Dose Response - A) Percent mean lethality at 5 days post-fertilization (dpf) correlated to the mean Pt equivalents determined per organism, B) Percent mean delayed hatching at 5 dpf correlated to the mean Pt equivalents per organism. Lethality: N = 40 per dose; Pt (ng) per Organism: >4 composite samples per dose; 2 experimental replicates

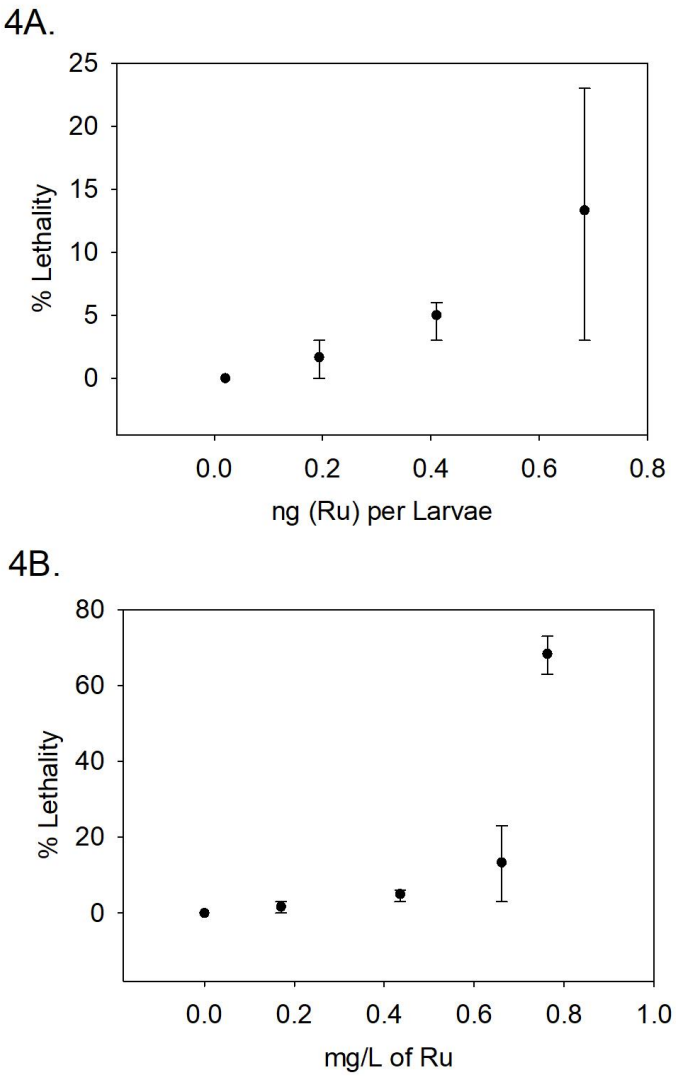

Figure 4. PMC79 Dose Response - A) Percent mean lethality was correlated to the analytically determined mean Ru equivalents in solution (mg/L). and B) Percent mean lethality at 5 dpf from the same experiment was correlated to the mean Ru equivalents per larvae. Lethality: N = 40 per dose; mg/L Ru: N = 6 composite samples per dose; ng (Ru) per larvae >4 composite samples per dose; 2 experimental replicates.

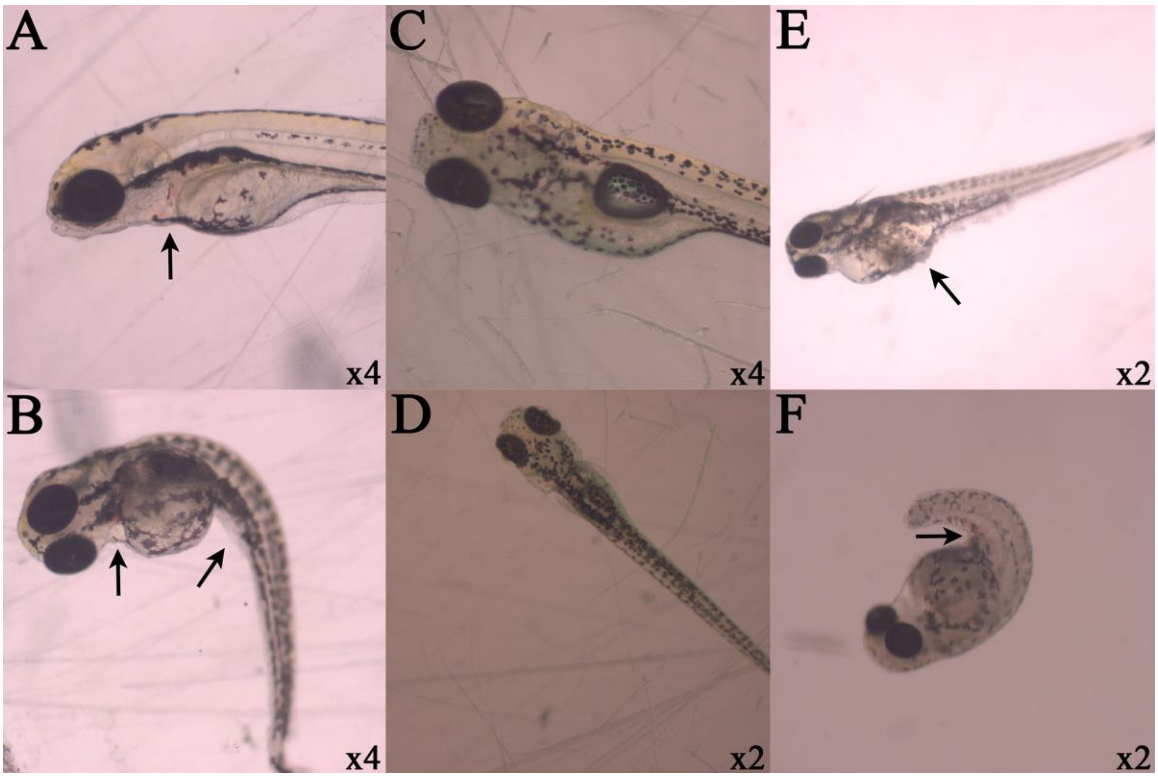

Figure 5. Lesion Identification - Observed lesions in zebrafish larvae after dechorionation were obtained with Olympus SZ-PT dissecting microscope equipped with Scion digital camera model CFW-1310C and analyzed with Adobe Photoshop software. Respective magnifications are displayed in the lower right hand corner of each photograph, and black arrows indicate lesions of interest. Cisplatin exposure at 30 mg/L demonstrate pericardial sac hemorrhaging (A and B) and spinal curvature (B) after dechorionation. Control organisms without lesions are centered (C and D). PMC79 exposure at arrows indicate yolk sac edema and protein coagulation and precipitation (E) and hemorrhaging along caudal vein or tail artery (F).

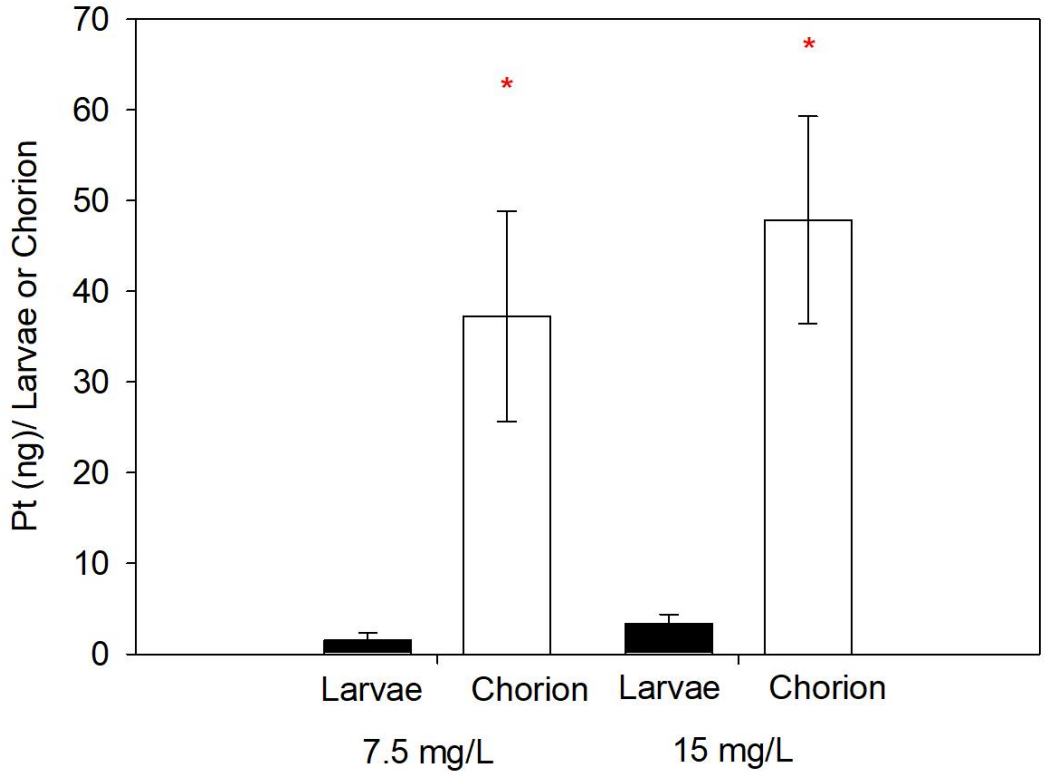

Figure 6. Chorionic Accumulation of Platinum (Pt) - Comparison of Pt (ng) present in the larvae and in the chorion after exposure to 7.5 mg/L or 15 mg/L. Composite >3 larvae or chorions per sample; from left to right N = 13, 10, 10, and 11. Mann-Whitney Rank Sum Test $P < 0.001$ between larvae and chorion for both doses.

CHAPTER 3. ANTI-PROLIFERATIVE AND ANTI-ANGIOGENIC EVALUATION OF NOVEL RUTHENIUM METALLODRUGS IN THE ZEBRAFISH MODEL

3.1 BACKGROUND

Cisplatin and alternative platins (platinum-based chemotherapeutics) have had great success in cancer treatment, however their dose-limiting side effects and spontaneous and/or acquired drug resistance cannot be ignored (Hall et al., 2008b; Lieberthal et al., 1996; NCI, 2007). In order to overcome these limitations, an alternative transition metal, ruthenium (Ru), has become popular as a structural core. With the advantage of increased versatile design due to octahedral geometry and strategic ligand design, these Ru metallodrugs may be able to out-perform the platins in terms of decreased toxicity and targeted efficacy (Noffke et al., 2012). Two Ru-based drugs, NAMI-A ((ImH)[*trans*-$RuCl_4$(dmso-S)(Im)], Im = imidazole) and KP1019 ((IndH)[*trans*-$RuCl_4(Ind)_2$], Ind = indazole), had successfully entered clinical trial. NAMI-A, which demonstrated potent anti-metastatic properties in pre-clinical trials did not recapitulate the same results in patients. KP1019 showed reasonable anti-solid tumor effects and the molecular formula has been improved upon and is currently being re-trialed (Burris et al., 2016; Leijen et al., 2015). Improvements in these metallodrugs have involved manipulating the molecule to target specific characteristics of cancer, thereby improving delivery and limiting off-target effects. Studies have shown that polymer-metal complexes, such as nanoparticles with polymer conjugates, can improve solubility, *in vivo* stability, pharmacokinetics and, most importantly, efficacy (Avgoustakis et al., 2002; Cabral et al., 2005; Yang et al., 2011). Here we compare two Ru-cyclopentadienyl (CP) − (η^5-C_5H_5) structures as potential anticancer agents: PMC79, the CP parental

compound, and LCR134, a CP derivative conjugated and biotin; [Ru(η^5-C_5H_5)(PPh_3)(2,2 bipy-4,4-CH_2OH)] and [Ru(η^5-C_5H_5)(PPh_3)(2,2 bipy-4,4-dibiotin ester)], respectively (**Figure 1**) (Corte-Real et al., 2019; Karas et al., 2019). These compounds belong to a novel class of Ru-based compounds which bear an organometallic fragment with proved cytotoxicity and improved aqueous stability (Moreira et al., 2019). These structures were designed to passively target cancer tissue by exploiting the enhanced permeation and retention (EPR) effect in which macromolecules selectively accumulate in solid tumors due to increase tissue fenestration and poor lymphatic drainage (Hoshida et al., 2006; Yamasaki et al., 2012). In addition, LCR134 contains a biotin (vitamin B7) conjugate for active targeting. Vitamin-drug targeting is a well-documented clinical approach due to the upregulated expression of vitamin receptors on cancer cells due to intense metabolic activity (Chen et al., 2010; Shi et al., 2014). Specifically, biotin has been one of the more successful conjugates exemplified in paclitaxel, doxorubicin and gemcitabine (Tripodo et al., 2014) and its receptor, sodium-dependent multivitamin transporter (SMVT), has been shown to be overexpressed various cancer cells lines including MCF7 and MDA-MB-231 cancer cell lines (Ren et al., 2015).

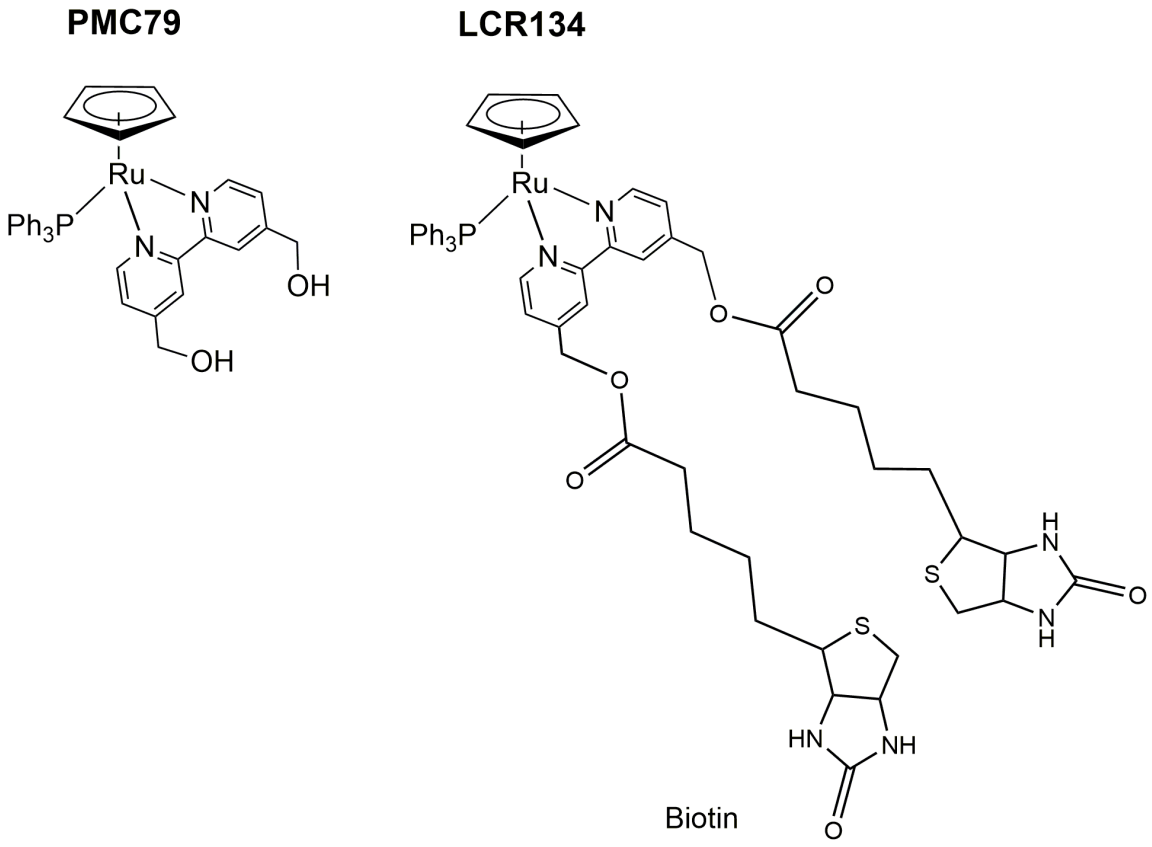

Figure 1. Chemical Structures of PMC79 and LCR134 – Two cyclopentaldienyl ruthenium (Ru) metallodrugs: PMC79 (left) the parental compound of LCR134 and LCR134 (right) the polymer-metal complex containing two poly(lactic acid) conjugates bound to biotin.

In this study, we establish whole organism response of PMC79 in comparison with previously investigated tolerability of LCR134 and cisplatin using the zebrafish model (Corte-Real et al., 2019). Anti-proliferative capacity was evaluated for these compounds using gene expression analysis and tail fin regeneration coupled with immunofluorescent staining for markers of increased cell count and proliferation. Due to a reproducible hemorrhaging lesion identified after PMC79 exposure, the perturbation of blood vessel development was investigated in the Tg(fli1”EGFP)y1 transgenic line (expression of green

fluorescent protein in vascular endothelial cells). As angiogenesis is a process for solid tumor growth and metastasis, inhibition of this process could indicate promising candidacy for further evaluation.

3.2 MATERIAL AND METHODS

Zebrafish Husbandry

The AB or the eGFP vascularly labeled transgenic Tg(fli1:EGFP)y^1 strain zebrafish (Zebrafish International Resource Center, Eugene, OR) was used for all experiments. Breeding stocks were bred and housed in Aquatic Habitats (Apopka, FL) recirculating systems under a 14/10 h light/dark cycle. System water was obtained by carbon/sand filtration of municipal tap water and water quality was maintained at <0.05 ppm nitrite, <0.2 ppm ammonia, pH between 7.2 and 7.7, and water temperature between 26 and 28 ºC. All experiments were conducted in accordance with the zebrafish husbandry protocol and embryonic exposure protocol (#08-025) approved by the Rutgers University Animal Care and Facilities Committee. Males and females were maintained separately and co-mingled the night before breeding to allow spawning the next morning. Spawning substrates were placed into the fish tanks on the day prior to spawning. In case eggs were obtained from more than one set of breeders all eggs that were fertilized and progressing normally through development were mixed. Embryos were collected within 1 hour after fertilization, washed with egg water (60 µg/ml Instant Ocean in DI water), and cleaned thoroughly.

PMC79 Treatment and Morphometric Analysis

Zebrafish embryos were exposed to concentrations of PMC79 solutions (mg/L) at 0.05% of DMSO in individual glass vials through a waterborne exposure from 3 hours post fertilization (hpf) until 120 hpf (5 days) in a static non-renewal protocol. Nominal zebrafish dose response concentrations 0, 3.1, 6.2, 9.2, 12.4 mg/L were determined using derivatives of an IC_{50} value (3.1 mg/L) established following A2780 human ovarian cancer cells after 72 hours (Corte-Real et al., 2019). These doses were analytically determined to contain 0, 0.17, 0.44 0.66, and 0.76 mg/L of Ru in previous work (Karas et al., 2019). The exposure vials were continuously rocked on shaker platforms at 26°C for the duration of the study to insure constant egg exposure. PMC79 experiments were conducted as static non-renewal. Two experimental replicates were conducted with 20-30 embryos per dose. The controls had >90 % survival rate.

The exposure followed a modified OECD 236 protocol (OECD, 2013) where the endpoints of lesion presence and mortality were recorded, during the major stages of organ development. A randomized portion of larvae surviving at the end of the toxicological experiment (120 hpf) were used for morphological data. Remaining larvae were quantified by ICP-MS Ru quantification analysis reported by (Karas et al., 2019).

Cisplatin Treatment and Morphometric Analysis

Group-housed zebrafish embryos were exposed to 15 mg/L cisplatin at 0.05% of DMSO in 20 ml glass vials through a waterborne exposure from 3 hours post

fertilization (hpf) until 120 hpf (5 days) in a static renewal (every 24 hrs) solution. The concentration was chosen based on previous work establishing this dose as having the most counts of delayed hatching with the lowest lethality (Karas et al., 2019). In order to further investigate chorionic interference with cisplatin exposure, one treatment group and one control group were manually dechorionated at 48 hours to mimic a naturally hatching time point. Two experimental replicates were conducted with 20-30 embryos per dose. The controls had >90 % survival rate.

Staining and Morphometric Measurements

For morphological data, embryos were dechorionated (if needed) and fixed in 10% buffered formalin for 48 hours. They were then stained for bone and cartilage following a two-color acid free Alcian Blue/Alizarin red stain (Walker & Kimmel, 2007). Photographs were taken using a Scion digital camera model CFW-1310C mounted on an Olympus SZ-PT dissecting microscope and cartilage/bone were measured using Adobe Photoshop. Endpoints examined included total body length, intraocular distance, pericardial sac size and yolk sac size. These were used to assess larval growth, cranial facial development, cardiovascular system impact and nutrient storage and usage, respectively.

Blood Vessel Measurements

Group-housed zebrafish embryos were exposed to 50 uM sorafenib, or doses of PMC79 or LCR134 at or below the Lowest Observed Adverse Effect Level (LOAEL) established previously (Corte-Real et al., 2019; Karas et al., 2019). All treatments contained DMSO at or below 0.05%. The treatments were conducted

in 20 ml glass vials through a waterborne exposure beginning at 3 hours post fertilization (hpf) in a static non-renewal solution. Live animal imaging was conducted by anesthetizing larvae at 72 hpf in a 0.01% concentration of MS-222 (tricaine mesylate) solution. Larvae were then transferred onto 35mm glass bottom dishes in 5% methyl cellulose and imaged using an Olympus TH4-100 inverted microscope with X-cite 120 Fluorescent Illumination. The sub-intestinal basket (SIV) area and branching number, and the intersegmental blood vessels (ISV) were measured using NIH Image J software.

Reverse-transcriptase (RT) quantitative PCR

Group-housed zebrafish embryos were exposed to either egg water with DMSO vehicle or doses of PMC79 or LCR134 at or below the Lowest Observed Adverse Effect Level (LOAEL) established previously (Corte-Real et al., 2019; Karas et al., 2019). All treatments contained at or below 0.05% of DMSO. The treatments were conducted in 20 ml glass vials through a waterborne exposure beginning at 3 hours post fertilization (hpf) static non-renewal solution. At 24 hpf, samples were rinsed 3xs with DI water and snap frozen in liquid nitrogen. Total RNA was isolated from 50 embryo composite samples using RNAzol (Sigma-Aldrich). Reverse transcription was performed on 1 ug aliquots of RNA to produce cDNA for RT-PCR using a High-Capacity cDNA Reverse Transcription Kit (Thermofischer) using a PTC-200 Peltier Thermal Cycler. RT-PCR reactions were performed in triplicate using PowerUp SYBR Green Master Mix (ThermoFischer) and the primers listed in **Table 1**. cDNA amplification was performed for 40 cycles on a QuantStudio 3

(Applied Biosystems) and recorded with QuantStudio Design and Analysis Software and analyzed in Thermocloud (ThermoFischer). Analysis was conducted as ΔΔCT using 28S as an endogenous control.

Table 1. Primer Sequences Used to Determine Transcription Levels

Primer	Forward Sequence	Reverse Sequence	Citation
28s	CCTCACGATCCTTCTGGCTT	AATTCTGCTTCACAATGATA	(Hillegass et al., 2007)
hif1-α	TCTGGTTCTTGAGTGCAGGGTTCT	GTCCGATCTGCACGTTTTCA	(Bonventre et al., 2011)
vegfa	TGCTCCTGCAAATTCACACAA	ATCTTGGCTTTCACATCTGCA A	(Bonventre et al., 2011)
vegfc	ATAAACCACCCTGCGTGTCTGTCT	TCCTTGCTTGACTGGAACTGTGA	(Bonventre et al., 2011)
wnt3a	ATGGTGTCCCGAGAGTTTGCTGAT	AAGCCCGTGACACTTGCATTTCAG	(Bonventre, 2012)
wnt8a	GGACTACATGGAACTGAAGG	CTGTCTCAATCCTCCTCTCTT	(Bonventre, 2012)

Tail fin Regeneration and PCNA/DAPI Staining

Tg(fli1:EGFP)y^1 strain zebrafish embryos were raised to 48 hpf and anesthetized in 0.01% MS-222. Tail fins were manually cut using a razor blade posterior to the notochord. Immediately following amputation, larvae were imaged and individually housed. Larvae were treated with either egg water with DMSO vehicle or doses of PMC79 or LCR134 at or below LOAEL, as established previously, for 24 hours (Corte-Real et al., 2019; Karas et al., 2019). All treatments contained at or below 0.05% of DMSO and 0.0002% methylene blue to retard bacterial growth.

At 24 hours post-amputation (hpa), larvae were reimaged, sacrificed, and fixed in 4% paraformaldehyde (PFA) for 2-4 hrs at room temperature (RT). Fixed

larvae were rinsed with PBST (rinse indicates 3xs for 5 mins with Phosphate Buffered Saline + 0.1% Tween-20 [PBST]) and dehydrated in a methanol/PBST gradient (25%, 50%, 75%, 100%; 5 mins each) and stored at -20°C until rehydration was conducted in the reverse gradient. After rehydration, larvae were PBST rinsed, and subsequently washed (1x; 5mins) and incubated in 150 mM Tris HCl, pH 9.0 incubate at 70°C for 15 mins. Larvae were then permeabilized in pre-chilled acetone at -20°C for 10 mins. Samples were them incubated in 10% normal horse serum(NHS)/PBST blocking buffer at 4°C for 3 hours and subsequently Anti-PCNA antibody [PC10] (ab29) (Abcam, Cambridge, UK) 1:500 NHS at rocked at 4°C for 3 days. Samples were then washed in 1% NHS block (5xs; 10 mins) and incubated with DyLight 549 Horse Anti-Mouse IgG Antibody (Vector Labs) 1:1000 NHS at 4°C rocking for 2 days. After secondary incubation, samples were PBST rinsed and stored in Vectashield Antifade Mounting Medium with DAPI (Vector Laboratories, Burlingame, CA) until fluorescent confocal imaging. Z- stack images were taken on an Olympus FV1000MPE microscope (Olympus XLPlan N 25x objective NA 1.05) in 3 µm step size. Z-stacks were compressed and ImageJ was used to count DAPI, PCNA and co-stained cells.

3.3 RESULTS

PMC79 Treatment and Morphometric Analysis

A modified Fish Embryo Acute Toxicity OECD protocol (OECD, 2013) was used in order to establish adverse outcomes of altered physiology and tissue development during PMC79 exposure. Daily observations of embryos were recorded and

included lethality as well as lesions, such as pericardial sac and yolk sac edema, and hemorrhaging. Nominal doses of PMC79 and LCR134 were selected as derivatives of IC_{50} values (1x, 2x etc.) previously established. These doses were analyzed for Ru by ICPMS in water-born solutions and larval tissues (**Tables 3 and 4)**. The LOAEL doses for the metallodrugs are designated with a secondary box within each table and were established for PMC79 as $0.17 \pm 1.7e^{-3}$ mg/L analytically determined Ru water-borne concentration and corresponding tissue dose 0.19 ± 0.05 Ru (ng/organism). LCR134 was established as $0.27 \pm 4.6e^{-2}$ mg/L analytically determined Ru water-borne concentration and corresponding tissue dose 0.30 ± 0.06 Ru (ng/organism). Ru solutions were back-calculated using molecular weight to determine total metallodrugs concentrations. These data indicate that a LOAEL was established for LCR134 at approximately 1.5 times the water-borne and delivered tissue dose for PMC79.

Daily monitoring indicated that minimal lethality occurred at all but the highest dose (12.4 mg/L) of PMC79. In contrast, yolk sac edema was observed at all but the lowest dose (3.1 mg/L) and increased in the number of afflicted larvae after 72 hpf. Additionally, at or after 72 hpf, all but the lowest dose had hemorrhaging around heart, dorsal aorta, or posterior cardinal vein with slowed heartbeats (**Figure 2**). After 120 hours post fertilization (hpf) larvae were sacrificed, fixed and a dual Alcian blue/Alizarian red stain was carried out to improve visualization and highlight bone and cartilage development. Larvae were morphometrically evaluated for total body length as an indication of growth and development, pericardial sac size to evaluate cardiovascular impacts, yolk sac size

for metabolic function and nutrient deposition and intraocular distance as an indication of cranio-facial development (**Figure 3**). Results demonstrate a significant dose-dependent decrease in total body length mirrored with a dose-dependent increase in yolk sac size after exposure to the three highest doses (nominal values: 6.2, 9.3, and 12.4 mg/L) of PMC79. A significant decrease in the intraocular distance of the highest three doses was observe, and although this was not dose-dependent, the threshold dose of 3.1 mg/ml appeared to have a wider range of distribution than the top two doses. Lastly, pericardial sac did not appear to be significantly impacted by PMC79 exposure. However, as with intraocular distance, there appears to be a dose-dependent increase in size distribution and variability at the three highest doses (**Figure 4**). Because lesions and/or lethality were observed at all doses, no NOAEL was established for PMC79.

It has been well established that cisplatin caused delay hatching in zebrafish in low doses with no lethality or additional lesions and, strikingly, up to 5 days post-fertilization (dpf) (Karas et al., 2019; Kovacs et al., 2016). Notably this delayed hatching was not observed in PMC79 exposed embryos. In order to investigate chorionic interference, morphological evaluation was carried out in non-dechorionated (N-DC) and manually dechorionated (DC) fish. Dechorionation was conducted at 48 hpf to mimic a natural hatching time point (Kimmel et al., 1995). A 15 mg/L cisplatin dose was selected due to low lethality and high percent delayed hatching. Morphology results indicated similar results to PMC79, and LCR134 in which total body length was significantly decreased and yolk sac size was significantly increased. These alterations were further augmented by

dechorionation. Intraocular distance was decreased to a similar extent for N-DC and DC fish, however, the DC fish had a much broader range of intraocular distances or variability as demonstrated by the wider quartile range. Unlike PMC79, cisplatin treatment did not appear to alter pericardial sac size (**Figure 5**). **Table 4** summarizes the morphometric endpoints observed in all three metallodrugs. Exposure to each metallodrugs resulted in similar morphometric impacts including a decrease in total body length, and intraocular distance as well as increase in yolk sac size. However, PMC79 was the only compound tested that caused cardiovascular damage.

Gene Expression

RNA transcript levels of several genes involved in proliferation and angiogenesis were measured after 24 hours of exposure at or below the LOAELs of PMC79 and LCR134. These genes included vascular endothelial growth factors (*vegfa* and *c*), a mitogenic factor for angiogenesis; wingless-related integration (*wnt 3a* and *8a*), critical for upregulating *vegf*, cell growth, proliferation and migration; as well as an inducer for all of these genes, hypoxia inducible factor α (*hif1α).* The VEGF-HIF Pathway and its components (**Figure 6**) are often targeted in cancer therapy. Overexpression of genes in this pathway have been correlated with poor patient prognosis, increased vascular invasion, metastasis and tumor resistance (Baba et al., 2010; Campbell et al., 2019; Chen et al., 2014; Zhan et al., 2017). As such, these factors have become important targets in drug development. Exposure to the parent compound PMC79, resulted in a significant decrease in all investigated

genes (except *wnt3a*), with *hif1α* and *wnt8a* as the most impacted at a ~0.5-fold reduction. LCR134 exposure did not result in a significant alteration of gene expression in the pathway (**Figure 7**).

Angiogenesis Assay

Angiogenesis is pivotal in cancer development and progression as it provides a mechanism by which rapidly growing tissue can acquire nutrients, oxygen, deplete toxic waste. Furthermore, angiogenesis is a hallmark of metastasis, as increased blood vessel development provides additional opportunity for metastatic cells to intravasate and migrate (Zetter, 1998). As such, angiogenesis has been a primary target in chemotherapeutic treatment. However, anti-angiogenic drug discovery has been stymied by narrow therapeutic windows and off-target effects including thrombosis, ischemia and other hemostatic complications (Elice et al., 2009; Verheul & Pinedo, 2007). Zebrafish are in a unique position to provide a robust model of anti-angiogenic capabilities for translation to higher organisms. Vasculogenesis in zebrafish is similar to other vertebrates, in which hemangioblasts differentiate from the mesoderm and later forming angioblasts and endothelial cells. Zebrafish blood vessel formation is very characteristic and has been thoroughly investigated. Development begins at around 12 hpf with all functioning vasculature developed by 72 hpf; making this organism a relatively high through-put model compared to in vivo plug assays. A circulatory network containing the dorsal aorta (DA) and axial vein (AV) form around 24 hpf and blood circulates adjacent to the yolk sac through the Ducts of Cuvier (a large blood

circulation sinus on the yolk sac where anterior and posterior cardinal vessels join) to begin sprouting of the subintestinal vessels (SIVs) into the gut (Fouquet et al., 1997; Kimmel et al., 1995; Serbedzija et al., 1999). In addition, many genes and major regulatory factors of angiogenesis such as the VEGF-HIF pathway are conserved (Liang et al., 2001). Studies have shown pharmacological translatability between zebrafish and human responses and in fact small molecules identified in zebrafish are in clinical trial (MacRae & Peterson, 2015) Another advantage larvae offer is the ability to develop in the absence of functional vasculature and blood. This is due to the fact that larvae can survive by oxygen perfusion during early development and allow investigation at disruptive stages that may be lethal to higher organisms and mammals (Isogai et al., 2001; Wilkinson & van Eeden, 2014).

Vascular insult was investigated by assessing SIV vessel length and corresponding area, number of interconnecting vessels (branching) within the SIV, and inhibition of blood vessel length extension from DA to dorsal lateral vein (DLV) by a ISV to trunk width to vessel length ratio (Chimote et al., 2014; Delov et al., 2014; Serbedzija et al., 1999). In this study, we used sorafenib, a multi-kinase inhibitor that targets tumoral angiogenesis, and is used in the treatment of metastatic cancers. In almost all larval exposure to sorafenib, both SIV baskets and ISV blood vessels were severely inhibited or not formed (**Figure 8**). No significant blood vessel inhibition was found in the ISV vessels or decrease in basket area for either PMC79 or LCR134 (**Figure 9 and 10**). However, PMC79 appeared to cause perturbations. The lowest dose of PMC79 caused an increase

in basket area (**Figure 10**), while the highest treated dose caused a 57% reduction in SIV basket branching (**Figure 11**).

Tail Fin Regeneration

Zebrafish have the ability to regenerate certain tissue including the fins. The caudal fin located at the posterior end of the body makes it easily accessible for surgical amputation. Post-amputation, two key structures form and interact to initiate proliferation, a wound epithelium and a blastema, or highly proliferative tissue containing undifferentiated cells as shown in **Figure 12** (Pfefferli & Jaźwińska, 2015). Additionally, genes within the Wnt/β-catenin signaling pathway increase expression in response to amputation and has been shown to be essential for regeneration (Gemberling et al., 2013). Larval fin regeneration offers an assay to assess impaired proliferation and remodeling of tissue during metallodrugs exposure. Larvae tail fins were amputated and immediately placed in respective treatments. Tail fins were given 24 hours to regenerate in metallodrugs solutions. All three metallodrugs resulted in a significant reduction in the total area of regenerated tail fin compared with the cut control (**Figure 13 and 14**). PMC79 and LCR134 exposure resulted in significantly less overall DAPI labeled cells. Tail fins were additionally stained for proliferating cell nuclear antigen (PCNA) as a marker for cells undergoing proliferation. When PCNA was considered in terms of overall DAPI (PCNA/DAPI), exposure to each metallodrugs resulted in significantly less cells proliferation (**Figure 15 - 16**).

3.4 DISCUSSION

Gross Morphological Impact

Morphometric analysis demonstrated that PMC79 and LCR134 exposure resulted in reduced total body length complementary with increased yolk sac size in a dose-dependent manner (**Figure 4**). This observation was also observed after cisplatin exposure regardless of intact chorion, but more drastically when embryos were dechorionated, thus increasing exposure; neither Ru drugs caused delayed hatching (**Figure 5**). This indicates that for all compounds a reduction in total growth and proliferation was mirrored by a reduction in nutrient uptake and distribution from the yolk (Corte-Real et al., 2019). In addition, exposure to each metallodrugs resulted in decrease in intraocular distance, indicating an impact on cranio-facial development at higher doses in developing organisms. These results could indicate side effects or off-target involvement of tissues that could result in a drug failing clinical trials or side effects that should be monitored when administering the drug.

Tail Fin Regeneration

Whole organism anti-proliferative properties observed by stunted growth and nutrient uptake were further evaluated using tail fin regeneration coupled with immunofluorescent staining of PCNA and DAPI. The doses selected for further evaluation were based off the 5-day dose response curve. PMC79 and LCR134 were used for treatment at established LOAEL. However, the cisplatin dose was selected at the established 5-day $LC_{50,}$ which demonstrated minimal lethality for a

24 hr exposure. Although cisplatin exposure was conducted at a more toxic dose, exposure to each of the three metallodrugs demonstrated similar reduction in total area of regeneration and reduced PCNA signaling for proliferation (**Figure 13-16**). This complemented with cell culture IC_{50} results demonstrating increased sensitivity to the Ru drugs compared to cisplatin (Corte-Real et al., 2019). In addition, a study conducted by Wang et al., in 2009 demonstrated novel Ru drugs resulted in PCNA downregulation and a significant caudal fin-reduction phenotype compared with cisplatin and were less toxic, although fins in this study were not amputated. This suggests that the Ru drugs enact their anti-proliferative capabilities comparatively to cisplatin with the advantage of being well below a lethal endpoint. Additionally, PMC79 and LCR134, unlike cisplatin, did not appear to impact normal cell proliferation at the ventral posterior region which form independently of injury as demonstrated by Kawakami et al., in 2004 (**Figure 17**). The alkylating activity of cisplatin is unable to distinguish cancerous and normal proliferating cells, however, PMC79 and LCR134 show distinct targeting during tail fin regeneration studies. The repair of an epithelial wound involves transient activation of cellular mechanisms alongside proliferation including inflammatory response, angiogenesis, cellular migration, and tissue matrix remodeling (Eming et al., 2014). Due to differences in downregulation of normal and injury induced PCNA after metallodrugs treatment, Ru-drugs may be more selectively targeting signaling involved in these mechanisms.

Anti-Angiogenic Properties

Although each Ru drug affected PCNA, gene transcription analysis demonstrated that PMC79 impacted the HIF-VEGF pathway at 24 hpf while LCR134 did not (**Figure 7**). As the parent compound of LCR134, PMC79 may be inducing its anti-proliferative capabilities through a separate cellular pathway and this difference in gene regulation suggests LCR134 is not cleaved to form its parental structure during interaction with the cell. This is supported by a unique hemorrhaging lesion observed after the three highest doses of PMC79 exposure (**Figure 2**) and localized near the dorsal aorta (DA), as well as 57% inhibition in basket branching within the SIV at the lowest dose: 3.1 mg/L (**Figure 11**). Sorafenib exposure in developing zebrafish embryos caused a near complete inhibition of blood vessels within the trunk as well as the yolk sac (**Figure 8**). This was almost always visualized with significant pericardial sac edema and is commonly associated with VEGFR inhibitors in zebrafish as well as clinically (Chimote et al., 2014; Chu et al., 2007). However, treatment of PMC79 resulted in specific impact to the SIV without pericardial sac or ISV insult (**Figures 9-11**). SIVs are outgrowths of the posterior cardinal vein (PCV) and subsequently form a plexus with organized branching, while the ISVs are a retained primary structure (Childs et al., 2002). Although there are regional differences in angiogenesis signaling and physiology, sorafenib was able to inhibit both ISVs and SIVs, most likely due to its non-specific kinase targeting. However, PMC79 appears specifically cause insult during the organization branching of the sub-intestinal plexus. Here the zebrafish model was able to elucidate distinct regional angiogenic impacts that would have been unable

to be observed without the context of *in vivo* heterogeneity. Although alternative *in vivo* angiogenic assays exists, such as the matrigel plug and chick chorioallantoic membrane assays they are limited by their throughput capacity. However, given the distinction in results, it is important for future studies of novel compounds to evaluate both regions of blood vessels due to potential targeting selectivity.

Summary

PMC79 and LCR134 are next generation Ru-based metallodrugs. Ru-based drug candidates were designed with the intent to improve upon the broad spectrum and resulting off-target toxicity of cisplatin. Furthermore, our candidates were modeled after the first generation Ru drug, NAMI-A, which showed promising anti-metastatic potential *in vivo* but under-performed during clinical trial.

In this study, we showed two Ru drugs with anti-proliferative capacity at doses at or below established LOAELs with comparative capacity at toxic doses of cisplatin in the zebrafish model. We also established that PMC79 may have anti-angiogenic capabilities specific for areas of blood vessel remodeling which may be pertinent to the tumor microenvironment. However, careful consideration of this model for blood vessel functionality, not just inhibited formation, should be taken, considering developmental zebrafish survivability in the absence of blood vessels by passive oxygen diffusion (Wilkinson & van Eeden, 2014). In conclusion, PMC79 and LCR134 show promising anti-cancer properties and warrant further investigation in higher vertebrate models.

Future studies could examine zebrafish tumor xenograft screening. These screenings have shown to be useful in elucidating solid tumor proliferation, tumor inducible neovascularization, and cancer cell invasion (Au - Ren et al., 2017; Lee et al., 2009; Marques et al., 2009; Nicoli et al., 2007). Recently, the zebrafish tumor xenograft screening tool has been exploited in personalized medicine for patient specific efficacious drugs (Veinotte et al., 2014). Given the heterogeneity of cancers, the success of these screening xenografts could by-pass patient chemotherapeutic trial and error which result adverse side effects and lower quality of life. These studies have shown promising anti-proliferative potential of Ru metallodrugs in a higher throughput *in vivo* model. Although, the mechanisms by which these compounds are still unknown, the zebrafish have shown to be a successful platform in elucidating relative efficacy and toxicity of novel Ru metallodrugs.

Table 2 – PMC79 and LCR134 Larval Water-borne Exposure Doses at Nominal and Analytically Determined Concentrations

PMC79 (MW 793.76)	**Nominal PMC79**		**Analytical**	
	(uM)	**(mg/L)**	**Ru (mg/L)**	**PMC79 (mg/L)**
1x	**3.9**	**3.1**	**$0.17 \pm 1.7e^{-3}$**	**1.33**
2x	7.8	6.2	$0.44 \pm 2.2e^{-2}$	3.43
3x	11.7	9.3	$0.66 \pm 1.0e^{-2}$	5.15
4x	15.6	12.4	$0.76 \pm 6.3e^{-2}$	5.93
LCR134 (MW 1292.46)	**Nominal LCR134**		**Analytical**	
	(uM)	**(mg/L)**	**Ru (mg/L)**	**LCR134 (mg/L)**
1/4x	1.1	1.5	$0.01 \pm 3.9e^{-3}$	0.15
1/2x	2.3	2.9	$0.04 \pm 8.2e^{-3}$	0.47
1x	4.5	5.8	$0.09 \pm 1.9e^{-2}$	1.17
2x	9	11.6	$0.17 \pm 3.0e^{-2}$	2.18
3x	**13.5**	**17.4**	**$0.27 \pm 4.6e^{-2}$**	**3.48**
4x	18	23.3	$0.33 \pm 4.6e^{-2}$	4.24
5x	22.5	29.1	$0.40 \pm 4.5e^{-2}$	5.12
6x	27	34.9	$0.51 \pm 5.0e^{-2}$	6.57

*The first column values indicate nominal concentrations chosen as derivatives of previously established IC_{50} values in cancer cells, i.e. 1x the IC_{50}. Analytically determined concentrations of ruthenium (Ru) are shown with standard deviation; these values were used to back-calculate the metallodrugs concentrations using their respective molecular weights (MW). Bolded and boxed values designate the established lowest observed adverse effect level (LOAEL).

Table 3 – PMC79 and LCR134 Analytically Determined Larval Tissue Concentrations

<table>
<tr><th rowspan="2">Dose</th><th>PMC79</th><th>LCR134</th></tr>
<tr><th colspan="2">Ru (ng / Larvae)</th></tr>
<tr><td>1/4x</td><td rowspan="2"></td><td>0.06 ± 0.06</td></tr>
<tr><td>1/2x</td><td>0.14 ± 0.08</td></tr>
<tr><td>1x</td><td>0.19 ± 0.05</td><td>0.19 ± 0.05</td></tr>
<tr><td>2x</td><td rowspan="2">0.41 ± 0.12</td><td>0.25 ± 0.08</td></tr>
<tr><td>3x</td><td>0.30 ± 0.06</td></tr>
<tr><td>4x</td><td rowspan="2">0.68 ± 0.14</td><td>0.29 ± 0.07</td></tr>
<tr><td>5x</td><td>0.29 ± 0.04</td></tr>
</table>

*The first column values indicate nominal concentrations chosen as derivatives of previously established IC_{50} values in cancer cells, i.e. 1x the IC_{50}. Analytically determined concentrations of ruthenium (Ru) in nanograms (ng) per larvae are shown with standard deviation. Bolded and boxed values designate the established lowest observed adverse effect level (LOAEL).

Table 4 – Morphometric Impacts of Three Anti-Cancer Metallodrugs

	Total Body Length	Intraocular Distance	Yolk Sac Size	Pericardial Sac Size
Cisplatin	(-)	(-) & IV	(+)	NC
PMC79	(-)	(-) & IV	(+)	IV
LCR134	(-)	(-) & IV	(+)	NC

*NC=No Change; IV=Increase Variability, - = decreased, + = increased

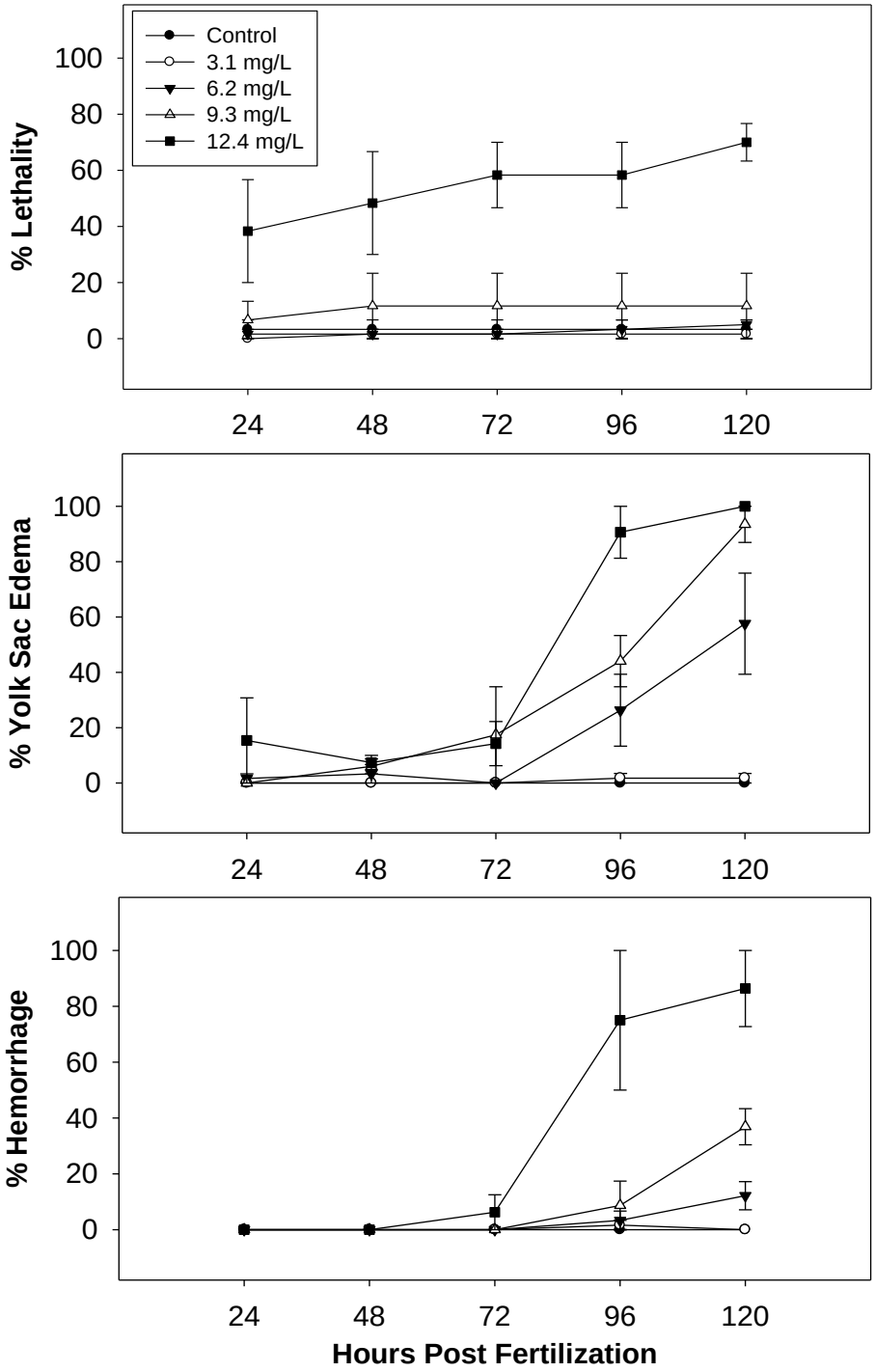

Figure 2. PMC79 Daily Observations – Four waterborne concentrations of PMC79 (3.1, 6.2, 9.3 and 12.4 mg/L) were used as exposure treatments in comparison to a 0.05% DMSO vehicle control over the course of 5 days. Lethality, hemorrhaging, and yolk sac edema counts were measured cumulative. Two experimental replicates were conducted, the ranges of which are displayed. N = 60.

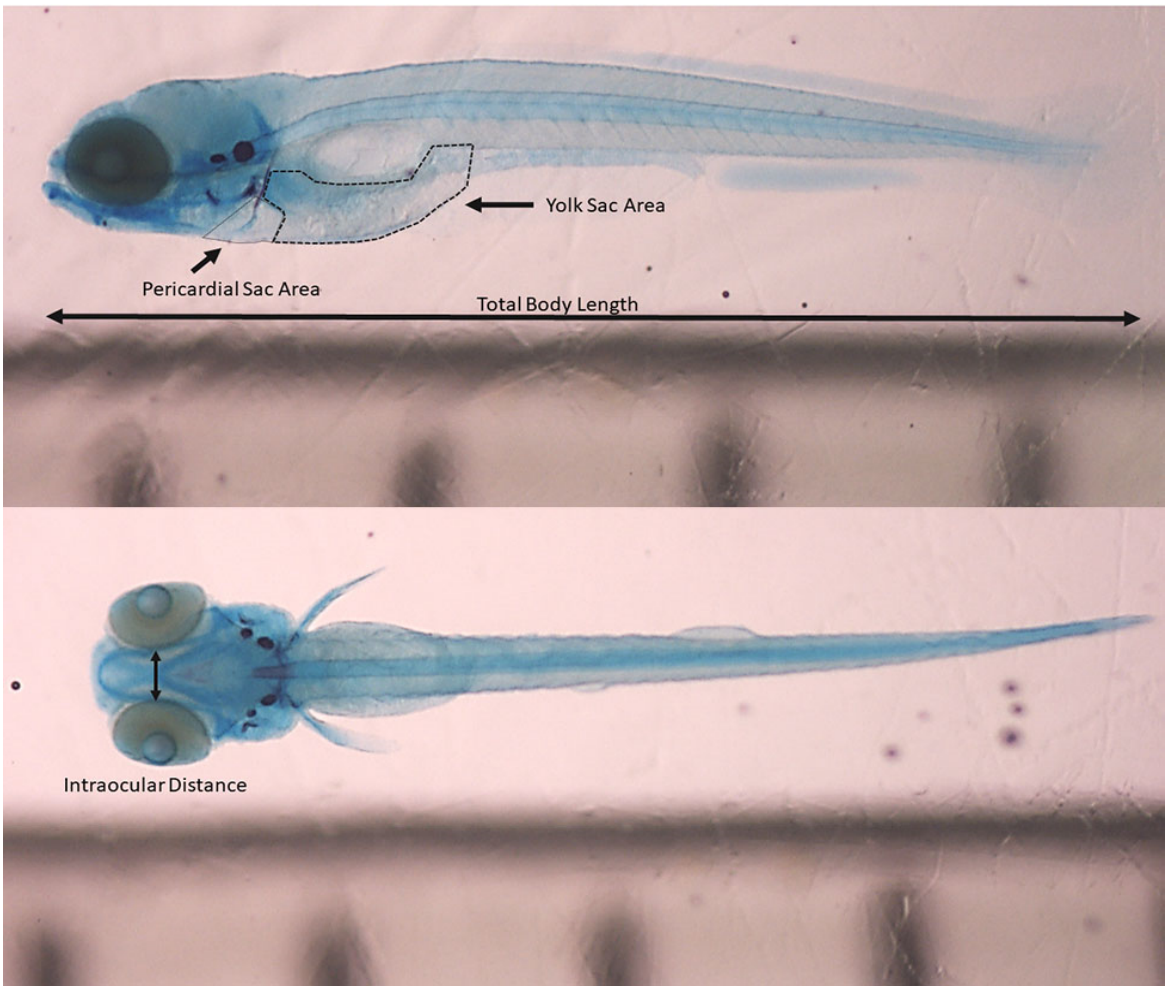

Figure 3. Morphometric Measurements – The zebrafish larvae in this image was fixed and stained with a dual cartilage and bone stain (Alcian Blue/Alizarian Red). The top image demonstrates how both the pericardial sac and yolk sac area are defined and quantified. The lower image demonstrates the length taken for intraocular distance.

A.

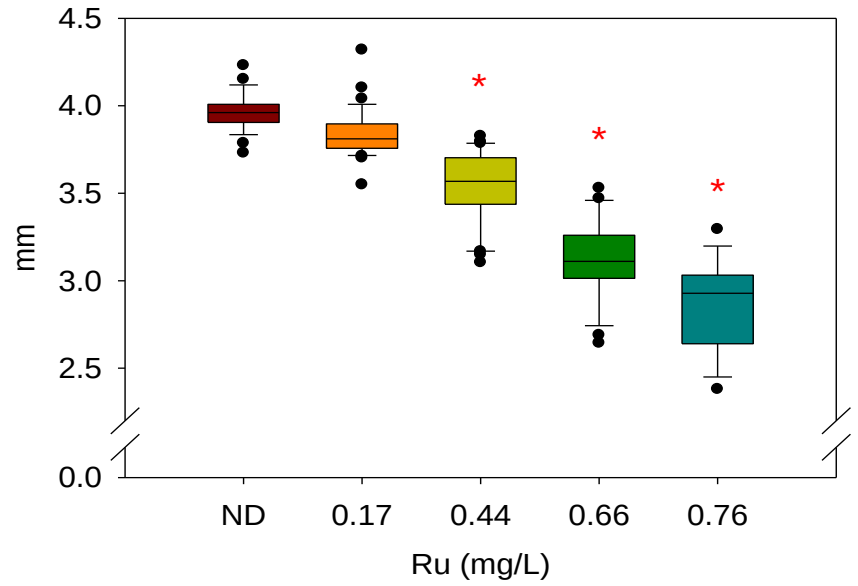
4.5
4.0
3.5
3.0
2.5
0.0
mm
*
*
*
ND
0.17
0.44
0.66
0.76
Ru (mg/L)

B.

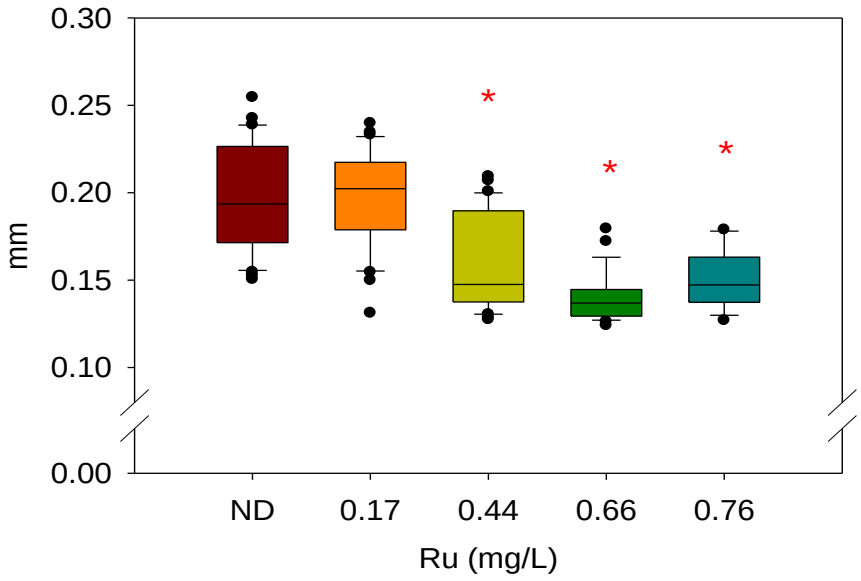
0.30
0.25
0.20
0.15
0.10
0.00
mm
*
*
*
ND
0.17
0.44
0.66
0.76
Ru (mg/L)

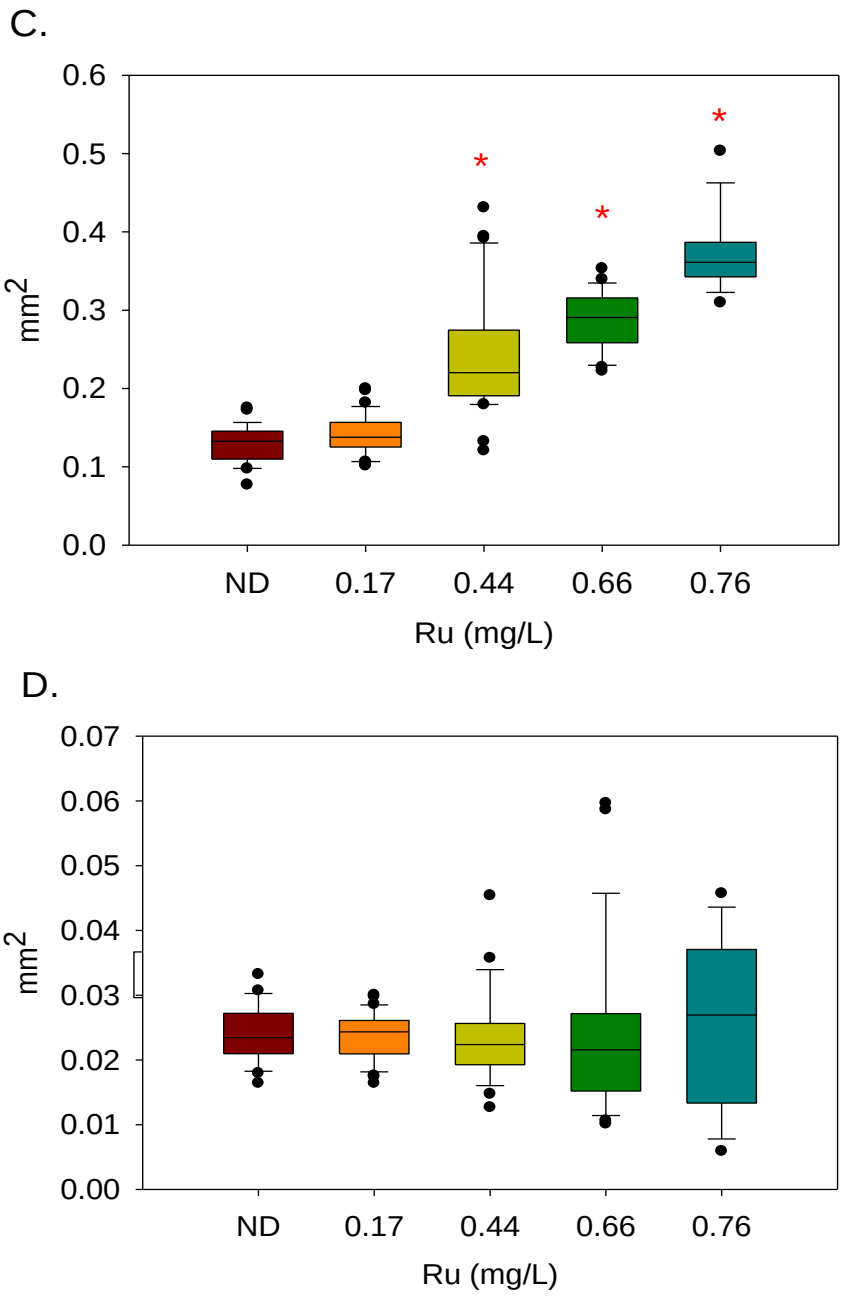

Figure 4. PMC79 Morphometric Analysis – Morphometric measurements were conducted after fixing and staining of tissue and included (A) total body length, (B) intraocular distance, (C) yolk sac size, and (D) pericardial sac size. Outliers parameters were identified as outside twice the standard deviation and removed from analysis. Asterisks indicate significant difference from the control. One Way Analysis of Variance, with posthoc Holm-Sidak (or Dunn's method for nonparametric data) with overall significance level = 0.05. Two experimental replicates were conducted; N= 14-33. Measurements were taken using ImageJ software.

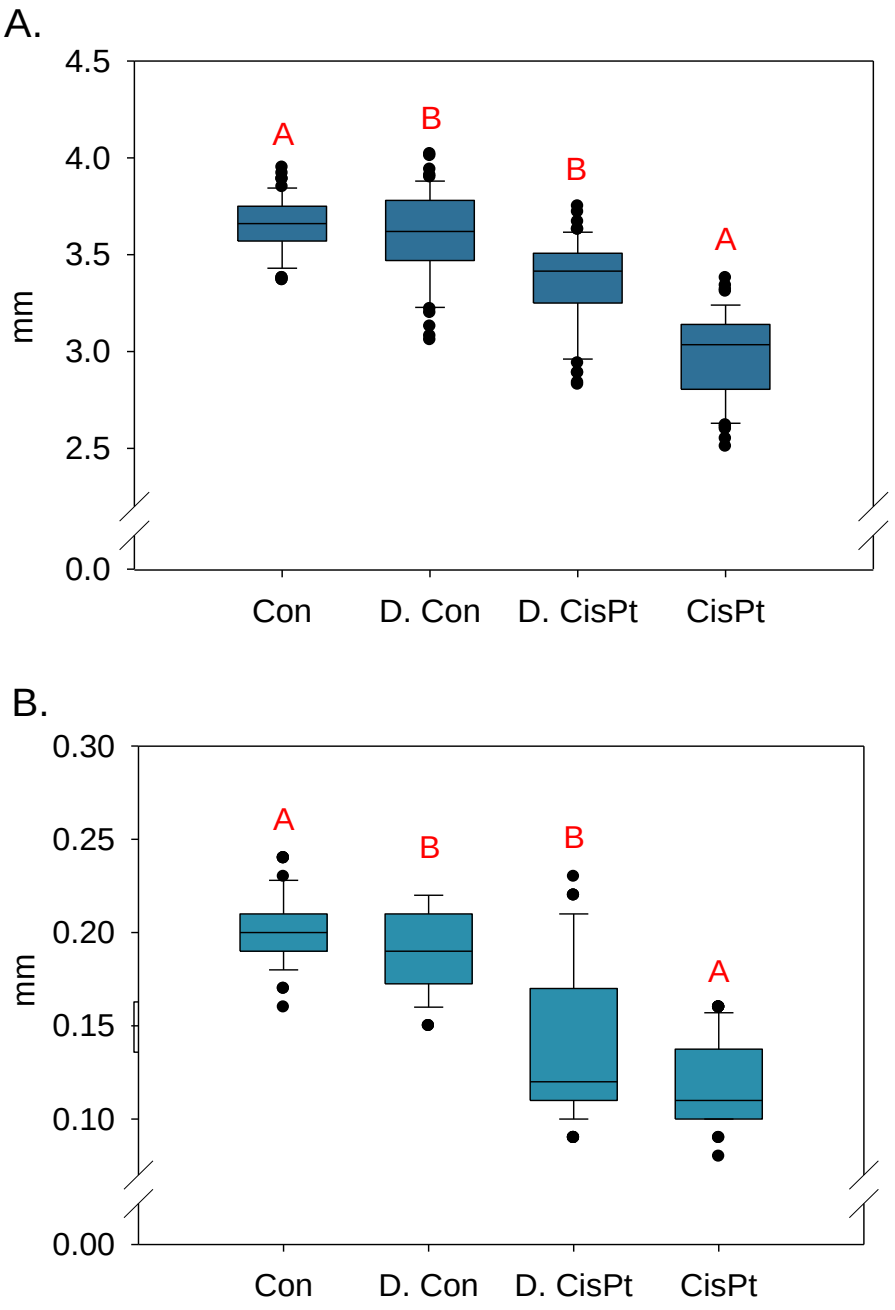
A.
4.5
4.0
3.5
3.0
2.5
0.0
mm
A
B
B
A
Con
D. Con
D. CisPt
CisPt
B.
0.30
0.25
0.20
0.15
0.10
0.00
mm
A
B
B
A
Con
D. Con
D. CisPt
CisPt

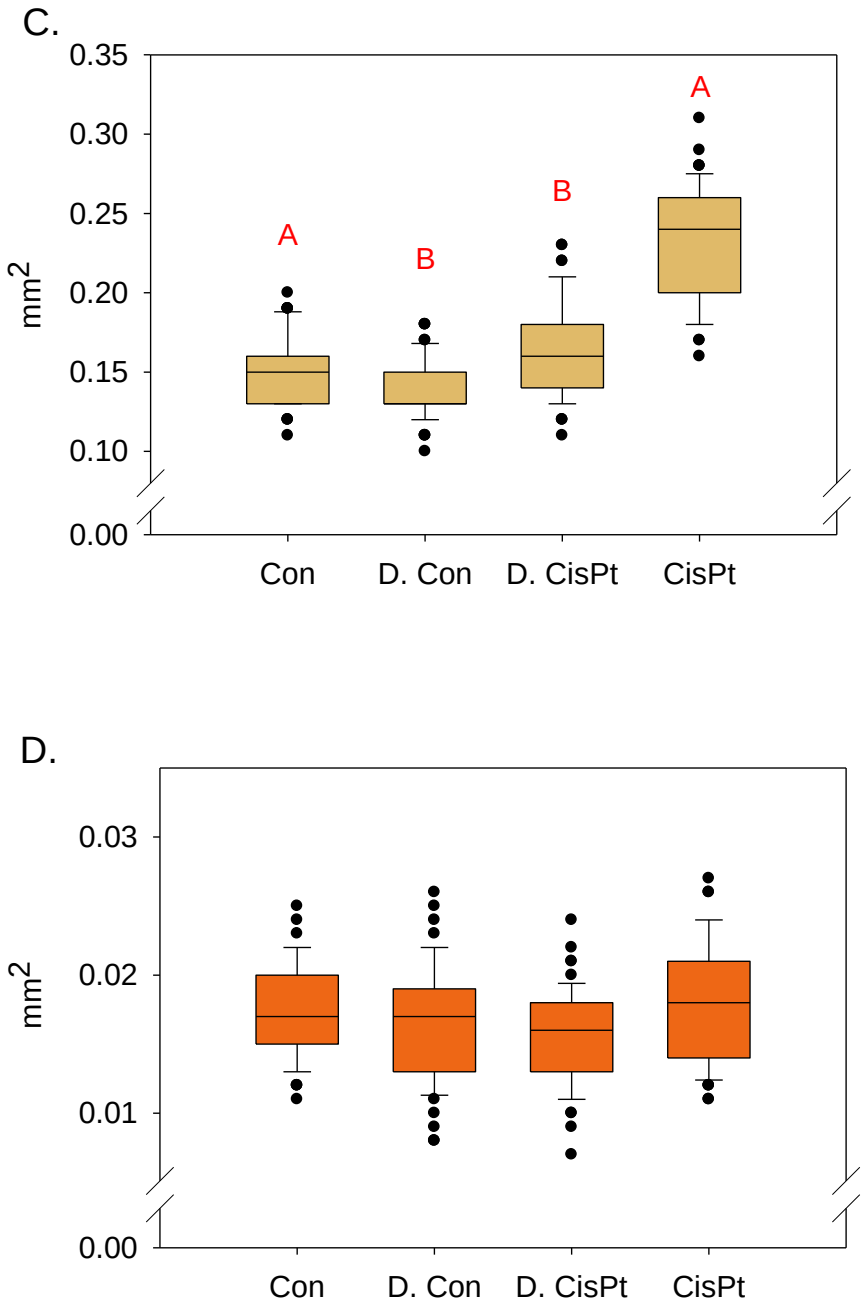

Figure 5. Cisplatin Morphometric Analysis – Morphometric measurements of 15 mg/L cisplatin treated larvae were conducted after staining and fixing of tissue. Measurements included (A) total body length, (B) intraocular distance, (C) yolk sac size, and (D) pericardial sac size. Control (Con) and treated (CisPt) embryos were divided into non- and manually dechorionated (D.) groups. Outliers parameters were identified as outside twice the standard deviation and removed from analysis. Similar letters indicate significant difference. One Way Analysis of Variance, with posthoc Holm-Sidak (or Dunn's method for nonparametric data) with overall significance level = 0.05. Two experimental replicates were conducted; N= 52-54. Measurements were taken using ImageJ software.

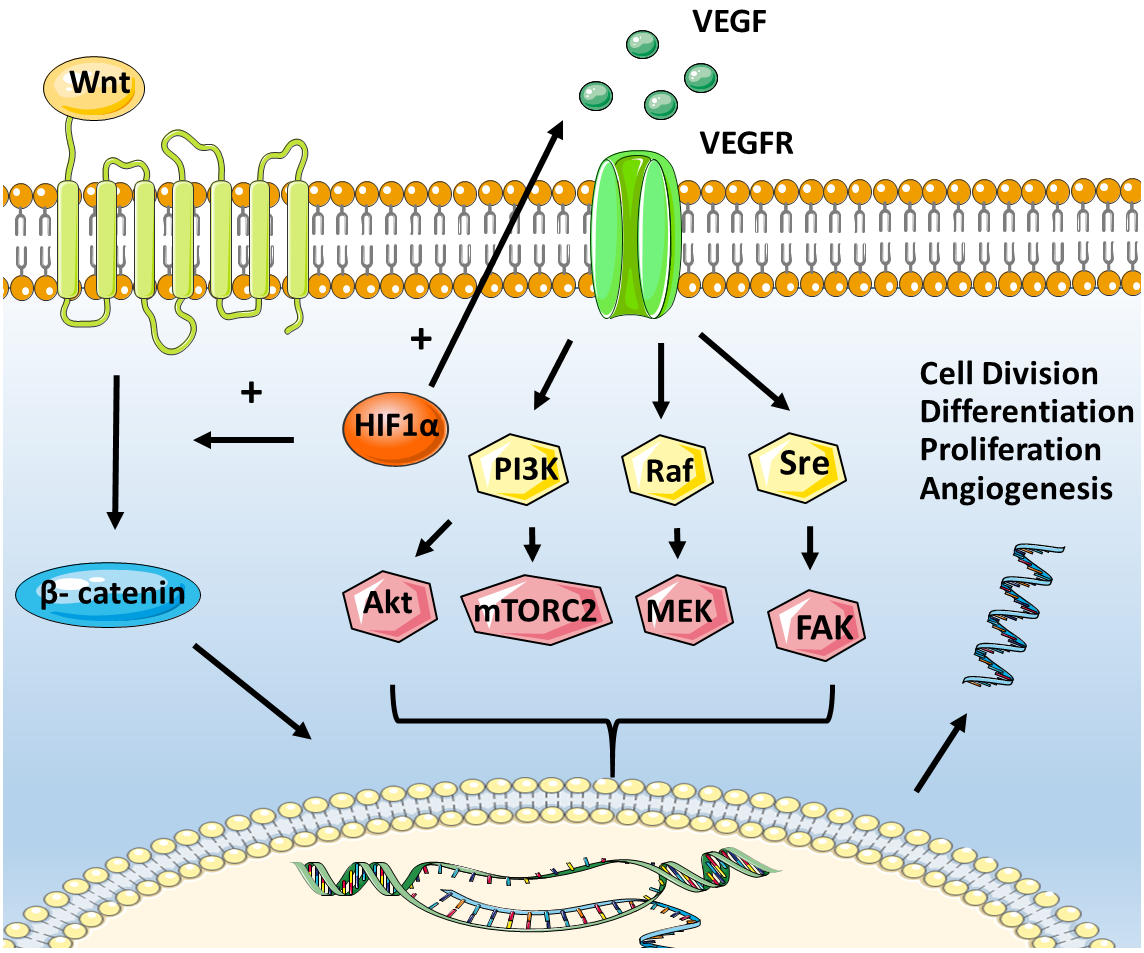

Figure 6. Gene Expression Pathway Interaction – Genes related to proliferation and angiogenesis including *hif1α, vegfa, vegfc, wnt3a, and wnt8a* have interactions bridging transcriptional levels. This figure was created using Servier Medical Art templates, which are licensed under a Creative Commons Attribution 3.0 Unported License; https://smart.servier.com.

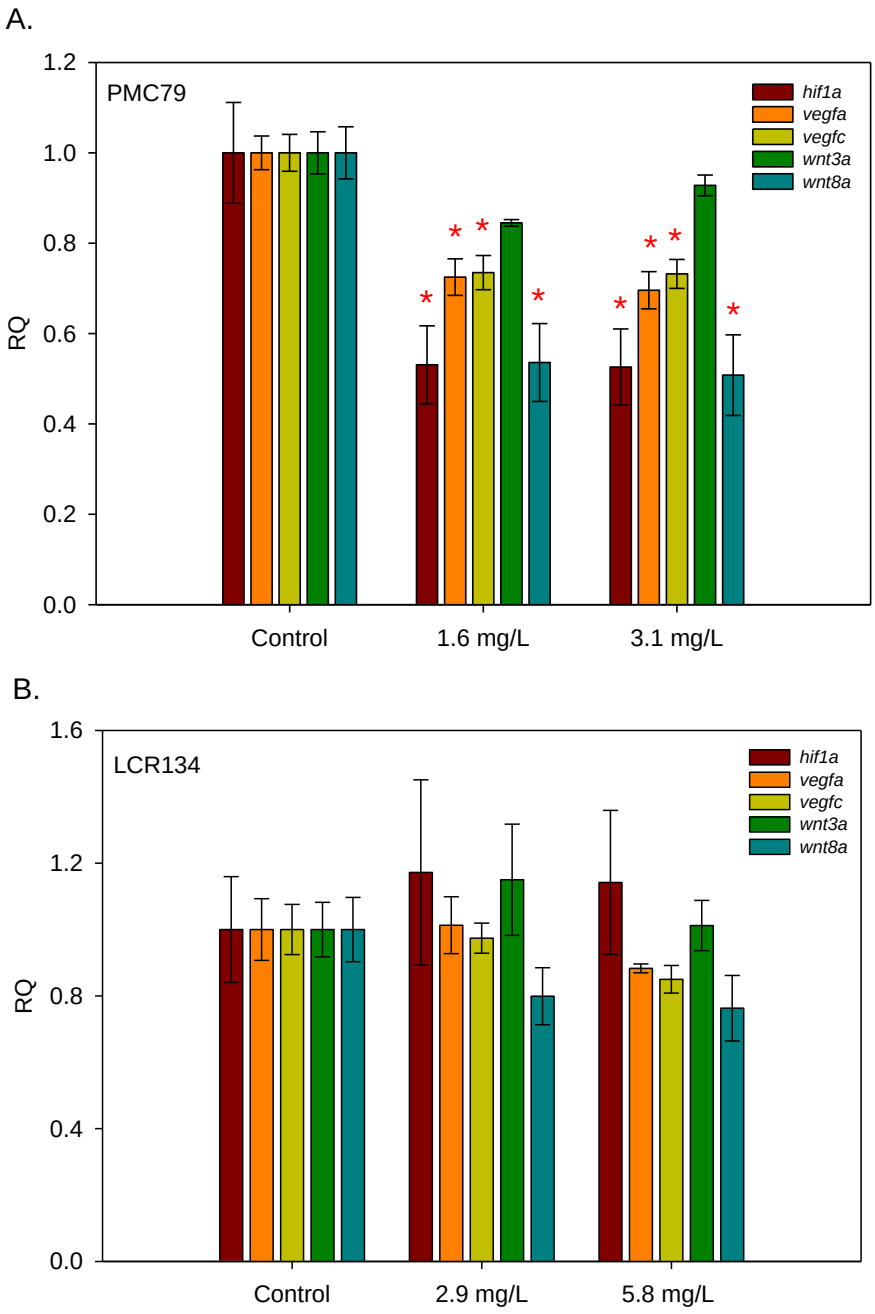

Figure 7. Gene Expression Analysis – RNA transcript levels of genes for proliferation and angiogenesis were assayed after 24 hours of exposure and included *hif1α, vegfa, vegfc, wnt3a, and wnt8a*. Graphs represent the mean relative quantification (RQ) +/- the S.E.M. of three experimental replicates (N=3). A one-way ANOVA or Kruskal-Wallis Anova on Ranks were used to determine a significant effect of metallodrugs PMC79 (A) and LCR134 (B) on transcript levels. * indicates a significant difference versus control as determined by Holm-Sidak or Dunn's post hoc analyses ($p \leq 0.05$).

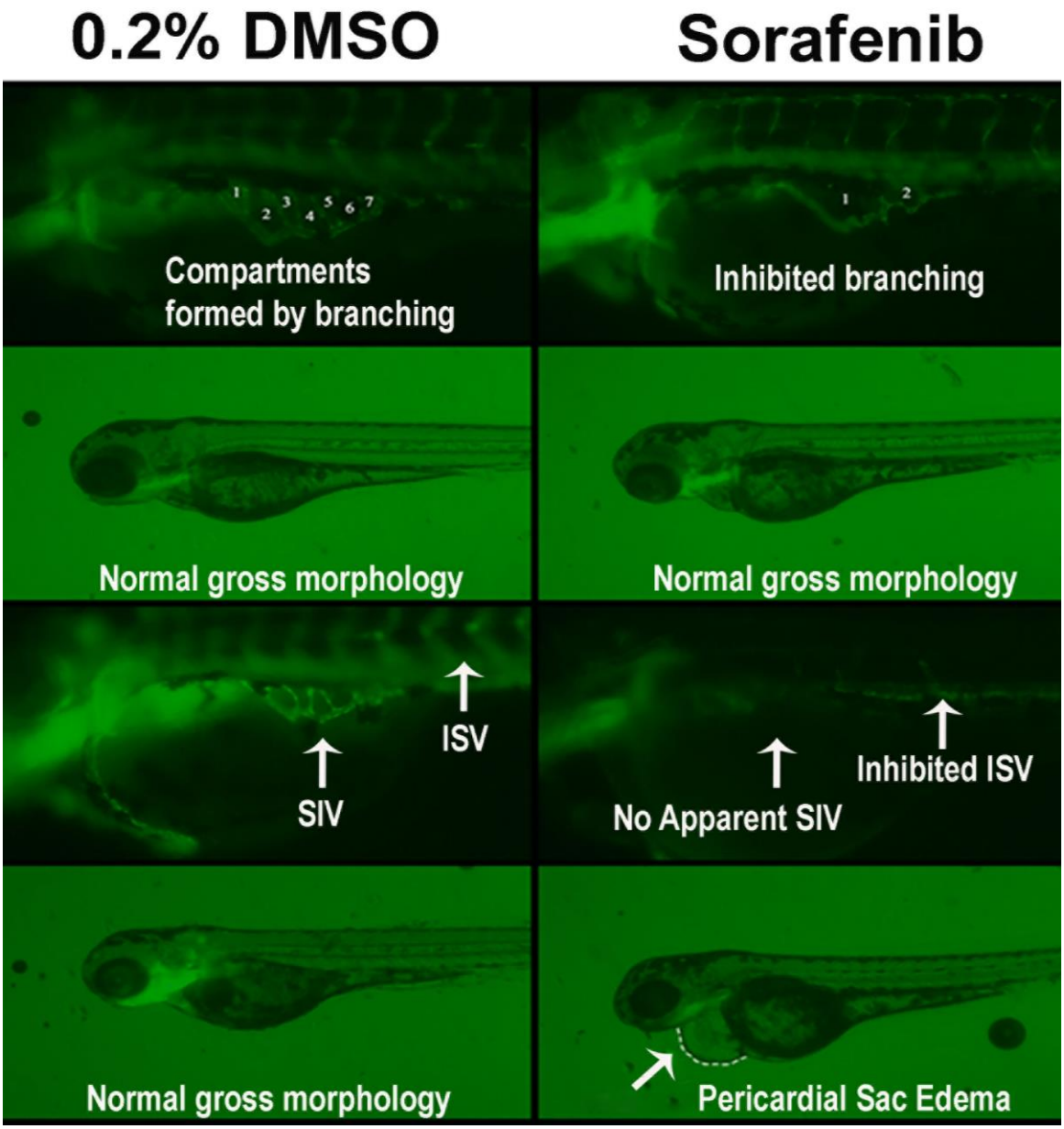

Figure 8. Zebrafish Blood Vessel Inhibition – Exposure to the potent anti-angiogenic compound sorafenib, caused severe inhibition of blood vessel development and branching. Numbers refer to the compartments formed by sub-intestinal interconnecting vessels or branching. Vehicle control organisms demonstrate normal subintestinal vessel (SIV) development as well as intersegmental vessels (ISV). Sorafenib treated larvae demonstrated inhibited branching, SIV, and ISV formation.

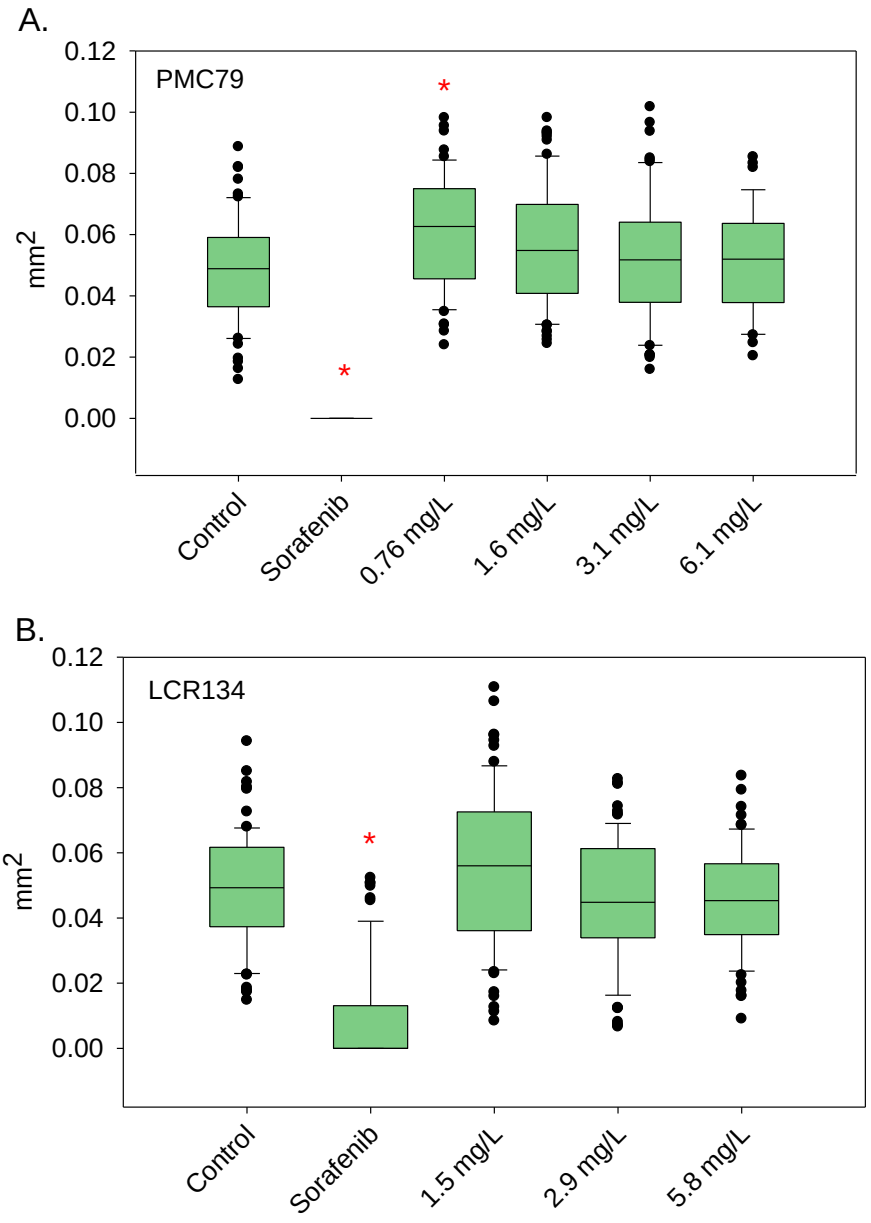

Figure 9. Basket Area Assessment – Live animal fluorescent imaging was conducted at 72 hpf. Graphs represent the average area of the sub-intestinal basket after exposure to either PMC79 (A) or LCR134 (B) of three experimental replicates. T-tests were conducted between Sorafenib and the control and Kruskal-Wallis Anova on Ranks with Dunn's post hoc was used to determine a significant effect of metallodrugs. * indicates a significant difference analyses ($p \leq 0.05$). Measurements were taken using ImageJ software. N = 39-80.

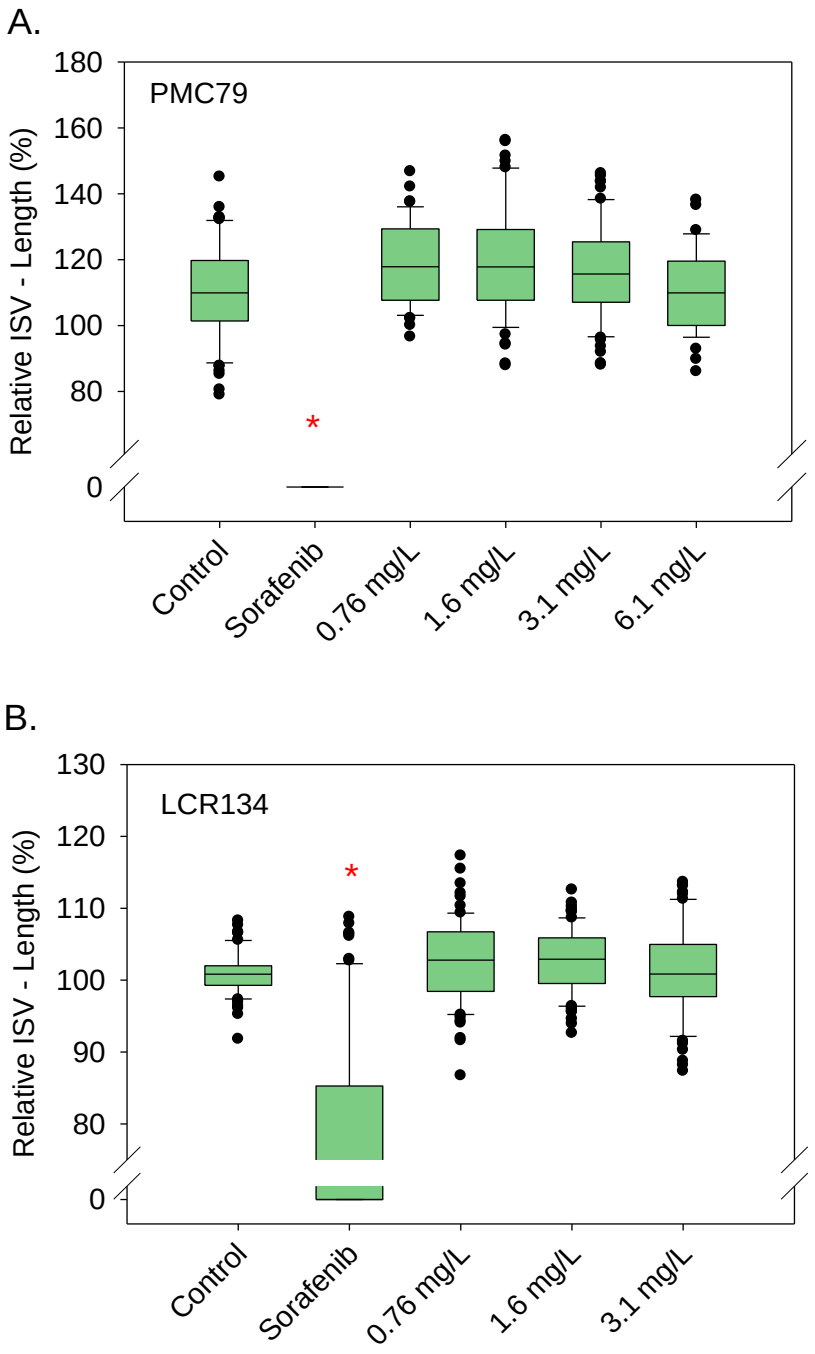

Figure 10. Intersegmental Vessel Assessment – Live animal fluorescent imaging was conducted at 72 hpf. Graphs represent the average length of 6 blood vessels per fish within the trunk after exposure to either PMC79 (A) or LCR134 (B) of three experimental replicates. T-tests were conducted between Sorafenib and the control and One Way Analysis or Kruskal-Wallis Anova on Ranks were used to determine a significant inhibitory effect of metallodrugs. * indicates a significant difference analyses ($p \leq 0.05$). Measurements were taken using ImageJ software. N = 39-80.

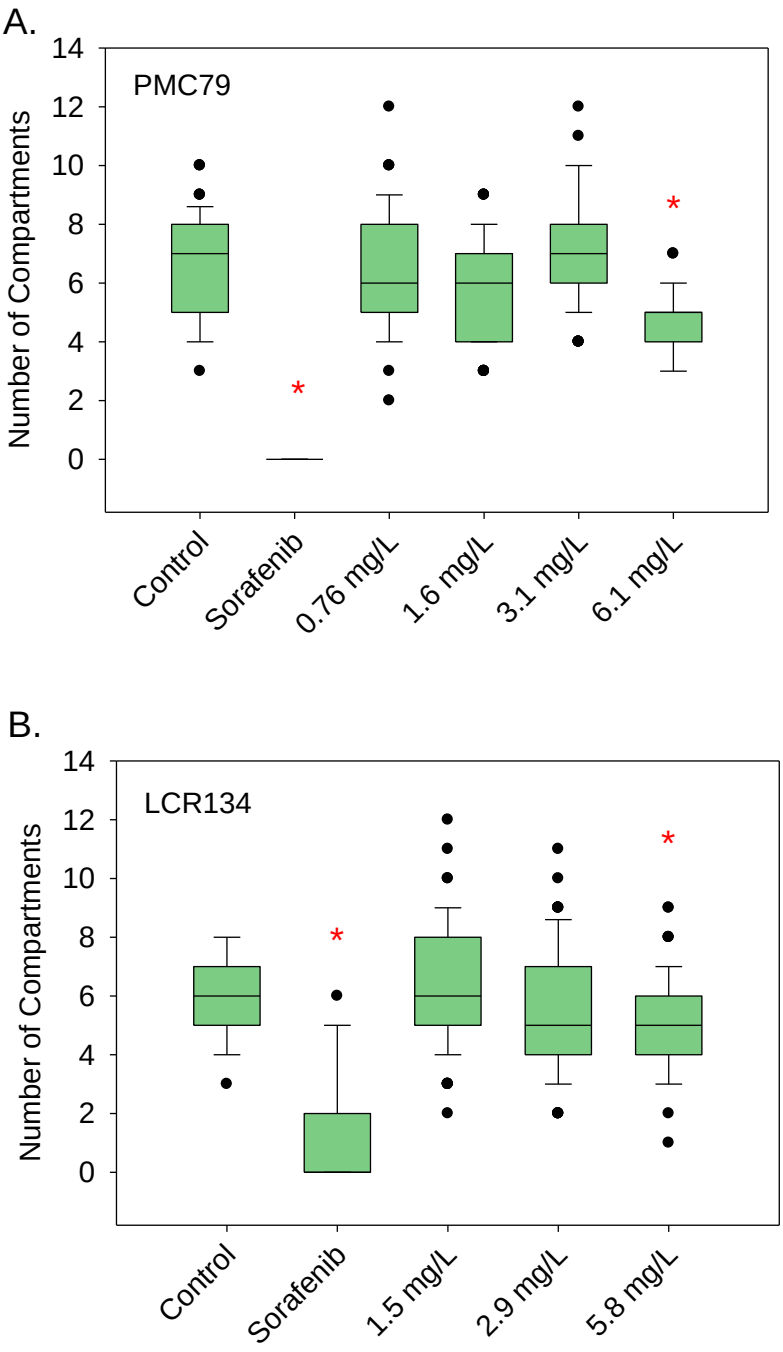

Figure 11. Basket Branching – Live animal fluorescent imaging was conducted at 72 hpf. Graphs represent the average total number of compartments formed by sub-intestinal basket branching after exposure to either PMC79 (A) or LCR134 (B) of three experimental replicates. The highest dose of PMC79 showed a 57% reduction in the average number of compartments. Kruskal-Wallis One Way Analysis of Variance on Ranks with Dunn's post hoc was used to determine significance; * indicates $P < 0.05$. Counts were taken using ImageJ software. N = 39-80.

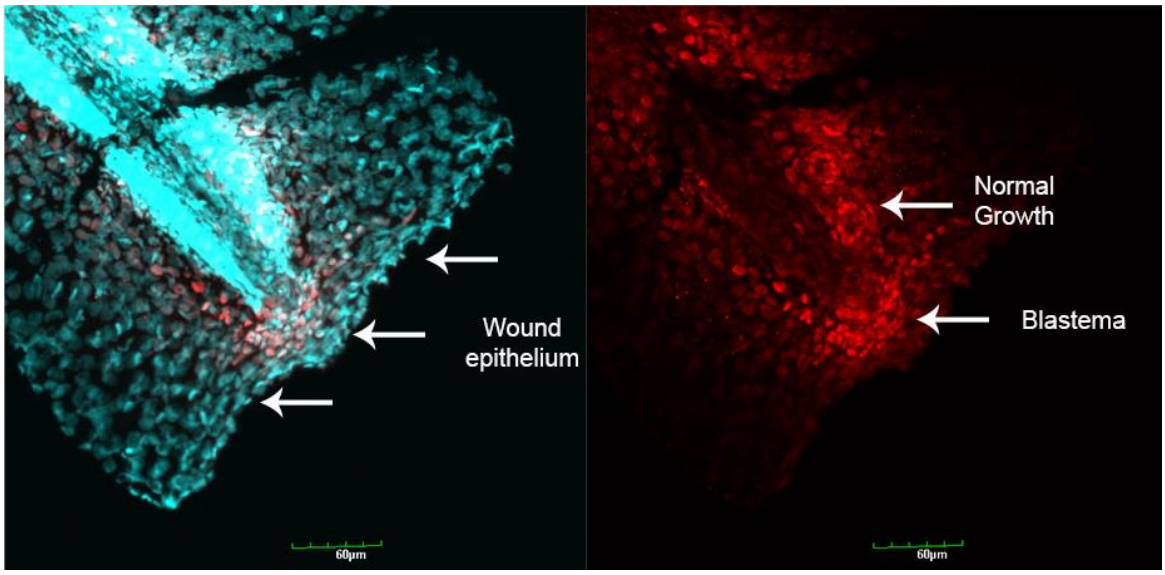

Figure 12. Tail Fin Wound Repair – During wound repair tail fins begin to heal by forming a wound epithelium, depicted here as a dense area of cells along the point of amputation (left image). Normal proliferative growth at the ventral posterior region occurs simultaneously as a blastema, or mass of proliferating mesenchymal cells, forms for regeneration. DAPI a cellular marker is stained as cyan and proliferating cell nuclear antigen (PCNA) a marker for proliferation is stained red; green rulers in each image designate a length of 60 µm.

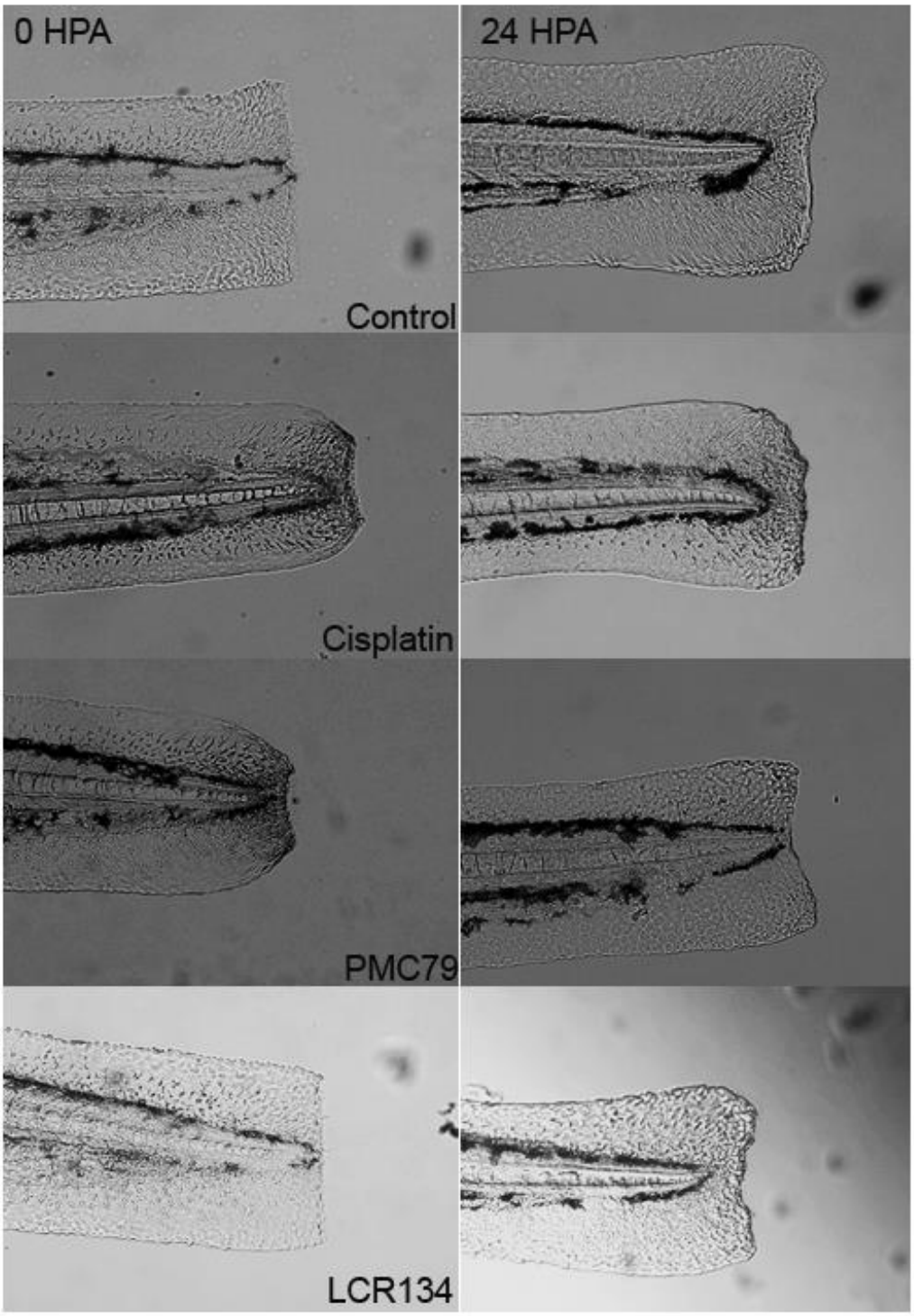

Figure 13. Tail Fin Regeneration – Live animal imaging was conducted immediately following fin amputation and after allowing 24 hours of regeneration (hours post amputation HPA) in selected media: vehicle control, 30 mg/L cisplatin, 3.1 mg/L PMC79, and 5.8 mg/L LCR134.

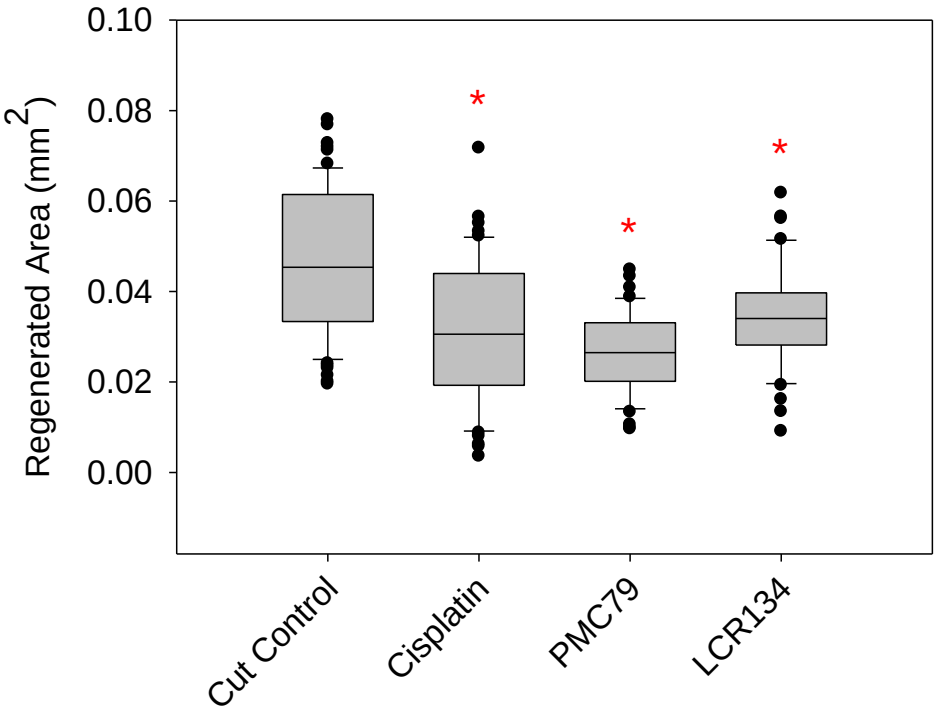

Figure 14. Area of Tail Fin Regeneration Analysis – Live animal fluorescent imaging was conducted after 24 hours of regeneration in selected media: vehicle control, 30 mg/L cisplatin, 3.1 mg/L PMC79, and 5.8 mg/L LCR134. The graph depicts the average area of regeneration for three experimental replicates. Kruskal-Wallis Anova on Ranks was used to determine a significant inhibitory effect of metallodrugs. * indicates a significant difference analyses with post hoc Dunn's method ($p \leq 0.05$). Measurements were taken using ImageJ software. N = 26-44.

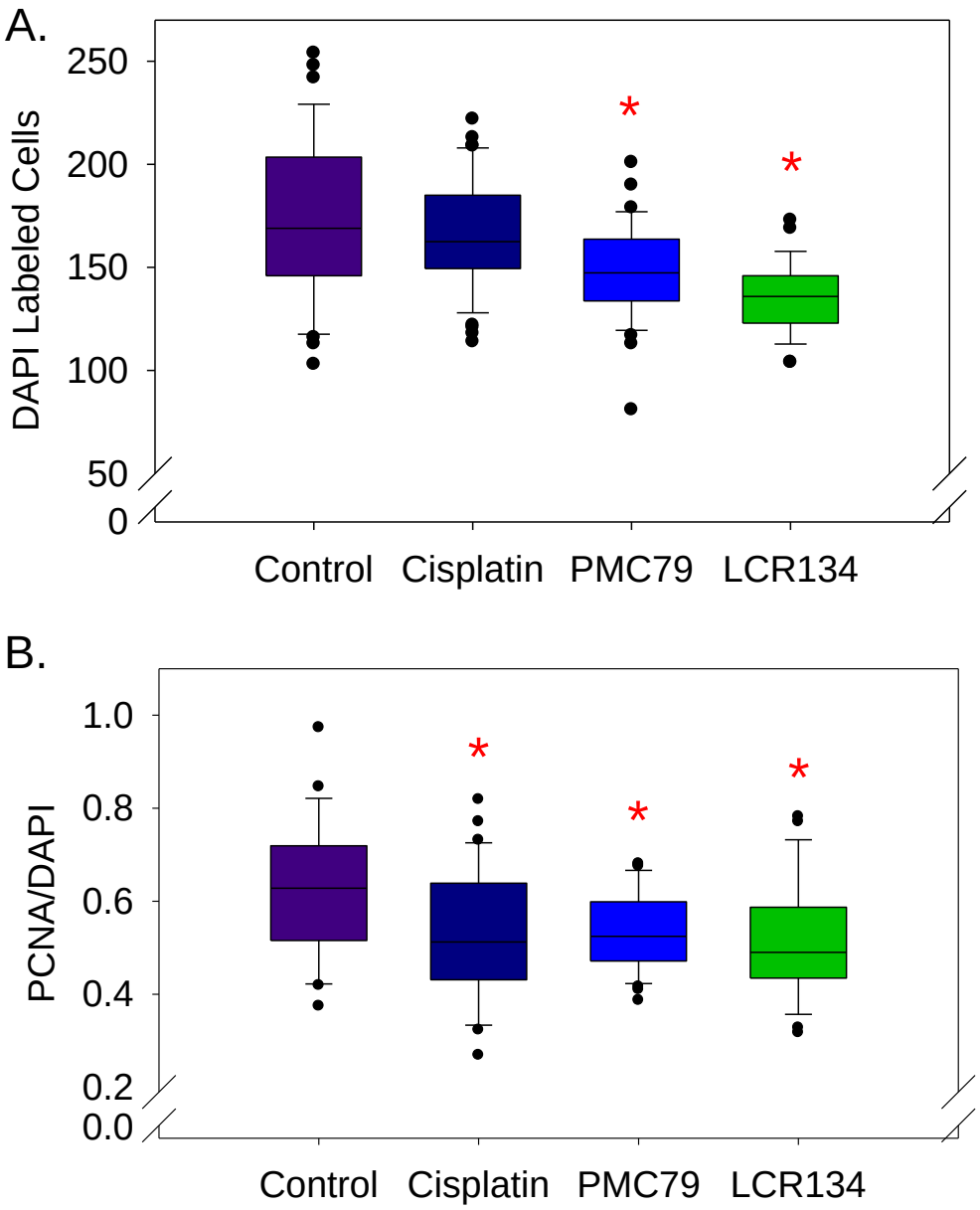

Figure 15. Immunofluorescent Labeling Analysis – Whole mount fluorescent imaging was conducted after 24 hours of regeneration in selected media: vehicle control, 30 mg/L cisplatin, 3.1 mg/L PMC79, and 5.8 mg/L LCR134. (A) DAPI stained cells, (B) proliferating cell nuclear antigen (PCNA) stained cells and (C) the relative number of PCNA to DAPI labeled cells. Kruskal-Wallis Anova on Ranks was used to determine a significant effect of metallodrugs. * indicates a significant difference analyses with post hoc Dunn's method ($p \leq 0.05$). Counts were conducted using ImageJ software. Three experimental replicates; N = 41-66.

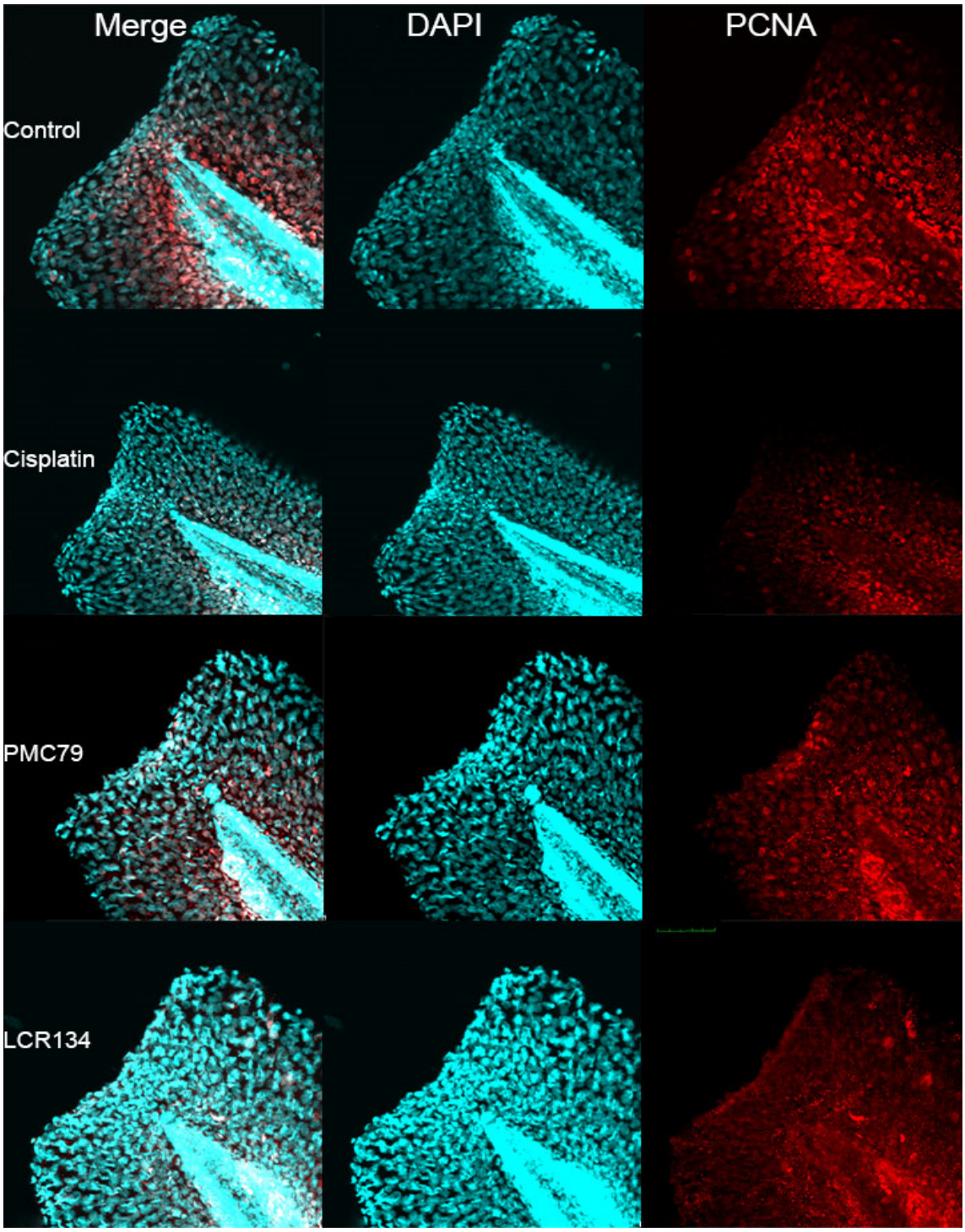

Figure 16. Immunofluorescent Labeling – Whole mount fluorescent imaging was conducted after 24 hours of regeneration in selected media: vehicle control, 30 mg/L cisplatin, 3.1 mg/L PMC79, and 5.8 mg/L LCR134. The first column depicts a merged image of proliferating cell nuclear antigen (PCNA) and DAPI, while the second two columns depict DAPI and PCNA, respectively. The green ruler in the bottom right image is set at 60 µm.

CHAPTER 4. *IN VIVO* RECAPITULATION OF METALLODRUG MECHANISTIC ACTIVITY IN THE ZEBRAFISH MODEL

4.1 BACKGROUND

The intricacies of mechanistic impact on whole organisms cannot be solely evaluated in *in vitro* models. However, *in vivo* adverse pathway analysis is often limited by time and financial commitments which may not provide conclusive information. Anti-cancer metallodrugs are being developed at an increasing rate which drives a need for a higher through-put toxicological assessment to keep pace. The zebrafish model has become a powerful platform for screening large numbers of novel compounds and may be in a unique position to provide a robust evaluation of *in vitro* endpoints. Zebrafish show great promise as an asset to pharmacology and toxicology. This model allows for examining adverse outcome pathways from biochemical to whole organism endpoints, in which cell culture lacks the complexity and testing in a rodent model are cost-limiting. Large screening for drug activity and toxicity have already been conducted in zebrafish and have successfully identified compounds tested in clinical trials (Leonard & Randall, 2005; Santoriello & Zon, 2012; Tan & Zon, 2011). In this study, we used the zebrafish model to evaluate novel ruthenium-based metallodrugs in comparison to cisplatin, a widely used metal-based chemotherapeutic. Our treatments included two Ru-cyclopentadienyl (CP) − (η^5-C_5H_5) structures as potential anticancer agents: PMC79, the CP parental compound, and LCR134, a CP derivative conjugated with poly(lactic acid) (PLA) and biotin; [Ru(η^5-C_5H_5)(PPh_3)(2,2 bipy-4,4-CH_2OH)] and [Ru(η^5-C_5H_5)(PPh_3)(2,2 bipy-4,4-dibiotin ester)], respectively (Corte-Real et al., 2019; Karas et al., 2019). Both compounds

exhibited promising anti-proliferative capabilities in several human cancer derived cell lines, with PMC79 demonstrating a low IC_{50} with ovarian A2780cis, a cisplatin resistant cancer cell line (Corte-Real et al., 2019; Moreira et al., 2019).

PMC79 has been shown to accumulate in the membrane fraction and cause disorganization of the cytoskeleton, specifically by depolymerization of F-actin. Although, cytoskeletal inhibitors like the taxanes, have been investigated as chemotherapeutics, anti-actin compounds have been limited by their inability to differentiate between healthy and cancerous cell and therefore cause broad spectrum toxicity (Bonello et al., 2009; Stehn et al., 2013). As such, compounds with anti-proliferative properties *in vitro* like cytochalasins have not successfully passed clinical trials, but are being investigated in more targeted approaches (Trendowski, 2015). Because PMC79 has been designed to exploit enhanced permeation and retention (EPR), it may provide a more targeted therapy and warrants further investigation *in vivo*.

LCR134 also accumulates in the cell membrane, but its cellular interactions are very distinct. Whereas PMC79 was shown to be transported by P-glycoprotein efflux transporter (P-gp pump), LCR134 caused an inhibition of P-gp pump specific activity in NIH3T3 cells overexpressing this transporter. This *in vitro* endpoint has implications in chemotherapeutic treatment, as this transporter is one of the most prominent causes of multidrug resistance (Pluchino et al., 2012; Shaffer et al., 2012). As such, this promising property must be evaluated in the context of a living organism.

In addition, we were able to observe effects *in vivo* caused by the well-characterized mechanism and toxicity of cisplatin. Previously, we had reported a delayed hatching phenomenon not observed in the Ru metallodrugs and observed by other researchers (Kovacs et al., 2016). This was hypothesized to be due to cross-linking between proteins in the chorion causing resistance to enzyme degradation, which was further investigated by pronase exposure and analysis of zebrafish hatching enzyme transcript levels. Lastly, a dual cartilage and bone stain revealed lesions within the ototic capsule supported by previous work by Ou et al. (2007) who reported ocular hair cell damage in zebrafish due to cisplatin exposure. In these studies, we have found that the zebrafish model is adequate to evaluate both novel and well-established mechanisms of metallodrugs.

4.2 MATERIALS AND METHODS

Zebrafish Husbandry

The AB or the eGFP vascularly labeled transgenic Tg(fli1:EGFP)y^1 strain zebrafish (Zebrafish International Resource Center, Eugene, OR) was used for all experiments. Breeding stocks were bred and housed in Aquatic Habitats (Apopka, FL) recirculating systems under a 14/10 h light/dark cycle. System water was obtained by carbon/sand filtration of municipal tap water and water quality was maintained at <0.05 ppm nitrite, <0.2 ppm ammonia, pH between 7.2 and 7.7, and water temperature between 26 and 28 ºC. All experiments were conducted in accordance with the zebrafish husbandry protocol and embryonic exposure protocol (#08-025) approved by the Rutgers University Animal Care and Facilities

Committee. Males and females were maintained separately and co-mingled the night before to allow spawning the next morning. Spawning substrates were placed into the fish tanks on the day prior to spawning. In case eggs were obtained from more than one set of breeders all eggs that were fertilized and progressing normally through development were mixed. Embryos were collected within 1 hour after fertilization, washed with egg water (60 µg/ml Instant Ocean in DI water), and cleaned thoroughly.

SDS PAGE

Group-housed zebrafish embryos were exposed to 30 and 60 mg/L cisplatin at 0.05% of DMSO in glass dishes through a waterborne exposure at 3 hours post fertilization in a static non-renewal solution. The concentration was chosen based on previous work establishing this dose as having the most counts of delayed hatching with the lowest lethality within 22 hrs (Karas et al., 2019). At 22 hpf, prior to the release of hatching enzyme , embryos were manually dechorionated (Sano et al., 2008). Chorions were centrifuged at 12,000G for 5 mins to form a pellet, and supernatant was removed. Chorions per dose were either non-pronase treated, pronase treated, or pronase treated and rinsed with DI water. Pronase concentrations for treatments were 2 mg/ml, for 5 mins, and re-centrifuged. All solution was removed; wash steps to remove excess pronase (if conducted) included three cycles of DI water and re-centrifugation. Pronase solution as a mixture of several nonspecific endo- and exo-proteases was purchased from Millipore Sigma, St. Louis, MO.

Samples were then incubated in Lammeli sample buffer (Bio-Rad), at 60C for 15 mins and were then run on NuPage 4-12% bis-tris gel (Thermofischer) at 120V for approximately 1 hour. Each treatment group consisted of a composite sample of 15 chorions. The controls had >90 % survival rate. Three experiment replicates were conducted.

Reverse-transcriptase (RT) quantitative PCR

Group-housed zebrafish embryos were exposed to either egg water, 7.5mg/L or 15mg/L cisplatin in order to evaluate the transcript levels of *zebrafish hatching enzyme 1* (*zhe1*). Transcript levels of *multi-drug resistance 1* (*mdr1*) and *b-actin* were evaluated after exposure to either egg water with DMSO vehicle or doses of PMC79 or LCR134 at or below the LOAEL as established previously (Corte-Real et al., 2019; Karas et al., 2019). PMC79 and LCR134 treatments contained at or below 0.05% of DMSO. The treatments were conducted in 20 ml glass vials through a waterborne exposure beginning at 3 hours post fertilization (hpf) static non-renewal solution. At 24 hpf, samples were rinsed 3xs with DI water and snap frozen in liquid nitrogen. Total RNA was isolated from 50 embryo composite samples using RNAzol (Sigma-Aldrich). Reverse transcription was performed on 1 ug aliquots of RNA to produce cDNA for RT-PCR using a High-Capacity cDNA Reverse Transcription Kit (Thermofischer) using a PTC-200 Peltier Thermal Cycler. RT-PCR reactions were performed in triplicate using PowerUp SYBR Green Master Mix (ThermoFischer) and cDNA amplification was performed for 40 cycles on a QuantStudio 3 (Applied Biosystems) and recorded with QuantStudio

Design and Analysis Software and analyzed in Thermocloud (ThermoFischer). Analysis was conducted as ΔΔCT using 28S as an endogenous control.

Table 1. Forward and Reverse Primer Sequences used for RNA Transcription Analysis

Primer	Forward Sequence	Reverse Sequence	Citation
28s	CCTCACGATCCTTCTGGCTT	AATTCTGCTTCACAATGATA	(Hillegass et al., 2007)
b-actin	CGAGCAGGAGATGGGAACC	CAACGGAAACGCTCATTGC	(Hillegass et al., 2008)
mdr1	TTGGTCAACGCCGCTATCTT	TTCGGTGTAACAGTGTGCAATG	Primer Express 3.0, (Applied Biosystems)
zhe1	GCCCGGTCTGGAAACCA	GTCCGATCTGCACGTTTTCA	Primer Express 3.0, (Applied Biosystems)

Cytoskeletal Evaluation

Group-housed Tg(fli1:EGFP)y^1 strain zebrafish embryos were collected and treated at 3 hpf with egg water with DMSO vehicle, 1 ug/ml Cytochalasin D (Millipore, St. Louis, MO) or doses of PMC79 at or below LOAEL, as established previously, for 24 hours (Corte-Real et al., 2019; Karas et al., 2019). At 24 hours post exposure, larvae were manually dechorionated and fixed in 4% PFA for 2-4 hours at room temperature (RT). Samples were then PBST rinsed (2xs for 5 mins with Phosphate Buffered Saline + 0.1% Tween-20 [PBST]) and permeabilized for 2 hours in PBS + 2% Triton X100. After permeabilization, samples were PBST rinsed and subsequently stained at 250nM of Acti- stain 555 phalloidin

(Cytoskeleton, Inc., Denver, CO) for 1 hour at RT protected from light. Samples were then destained overnight and stored in Vectashield Antifade Mounting Medium with DAPI (Vector Laboratories, Burlingame, CA) until fluorescent confocal imaging. Z- stack images were taken on an Olympus FV1000MPE microscope (Olympus XLPlan N 25x objective NA 1.05) in 3 µm step size. Z-stacks were compressed and ImageJ was used to evaluate cytoskeletal disruption. Ten somites were evaluated for fluorescent intensity and filament fragmentation anterior to the tapered end of the yolk sac. Additionally, the first somite anterior and distal to the tapered yolk was used to count the number of filaments. During analysis, larvae without filaments were not considered outliers. Filament fragmentation and filaments per somite counts were conducted blind.

P-gp Pump Assay

At 48 hpf, AB strain zebrafish embryos were dechorionated and treated with egg water with DMSO vehicle, 10 µM cyclosporine (CSA) (Millipore, St. Louis, MO), or at or below the LOAEL for LCR134. All treatments contained at or below 0.05% of DMSO and 8 µM rhodamine (RH) 123 (Millipore, St. Louis, MO). Treatments were conducted in group housing with a maximum of 12 larvae; an N=4 per dose. Free swimming larvae were rocked in the dark at RT for 2 hrs. Larvae were then rinsed in ice cold DI water, moved into fresh vials and rinsed again 3xs. After the final rinse larvae were transferred into microcentrifuge tubes, mechanically homogenized for 1 min and sonicated for 5 mins. After sonication, samples were centrifuged with a quick spin, and aliquoted onto a black, clear bottom 96 well

plate. The plate was read on a Varioskan LUX Fluorometer. The optics were directed from the bottom at excitation: 505nm; emission: 530nm with a bandwidth of 5 nm. Measurements were collected on SkanIt RE 6.0.2 software and were averaged as measurements from 29 points per well. Concentrations were calculated from a 10-point standard curve of Rh123 dissolved in egg water. Images were taken immediately after treatment and rinsing. Larvae were anesthetized in 0.01% MS-222 and imaged on a Zeiss Axio Observer 1 microscope with a X-Cite XFO 120 Light Source, Liquid Light Guide and Microscope Adapter and images were collected using ZEN 2 (Blue Edition) software. Experiments were carried out in triplicate.

Alcian Blue/Alizarin Red Staining

Cisplatin treated larvae were dechorionated and stained for bone and cartilage following a two-color acid free Alcian Blue/Alizarin red stain (Walker & Kimmel, 2007). Photographs were taken using a Scion digital camera model CFW-1310C mounted on an Olympus SZ-PT dissecting microscope and cartilage/bone were measured using Adobe Photoshop.

4.3 RESULTS

Cisplatin

SDS PAGE and gene expression analysis were co-conducted in order to further investigate the mode of action for cisplatin-induced delayed hatching (**Figure 1**). Embryos were treated with egg water, 30 mg/L, or 60 mg/L doses of cisplatin. Cisplatin doses were chosen for maximum delayed hatching with minimum lethality

for an exposure from 3 to 22 hpf and embryos were manually dechorionated. Within the control groups (Lanes 2-4; **Figure 2**), pronase treated samples degraded larger proteins, which is evident by the attenuation of high molecular weight bands in lanes 3 and 4 with a complementary increase in the appearance and size of lower molecular weight bands. Cisplatin treated groups without the addition of pronase (Lanes 5 and 8) were extremely resistant to degradation even after incubation in laemmli denaturing agent as designated by white arrows; although some low molecular weight bands are apparent indicating minor degradation. Cisplatin treated chorions with subsequent pronase treatment were successfully degraded (Lanes 6, 7, 9 and 10) as evidenced by a lack of protein within the wells, and low molecular weight bands.

RNA transcript levels of zebrafish hatching enzyme 1 (*zhe1*) were assayed after manual dechorionation. Doses were lowered to 7.5 and 15 mg/L cisplatin in order to avoid non-lethal lesions such as decreased mobility while maintaining maximum percent of delayed hatching. No fold change was identified between control and either dose of cisplatin treated fish (**Figure 3**).

Cisplatin treated larvae were dually stained with Alcian Blue and Alizarin Red after a 5-day exposure to improve visualization and highlight insult to cartilage and bone development, respectively. In addition, approximately half of the samples were manually dechorionated (DC) at 48 hpf in order to evaluate the role of the chorion. Cisplatin treated fish, regardless of dechorionation, showed abrogration of bone development within the otic capsules located behind the eye. Additionally,

non-DC cisplatin exposed larval manifested impaired cranio-facial development (**Figure 4**).

P-gp Efflux Regulation

Adenosine triphosphate (ATP) – binding cassette B1 (ABCB1), Multidrug resistance 1 (MDR1) or P-glycoprotein (P-gp) efflux transporter is named for its ability to remove drugs from sites of action resulting in low efficacy and increased resistance. This resistance is correlated with poor patient prognosis and remains a limitation for chemotherapeutic treatment (Chung et al., 2016). As such, strategies to overcome P-gp mediated resistance have become a target of drug development. Zebrafish were found to express a gene orthologous to *ABCB1* called *abcb4* that form a protein with similar structure, function and pharmacological response (Cunha et al., 2017; Fischer et al., 2013; Zhu et al., 2019). These similarities have resulted in the successful use of the zebrafish model in evaluating P-gp protein activity. Specifically, the inhibition of this pump in zebrafish could have translational relevance result for overcoming chemotherapeutic resistance.

P-gp pump inhibition in the whole zebrafish was evaluated by the retention of the fluorescent substrate Rhodamine 123 (Rh123). Cyclosporine A treated larvae retained approximately twice the amount of Rh123 as control larvae (0.045 ± 0.012 and 0.026 ± 0.016 picomol/larvae), whereas two LOAEL treatments of LCR134 contained 7 and 44xs higher Rh123 compared to control: 0.181 ± 0.116 and 1.125 ± 0.420 picomol/larvae, respectively (**Figure 5 and 6**).

The mRNA levels of the P-gp gene (*mdr1*) was analyzed in zebrafish treated with LCR134. Relative expression of this gene was unchanged after 24 hours of exposure (**Figure 7**).

Cytoskeletal Evaluation

Cytoskeletal disruption by PMC79 was evaluated by fluorescent intensity, filament fragment number, and filament number within the area of a somite (**Figure 8**). The ten somites adjacent to the yolk extension were chosen in order to observe impacts on gradation of maturity due to anteroposterior development (Kimmel et al., 1995). A visual comparison of the level of disorganization caused by treatments can be seen in **Figure 9**. Results indicated that 3.1 mg/L and 6.2 mg/L of PMC79 showed significant and proportional reduction in fluorescent intensity as the positive control, Cytochalasin D (**Figure 10**). This is in agreement with the number of filaments per somite area in which PMC79 (6.1 mg/L) and Cytochalasin D exposure caused a significant reduction in filament density. However, Cytochalsin D exposure clearly caused a greater decrease compared with the negative control as opposed to the PMC79 at 6.1 mg/L (median values: 17, 2, and 14 filaments per 10^4 µm somite area; vehicle control, Cytochalasin D, and 6.1 mg/L PMC79, respectively) **Figure 10**.

The number of fragments within the ten somites anterior to the tapering of the yolk sac were evaluated. Results demonstrated that Cytochalasin D had approximately twice the occurrence of fragments compared with the negative control (medians: 25 and 13 fragments per 10^4 µm somite area). Both doses of

PMC79 showed a decrease in the number of fragments within this area compared to the negative control, although these data were not significant (median values: 13, 9, and 7, vehicle control, 3.1 and 6.2 mg/L PMC79, respectively) **Figure 10.**

The mRNA levels of *beta-actin* were analyzed in zebrafish treated with 1.6 and 3.1 mg/L PMC79. Relative expression of this gene was significantly reduced after 24 hours of exposure to both doses of the PMC79 metallodrug (**Figure 11**).

4.4 DISCUSSION

Cisplatin

The mechanism of cisplatin-induced apoptosis and anti-cancer has been well characterized as alkylating activity (Eljack et al., 2014). In addition to the mechanism, off target effects have also been investigated and include dose limiting side effects such as ototoxicity (de Jongh et al., 2003). In order to establish the zebrafish model for the study of anti-cancer metallodrugs, we demonstrated that evidence of these hallmarks can be established across vertebrates. The alkylating activity of cisplatin is not specific to DNA, and has been shown to cause protein adducts. We had hypothesized that cisplatin protein cross-linking within the chorion was causing a delayed hatching phenomenon, supported by our previous studies which demonstrate significant platinum accumulation in the chorion (Karas et al., 2019). Here we demonstrated that extracted chorions exposed to cisplatin are resistant to denaturing caused by heating and di-sulfide bond breakage. Only after exposure to a mixture of nonspecific endo-and exo-proteases were the chorions able to be digested (**Figure 2**). Furthermore, cisplatin impacts to the

transcript levels of *zebrafish hatching enzyme 1* (*zhe1*) were also investigated and showed no significant difference between mRNA levels of control fish and fish treated with two concentrations of cisplatin with confirmed delayed hatching (**Figure 3**) (Sano et al., 2008). As such, cisplatin may be causing a reinforcement effect of the chorion and/or binding to zhe1 rendering it ineffective. The mechanistic activity of cisplatin in zebrafish had been demonstrated, however, it is not at the molecule of interest for anti-cancer studies. Further studies should be conducted only after dechorionation in order to limit dose impediment by off-target adducting.

Alizarian Red staining used to locate calcium deposits and therefore bone, was used for both dechorionated and nondechorionated fish treated with cisplatin. Both treatment groups demonstrated complete loss of the otoliths as well as areas of bone formation involving the gills: the opercle, ceratobranchial, and cleithrum (**Figure 4**) **(**Strecker et al., 2013**)** . The molecular mechanisms of cisplatin-induced ototoxicity include the generation of reactive oxygen species that results in damage to various cell types associated with the ear. Specifically, the structures of the inner ear, contained in the cochlea, are most susceptible due to their high metabolic activity (Sheth et al., 2017). Additionally, cisplatin has limited clinical use due to bone marrow suppression and subsequent abnormal hematopoiesis (Park et al., 2017). These studies demonstrate that not only was recapitulation of mechanistic activity supported in zebrafish, but a highly relevant off-target toxicities were identified.

PMC79 and LCR134

LCR134 demonstrated an ability to inhibit the multidrug resistant P-gp transporter *in vitro* which was successfully recapitulated in the zebrafish model. Larvae treated with LCR134 showed a dose dependent increase in the amount of accumulated P-gp substrate, Rh123, during a 2-hour exposure both quantitatively and qualitatively (**Figure 5 and 6**). Unexpectedly, LCR134 showed a marked increase in accumulation compared to cyclosporine A, even at levels below the 120 hour LOAEL exposure dose established in zebrafish larvae. Additionally, *mdr1* RNA transcript levels of embryos exposed for 24 hrs were unaffected, further supporting a form of protein inhibition. The potency at which LCR134 inhibits P-gp transporters may suggest the clinical efficacy at very low doses, potentially limiting off-target effects and increasing compatibility with co-administered chemotherapeutics. In future studies, the compatibility and drug interaction of LCR134 with cisplatin and additional P-gp effluxed chemotherapeutics should be investigated.

Although PMC79 is the parental compound of LCR134, the *in vivo* activity appeared very different. Cytoskeletal impacts, i.e. the depolymerization of F-actin observed *in vitro,* were investigated in the zebrafish model. PMC79 significantly decreased the fluorescent intensity quantified within the somites of the fish in addition to increased disorganization. This was in agreement with a decrease in the number of filaments assessed per somite area (**Figure 9**). Overall, this suggests a decrease in the density of cytoskeleton within the area adjacent to the yolk extension. The number of fragments caused by disruption of cytoskeletal

development were also assessed. Significance was found between the vehicle control and cytochalasin D, which binds to the end of F-actin preventing the addition of new monomers (Cooper, 1987). However, PMC79 exposure did not cause an increase in fragment number. This may be due to a different mechanism of cytoskeletal impact in which PMC79 is depolymerizing and reducing the overall number of filaments and therefore fragmentation sites. Additionally, zebrafish RNA transcript levels of *beta-actin* were significantly reduced at both PMC79 exposure doses (**Figure 10**). Beta-actin is responsible for the maintenance of total actin and regulation of the cellular G-actin concentration (F-actin monomer), and as such may be interfering with actin formation signaling pathways (Bunnell et al., 2011).

To conclude, the mechanisms of three metallodrugs were successfully investigated and recapitulated in the context of a living organism. We found that LCR134 is a promising candidate to decrease chemotherapeutic resistance at low doses compared to a clinically relevant inhibitor (List et al., 2001). Further investigation should be conducted of alterations in cellular uptake, transport and half-lives of drugs susceptible to multi-drug resistance in the presence of LCR134.

Cytoskeleton inhibitors are a class of anti-cancer compounds, but not without inherent issues. Compound differentiation between healthy and cancerous cells continues to be a challenge, as actin cytoskeleton is essential for cell function. In these studies, previously established LOAEL doses based on morphometric evaluation were able to decrease cytoskeleton density. However, the zebrafish larvae are a particular sensitive model for cytoskeleton toxicity due to active

development. Further studies are warranted in adult organisms for off-target toxicity and specificity.

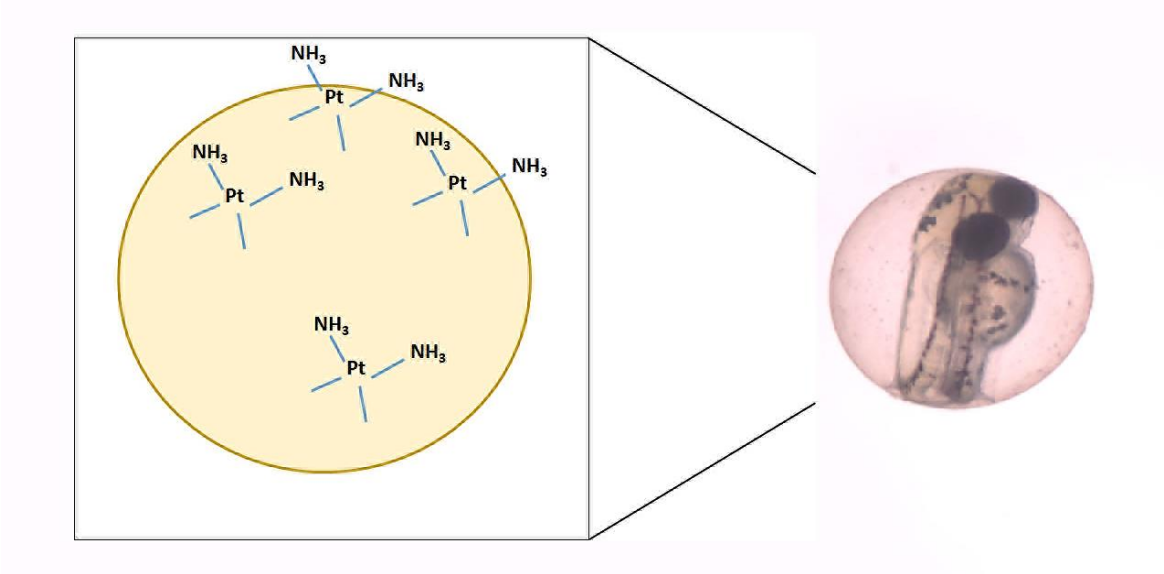

Figure 1. Cisplatin Chorionic Crosslinking – Cisplatin is an alkylating agent that has the potential to cross-link with nucleophilic molecules including the sulfur groups within proteins. Here we propose that the mode of action for delayed hatching is due to reinforcement of proteins by cisplatin crosslinking resulting in resistant degradation.

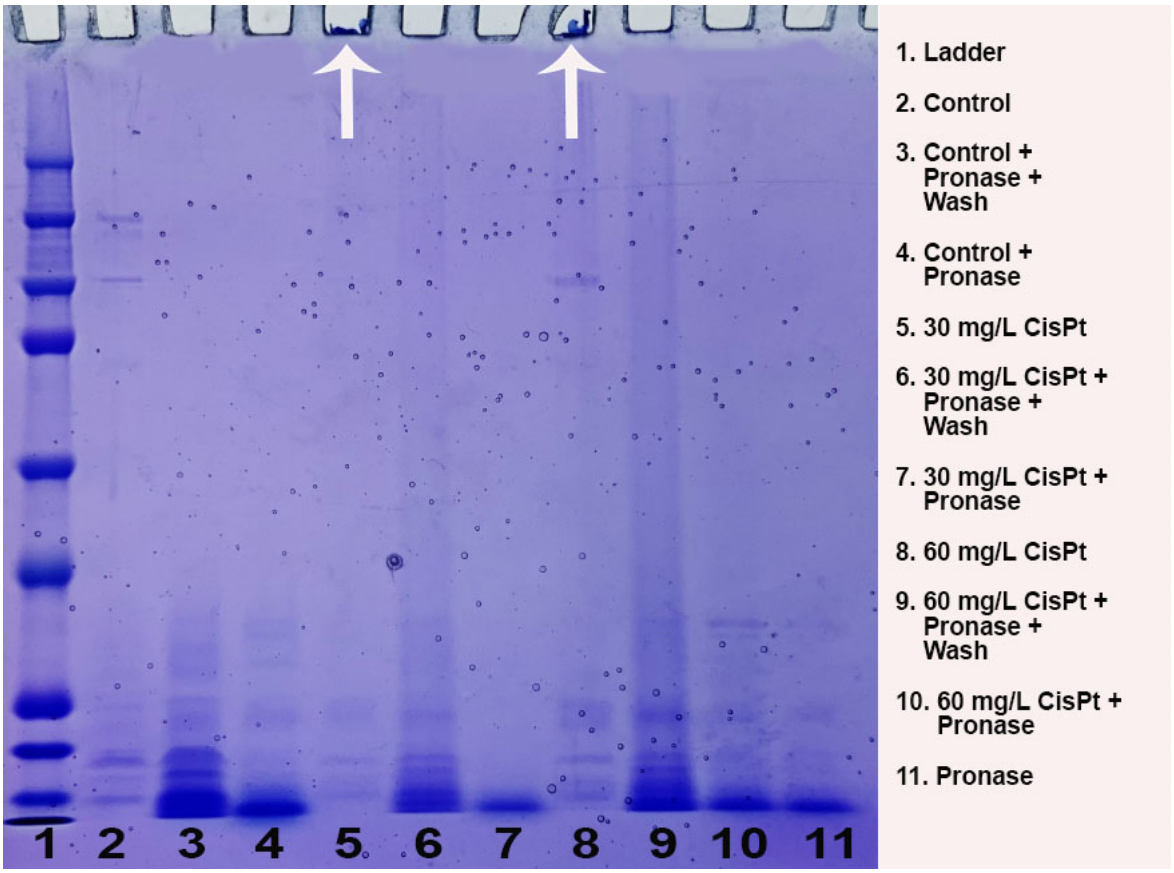

Figure 2. SDS PAGE, Cisplatin-Induced Resistant Degradation – Chorions treated with 30 or 60 mg/ml cisplatin are resistant to degradation and are too large to migrate through the SDS PAGE gel. High concentration of pronase are able to degrade cisplatin treated chorions and allow migration. 1) egg water control; 2) egg water + pronase + Rinse; 3) Egg water + Pronase; 4) 30 mg/L cisplatin; 5) 30 mg/L cisplatin + pronase + wash; 6) 30 mg/L cisplatin + pronase; 7) 60 mg/L cisplatin; 8) 60 mg/L cisplatin + pronase + wash; 9) 60 mg/L cisplatin + pronase; 10) pronase. The figure depicts cisplatin crosslinking with chorionic proteins, a potential interaction based on the well-known mechanistic activity of cisplatin.

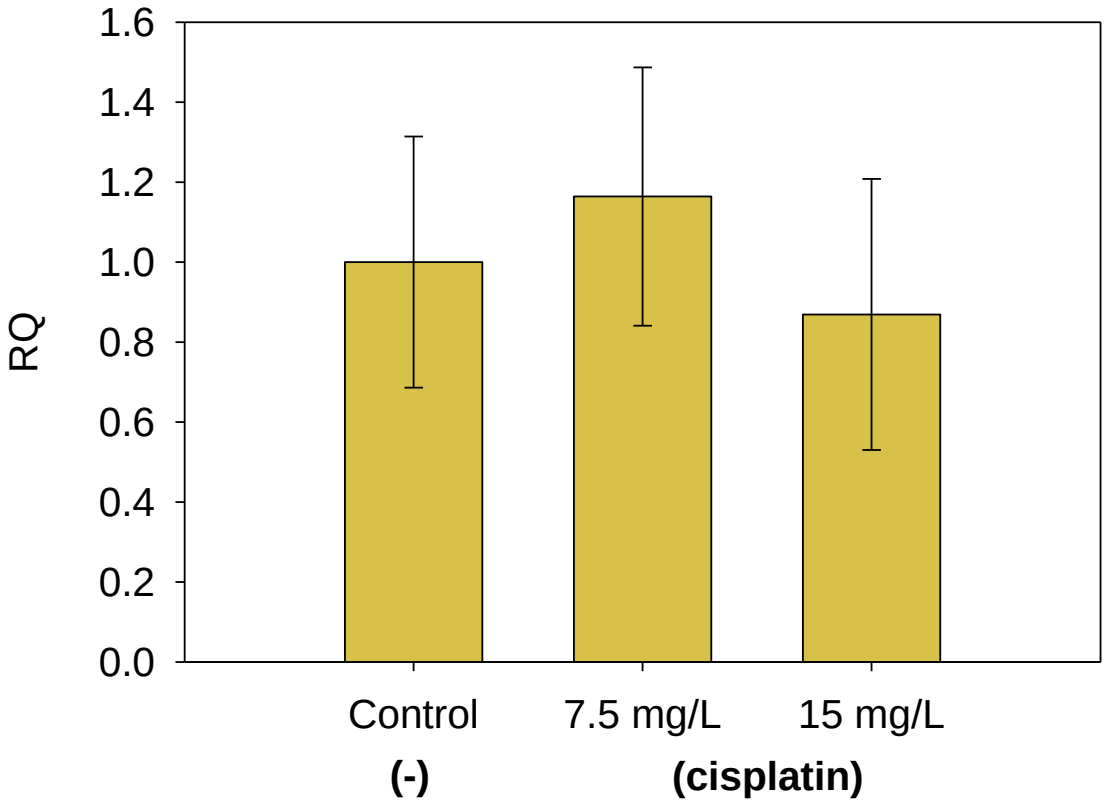

Figure 3. Gene Expression Analysis – RNA transcript levels of zebrafish hatching enzyme 1 (zhe1) were assessed after exposure to 7.5 and 15 mg/L cisplatin. Transcript levels were assayed after exposure from 3-22 hours post-fertilization (hpf). Graphs represent the mean fold change +/- the S.E.M. of three experimental replicates (N=3). No significance was identified between controls and cisplatin-treated transcript levels.

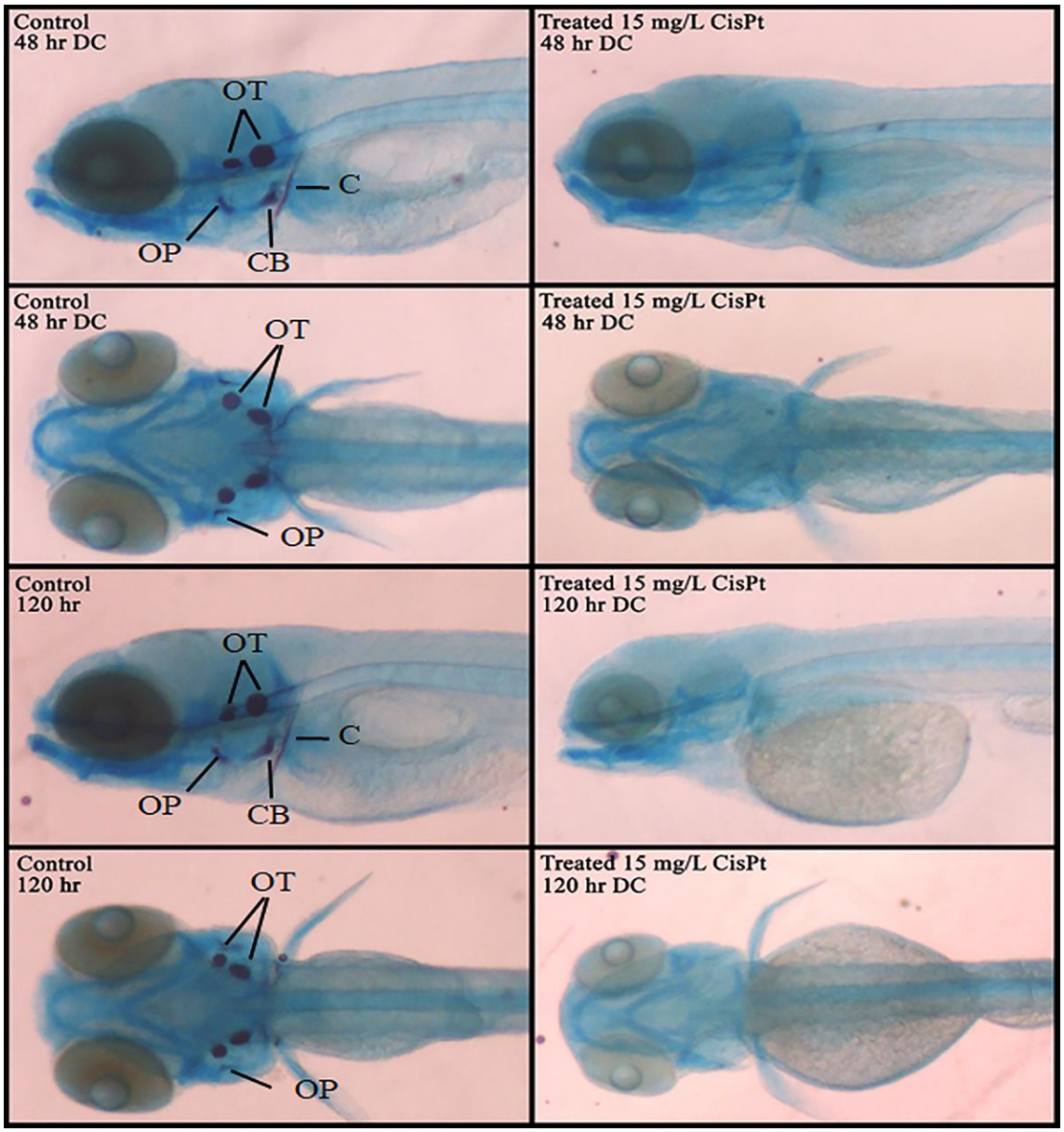

Figure 4. Cisplatin Toxicity – The zebrafish larvae in this image were fixed and stained with a dual cartilage and bone stain (Alcian Blue/Alizarian Red). The control fish (left panel) and the cisplatin treated fish (right panel) were either dechorionated at 48 hpf (48 hr DC) or dechorionated at 120 hpf (120 hr DC), necessary after cisplatin treatment. Both cisplatin treatments demonstrate a loss of calcium staining indicative of bone formation. OT- otoliths, OP – opercle, CB – ceratobranchial, and C – cleithrum.

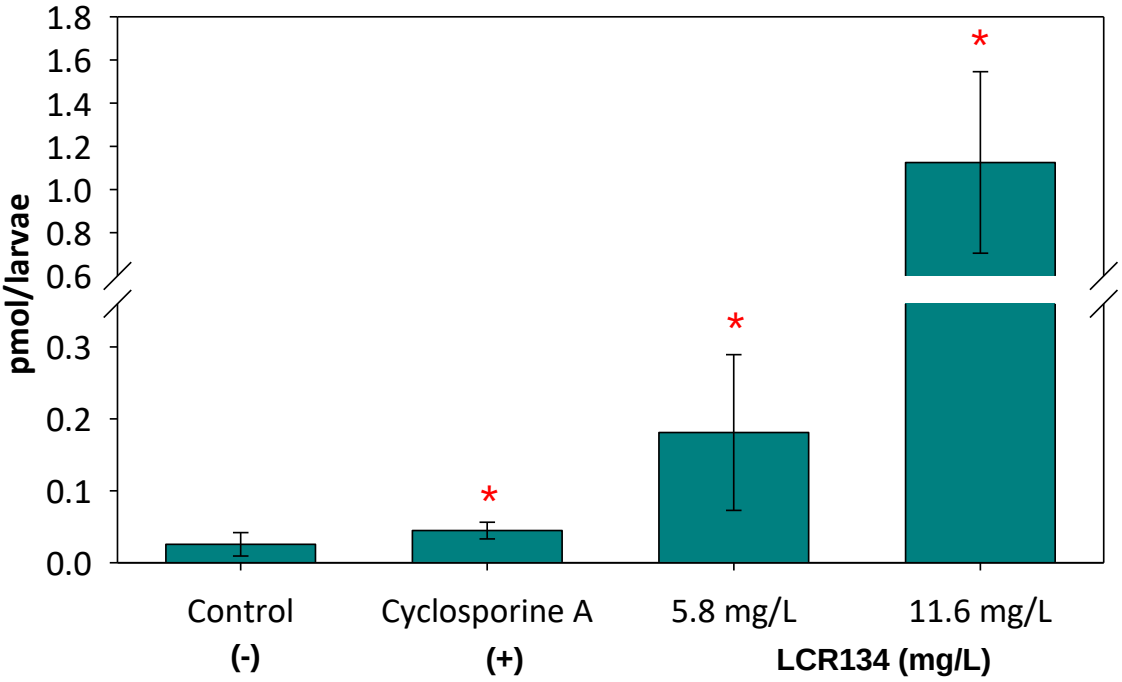

Figure 5. P-pg Inhibition – Free-swimming larvae at 48 hours post-fertilization (hpf) were co-incubated with Rhodamine 123 (Rh123), a fluorescent P-pg substrate and vehicle control (-), 10 µM cyclosporine A (+), 5.8 mg/L LCR134 or 11.6 mg/L LCR134. Larval tissue was analyzed using a Varioskan LUX Fluorometer. Optics were directed from the bottom at excitation: 505nm; emission: 530nm with 5nm bandwidth. Asterisks indicate significant difference from the control: $P<0.05$. A t-test was conducted between the two controls and Kruskal-Wallis One Way Analysis of Variance, with posthoc Dunn's method was conducted for the control and two doses of LCR134. Three experimental replicates were conducted; N = 11-12

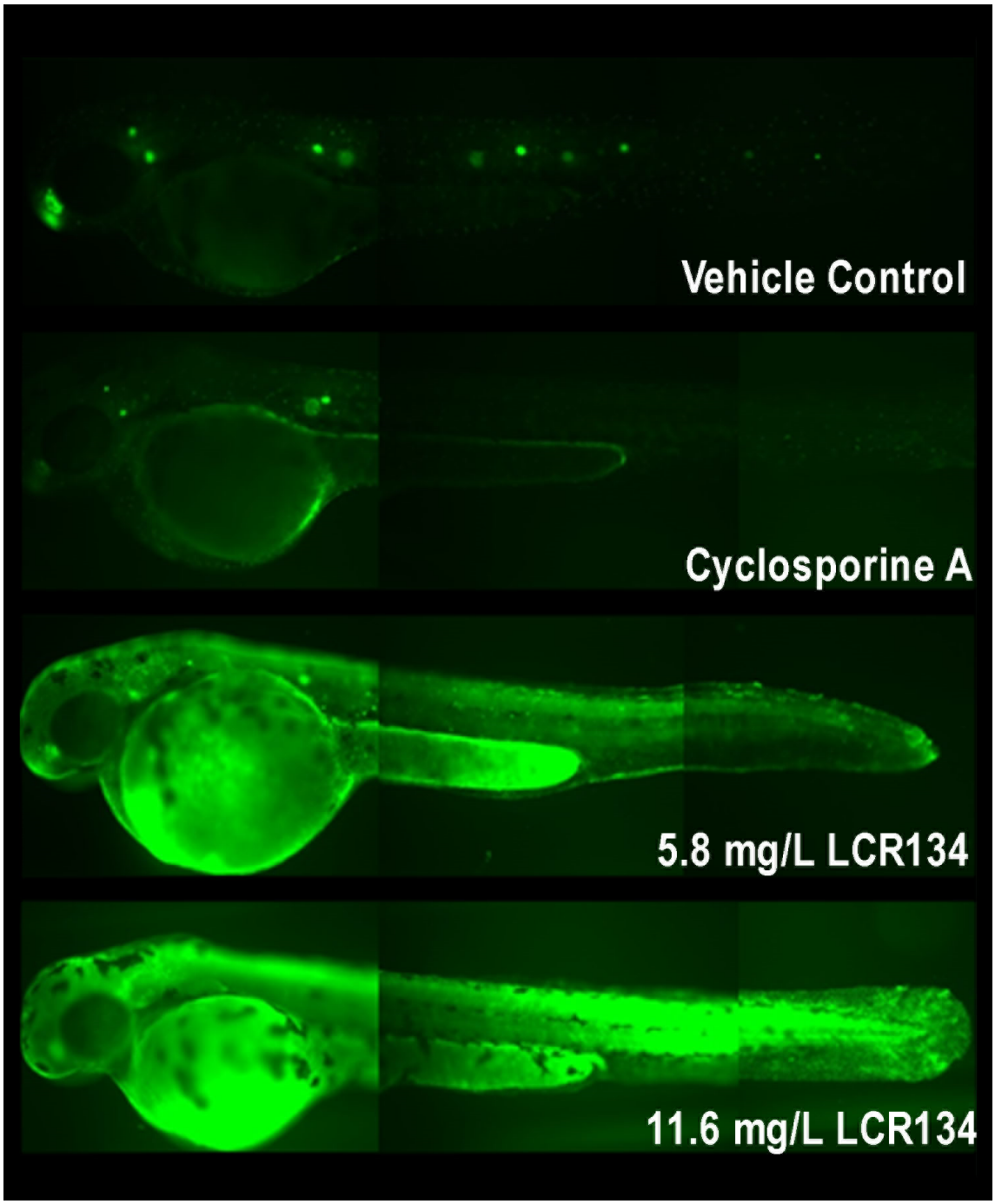

Figure 6. Rhodamine 123 Accumulation – Images of free-swimming larvae at 48 hours post-fertilization (hpf) after co-incubated with Rhodamine 123 (Rh123), a fluorescent P-pg substrate and vehicle control (-), 10 µM cyclosporine A (+), 5.8 mg/L LCR134 or 11.6 mg/L LCR134.

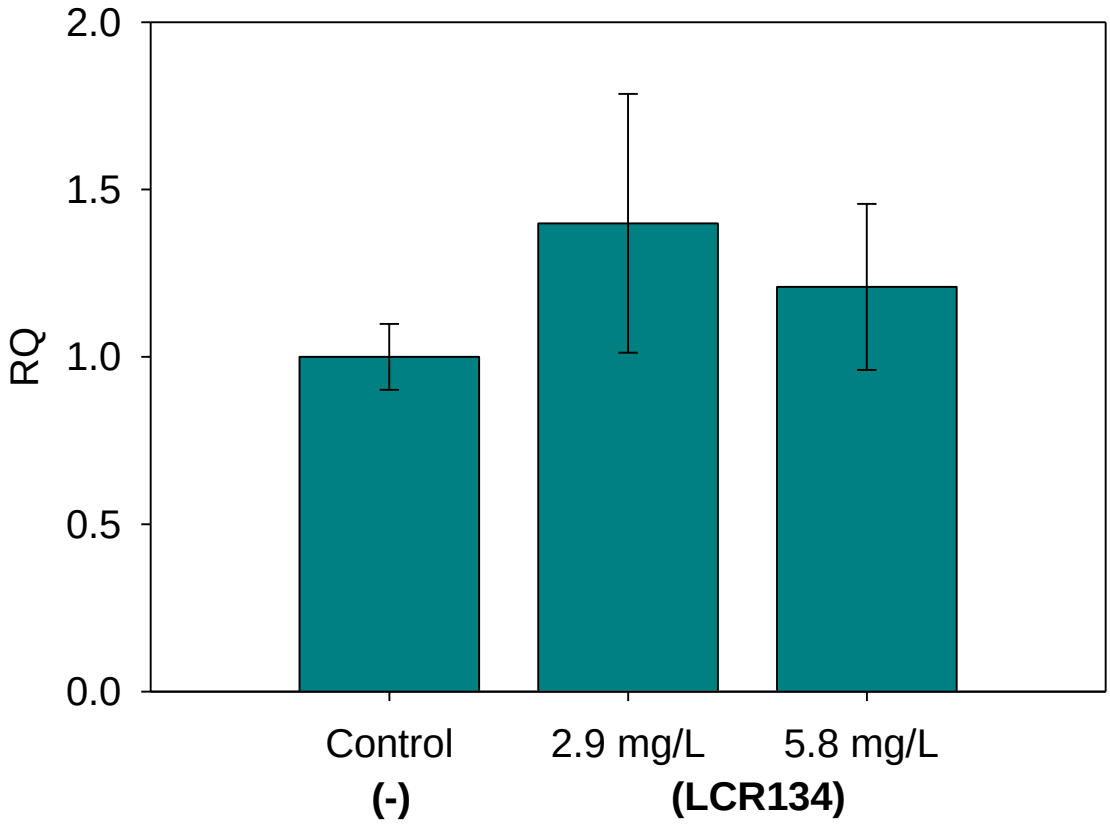

Figure 7. LCR134 Impacts on Gene Expression of *mdr1* – RNA transcript levels of zebrafish *mdr1* were assessed after exposure to 2.9 and 5.8 mg/L of LCR134. Transcript levels were assayed after exposure from 3-22 hours post-fertilization (hpf). Graphs represent the mean fold change +/- the S.E.M. of three experimental replicates (N=3). No significance was identified between controls and cisplatin-treated transcript levels.

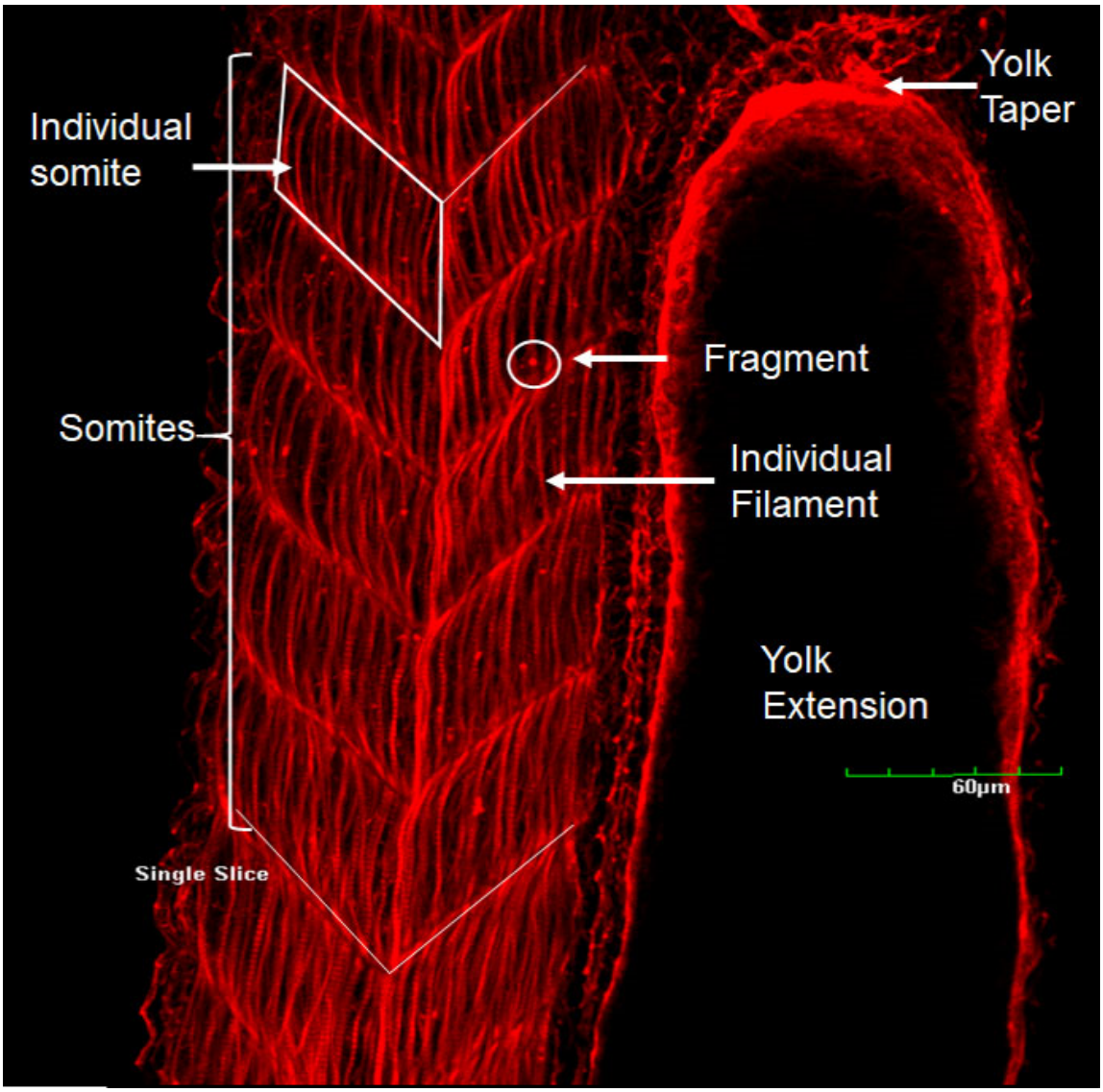

Figure 8. Cytoskeleton Quantification – Zebrafish embryo at 24 hours post-fertilization (hpf) stained with phalloidin to visualize cytoskeleton actin filaments (F-actin). Ten somites adjacent to the yolk extension and anterior to the end of the taper were chosen for quantification of fluorescent intensity and fragmentation count. The distal somite (outlined in white) was used to count number of filaments within a given somite.

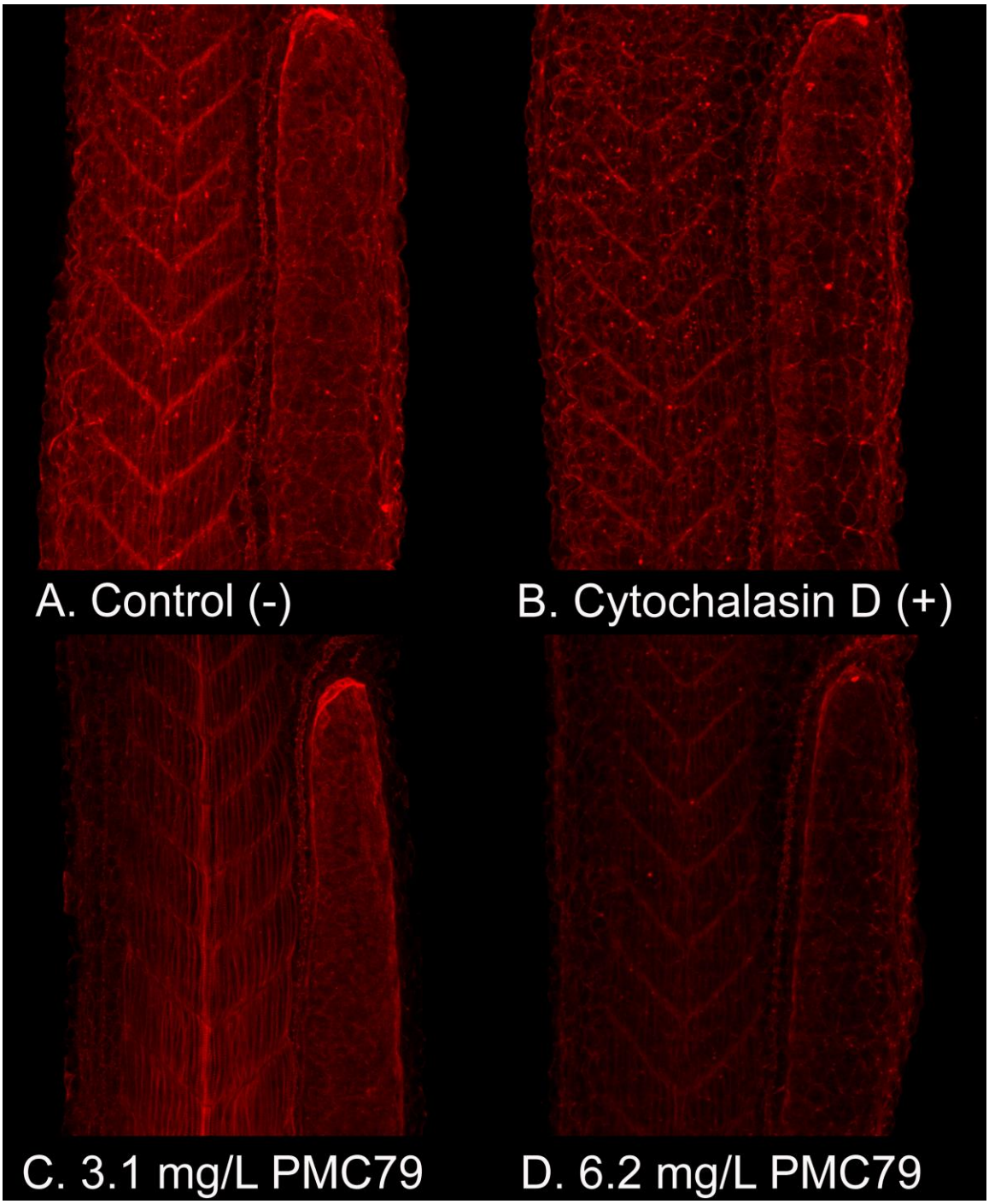

Figure 9. Cytoskeletal Evaluation – Zebrafish Larvae were exposed to vehicle control (A), Cytochalasin D (B), 2.9 mg/L PMC79 (C), and 5.8 mg/L PMC79 (D) and subsequently fixed and stained with phalloidin. Stacked images were taken on an Olympus FV1000MPE microscope (Olympus XLPlan N 25x objective NA 1.05) in 3 µm step size. Z-stacks were compressed and ImageJ was used to evaluate cytoskeletal disruption.

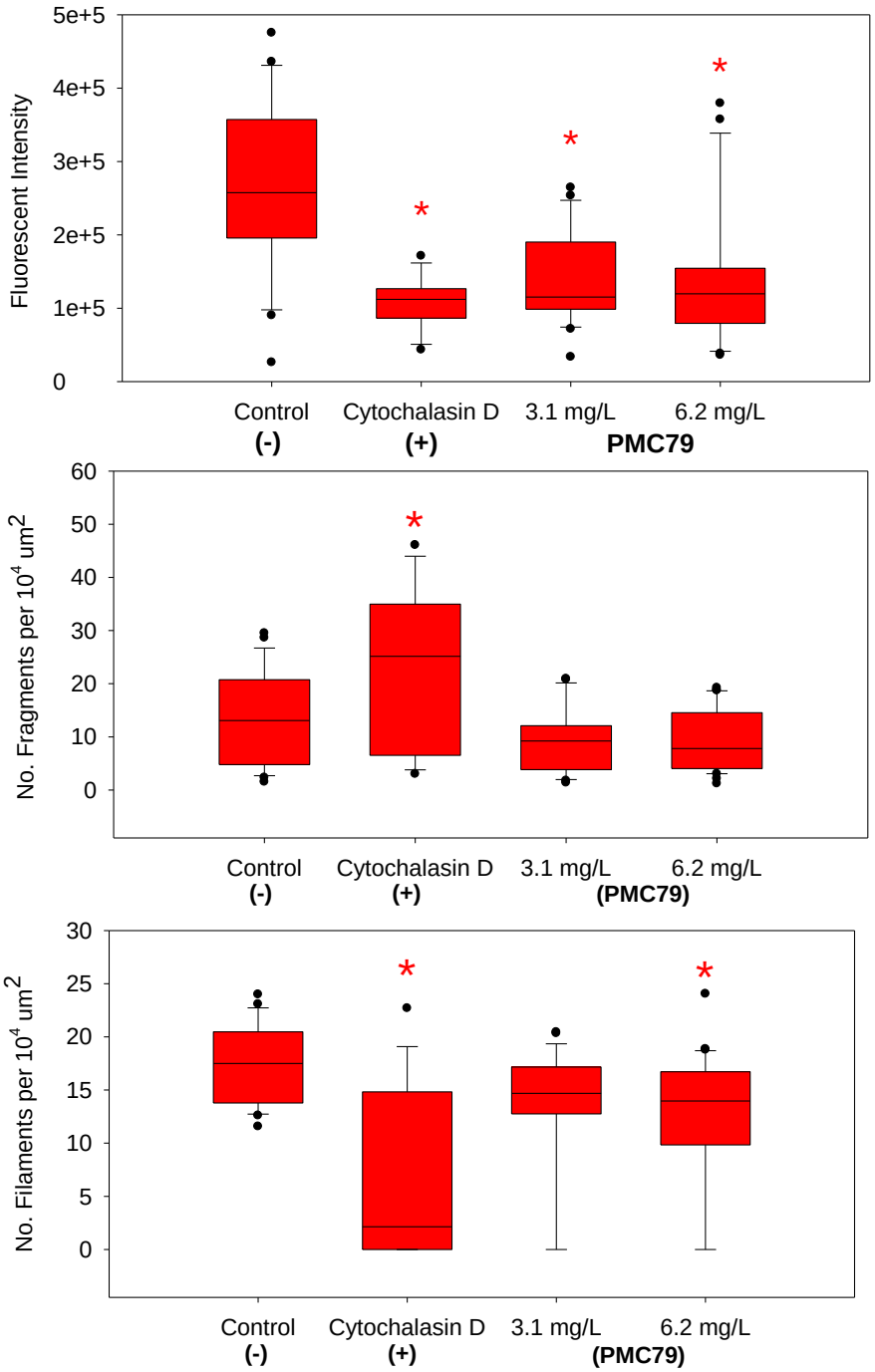

Figure 10. Cytoskeletal Evaluation – Zebrafish Larvae were exposed to vehicle control (A), 1 mg/L Cytochalasin D (B), 2.9 mg/L PMC79 (C), and 5.8 mg/L PMC79 (D) and subsequently fixed and stained with phalloidin. Fluorescent intensity (top), number of fragments (middle), and number of filmaments per 10^4 μm^2 somite area (bottom) were evaluated. T-tests were run between positive and negative controls. Kruskal-Wallis One Way Analysis were conducted with post-hoc Dunn's method. Asterisks indicate significance at $P<0.05$. Experiments were run in triplicate.

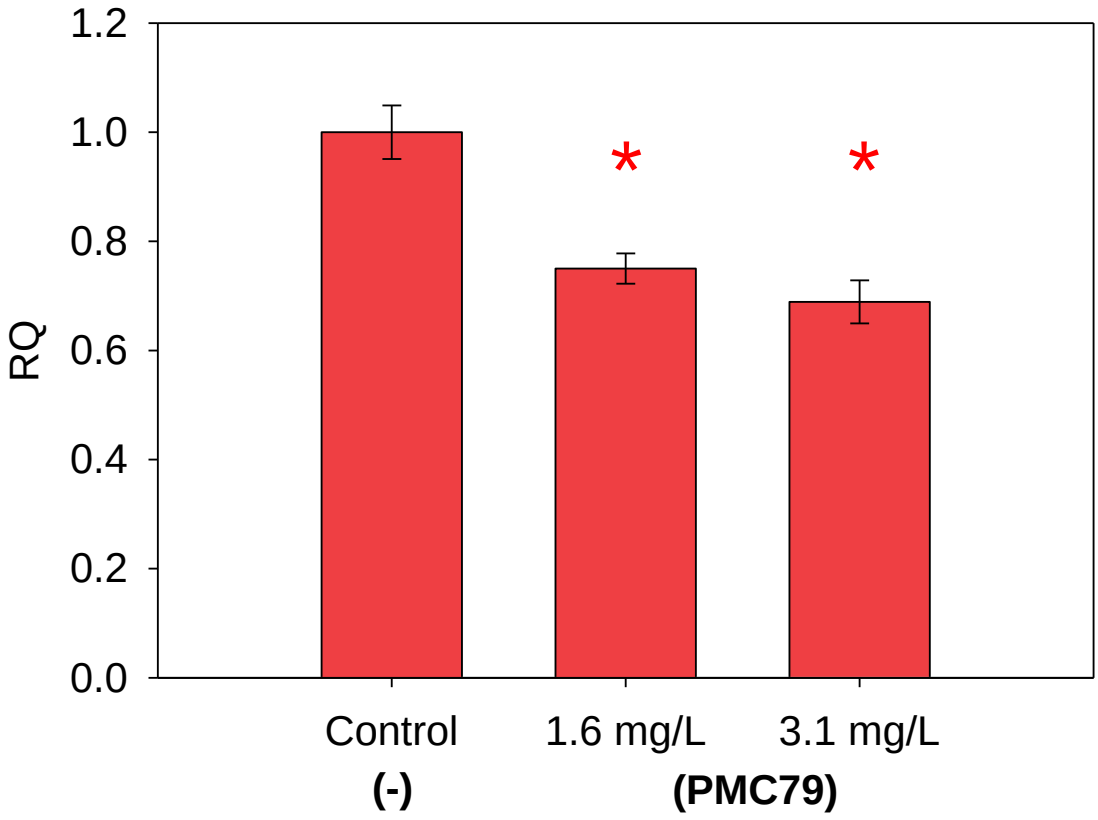

Figure 11. PMC79 Impacts on Gene Expression of *beta-actin* – RNA transcript levels of zebrafish *beta-actin* were assessed after exposure to 1.6 and 3.1 mg/L of PMC79. Transcript levels were assayed after exposure from 3-22 hours post-fertilization (hpf). Graphs represent the mean fold change +/- the S.E.M. of three experimental replicates (N=3). A one-way ANOVA was used to determine a significant effect of metallodrug PMC79 on transcript levels. * indicates a significant difference versus control as determined by Holm-Sidak post hoc analyses ($p \leq 0.05$).

CHAPTER 5. DISCUSSION, IMPLICATIONS AND FUTURE DIRECTIONS

Cancer is a global disease burden with large societal impacts; in 2015 alone, approximately 90.5 million people were diagnosed with cancer worldwide (G. B. D., 2016). As such, it is of paramount importance to understanding the mechanisms of disease in order to develop therapeutic targets. One of the major challenges of target development is the ability to distinguish between healthy and cancerous cells thereby limiting off target effects and toxicity. To this end, ruthenium (Ru) metallodrugs may play a pivotal role due to their structural diversity and relative ease of physiochemical manipulation, enhanced permeation and retention (EPR) and macromolecular accumulation (passive targeting), and ability to be conjugated to cancer-targeting molecules, such as biotin (active targeting) (Hoshida et al., 2006; Tripodo et al., 2014). Unfortunately, the rate at which these metallodrugs are being synthesized has out-paced the ability to assess their efficacy and toxicity.

In this dissertation, I explored the potential of the zebrafish model as an additional platform of the drug development paradigm. The zebrafish has been shown to be an advantageous model due to its higher throughput screening and translatability across vertebrate systems (Leonard & Randall, 2005). The intent was to expedite the establishment of critical pharmacological endpoints including drug delivery, benchmark doses, anti-proliferative and angiogenic efficacy, and recapitulation of *in vitro* mechanisms in an *in vivo* model. These studies focused on two novel Ru metallodrugs: the parental compound PMC79 and its conjugated biotin derivative, LCR134.

I successfully incorporated the use of inductively coupled plasma mass spectrometry (ICPMS) in order to determine drug delivery in waterborne exposures for cisplatin, PMC79, and LCR134 (**Chapter 2**). From these studies, I was able to elucidate the no observed adverse effect levels (NOAELs), lowest observed adverse effect levels (LOAELs), and LC_{50} doses (Corte-Real et al., 2019; Karas et al., 2019). Furthermore, morphological assessments demonstrated similar whole organism effects between all three metallodrugs including dose-dependent decreased body length complementary to increased yolk sac size as well as a threshold decrease of intraocular distance. This suggests an overall impediment of proliferation and growth, and a decreased or impaired nutrient uptake. Unique among the morphometric results was a potential impact on the cardiovascular system after exposure to PMC79 demonstrated by hemorrhaging after blood vessel development. This was further supported by evidence that PMC79 inhibited blood vessel branching within the yolk sac of exposed larvae, which was not seen with LCR134 (**Chapter 3**). However, the robust nature of this assay for means of evaluating anti-angiogenic properties may need further consideration. Potent anti-angiogenic substances like sorafenib almost completely impaired blood vessel growth within various regions of the animal (trunk and yolk sac). Whether or not the limited and regional inhibition of PMC79 is beneficial or ineffective for anti-cancer therapy must be further explored.

Anti-proliferative capabilities were investigated by a tail fin regeneration study coupled with immunofluorescent staining for proliferating cell nuclear antigen (PCNA). From these studies (**Chapter 3**), I was able to demonstrate that PMC79

and LCR134 has similar profiles of inhibition to cisplatin, although their concentrations were kept below previously established LOAEL concentrations and cisplatin was not. This may suggest lower doses are necessary in order to achieve the same efficacy as cisplatin.

In vitro systems often fail to elucidate the complex feedback mechanisms observed in *in vivo* models. For this reason, I sought to recapitulate *in vitro* observations using the zebrafish model. Here I observed consequences of the well-characterized alkylating activity of cisplatin through novel means. The hypothesis of a cross-linking effect with chorionic proteins was supported by chorion specific platinum accumulation, chorion resistant degradation, and no observable changes in hatching enzyme RNA transcript levels. Furthermore, notorious off target toxicities of cisplatin including ototoxicity and bone marrow suppression were suggested from lack of bone and otolith formation as evidenced by a complete lack of calcium-specific staining by Alizarian Red in cisplatin treated larvae (**Chapter 4**).

PMC79 and LCR134 demonstrated similar effects *in vivo* as *in vitro (*Corte-Real et al., 2019*;* Moreira et al., 2019*).* LCR134 exposure in zebrafish showed a potent capability to inhibit P-gp transporters compared to a well-documented clinical inhibitor, cyclosporine A. Additionally, PMC79 appeared to impair the formation of cytoskeleton within the developing organism, although the mechanism by which this happens is still unknown. Both of these mechanisms have implications in cancer therapy, potential side effects, and warrant further investigation.

In conclusion, both compounds have shown promising anti-cancer properties in the context of a living organism. Importantly, all studies were conducted at benchmark doses with the intent to uncover efficacy and limit off target effects. However, the mechanisms themselves, specifically PMC79, may inherently target healthy tissue or inhibit wound repair from impaired angiogenesis and cytoskeletal inhibition. Because this compound does not have a combination of passive and active targeting like LCR134, it may be the more cautious candidate for future consideration.

Future studies should focus on anti-primary tumor and anti-metastatic capabilities. Tumor xenograft in zebrafish has shown success in screening neovascularization, solid tumor proliferation, and the propensity for cancer cells to metastasize (Au - Ren et al., 2017; MacRae & Peterson, 2015). These screening tools have been coupled nicely with drug treatment in order to deduce efficacy. Furthermore, the success of these assays have even been used in personalized medicine in which a tumor biopsy is injected in zebrafish. These avatars can then elucidate successful treatments without subjecting patients to exhausting and deleterious chemotherapeutic trial and error. We would anticipate that PMC79 would be able to impede neovascularization of xenografted tumors as well as stymie the growth of the primary tumor. Additionally, LCR134 should be tested specifically with cell lines that have a high occurrence of drug resistance, and co-administer with P-gp transported therapies like cisplatin. Given our developed ICPMS methodology, it would be possible to excise the tumor and assess increases in cisplatin accumulation from inhibited efflux transport by LCR134.

Lastly, given that these structures were based on the ant-metastatic compound NAMI-A, xenografts should include cells that have a propensity to metastasize (Brown et al., 2017). Combining strong analytical capabilities with targeted mechanistic studies with the zebrafish animal model have proven to be a valuable screening tool for novel cancer therapeutic agents. These studies can provide the preliminary information needed to deduce the likelihood of success or off target effects in pre-clinical trials in higher organisms.

LITERATURE CITED

Aird, R. E., Cummings, J., Ritchie, A. A., Muir, M., Morris, R. E., Chen, H., . . . Jodrell, D. I. (2002). In vitro and in vivo activity and cross resistance profiles of novel ruthenium (II) organometallic arene complexes in human ovarian cancer. *British journal of cancer, 86*(10), 1652-1657. doi:10.1038/sj.bjc.6600290

Alessio, E. (2016). Thirty Years of the Drug Candidate NAMI-A and the Myths in the Field of Ruthenium Anticancer Compounds: A Personal Perspective. *European Journal of Inorganic Chemistry*. doi:10.1002/ejic.201600986

Andrews, P. A., Mann, S. C., Huynh, H. H., & Albright, K. D. (1991). Role of the Na⁺,K⁺-Adenosine Triphosphatase in the Accumulation of cis-Diamminedichloroplatinum(II) in Human Ovarian Carcinoma Cells. *Cancer Research, 51*(14), 3677-3681. Retrieved from https://cancerres.aacrjournals.org/content/canres/51/14/3677.full.pdf

Andrews, P. A., Velury, S., Mann, S. C., & Howell, S. B. (1988). cis-Diamminedichloroplatinum(II) accumulation in sensitive and resistant human ovarian carcinoma cells. *Cancer Res, 48*(1), 68-73.

Atilla-Gokcumen, G. E., Williams, D. S., Bregman, H., Pagano, N., & Meggers, E. (2006). Organometallic compounds with biological activity: a very selective and highly potent cellular inhibitor for glycogen synthase kinase 3. *Chembiochem, 7*(9), 1443-1450. doi:10.1002/cbic.200600117

Au - Ren, J., Au - Liu, S., Au - Cui, C., & Au - ten Dijke, P. (2017). Invasive Behavior of Human Breast Cancer Cells in Embryonic Zebrafish. *JoVE*(122), e55459. doi:doi:10.3791/55459

Avgoustakis, K., Beletsi, A., Panagi, Z., Klepetsanis, P., Karydas, A. G., & Ithakissios, D. S. (2002). PLGA-mPEG nanoparticles of cisplatin: in vitro nanoparticle degradation, in vitro drug release and in vivo drug residence in blood properties. *J Control Release, 79*(1-3), 123-135. doi:10.1016/s0168-3659(01)00530-2

Baba, Y., Nosho, K., Shima, K., Irahara, N., Chan, A. T., Meyerhardt, J. A., . . . Ogino, S. (2010). HIF1A overexpression is associated with poor prognosis in a cohort of 731 colorectal cancers. *The American journal of pathology, 176*(5), 2292-2301. doi:10.2353/ajpath.2010.090972

Bellon, S. F., Coleman, J. H., & Lippard, S. J. (1991). DNA unwinding produced by site-specific intrastrand cross-links of the antitumor drug cis-diamminedichloroplatinum(II). *Biochemistry, 30*(32), 8026-8035. doi:10.1021/bi00246a021

Bergamo, A., Gagliardi, R., Scarcia, V., Furlani, A., Alessio, E., Mestroni, G., & Sava, G. (1999). In vitro cell cycle arrest, in vivo action on solid metastasizing tumors, and host toxicity of the antimetastatic drug NAMI-A and cisplatin. *J Pharmacol Exp Ther, 289*(1), 559-564.

Bergamo, A., & Sava, G. (2007). Ruthenium complexes can target determinants of tumour malignancy. *Dalton Transactions*(13), 1267-1272. doi:10.1039/B617769G

Berger, M. R., Garzon, F. T., Keppler, B. K., & Schmahl, D. (1989). Efficacy of new ruthenium complexes against chemically induced autochthonous colorectal carcinoma in rats. *Anticancer Res, 9*(3), 761-765.

Blunden, B. M., Rawal, A., Lu, H., & Stenzel, M. H. (2014). Superior Chemotherapeutic Benefits from the Ruthenium-Based Anti-Metastatic Drug NAMI-A through Conjugation to Polymeric Micelles. *Macromolecules, 47*(5), 1646-1655. doi:10.1021/ma402078d

Brystol-Meyer Squibb. (2002). Platinol-AQ (cisplatin injection) prescribing information. In. Princeton, NJ.

Bonello, T. T., Stehn, J. R., & Gunning, P. W. (2009). New approaches to targeting the actin cytoskeleton for chemotherapy. *Future Medicinal Chemistry, 1*(7), 1311-1331. doi:10.4155/fmc.09.99

Bonventre, J. A. (2012). *Disruption Of Angiogenesis By Methyl Tert-Butyl Ether (Mtbe) Is Mediated By A Dysregulation Of The Vascular Endothelial Growth Factor (Vegf) Pathway.* (Doctor of Philosophy). Rutgers University, New Brunswick, NJ.

Bonventre, J. A., White, L. A., & Cooper, K. R. (2011). Methyl tert butyl ether targets developing vasculature in zebrafish (Danio rerio) embryos. *Aquat Toxicol, 105*(1-2), 29-40. doi:10.1016/j.aquatox.2011.05.006

Brady, H. R., Zeidel, M. L., Kone, B. C., Giebisch, G., & Gullans, S. R. (1993). Differential actions of cisplatin on renal proximal tubule and inner medullary collecting duct cells. *Journal of Pharmacology and Experimental Therapeutics, 265*(3), 1421. Retrieved from http://jpet.aspetjournals.org/content/265/3/1421.abstract

Bregman, H., Williams, D. S., Atilla, G. E., Carroll, P. J., & Meggers, E. (2004). An Organometallic Inhibitor for Glycogen Synthase Kinase 3. *Journal of the American Chemical Society, 126*(42), 13594-13595. doi:10.1021/ja046049c

Briz, O., Serrano, M. A., Rebollo, N., Hagenbuch, B., Meier, P. J., Koepsell, H., & Marin, J. J. (2002). Carriers involved in targeting the cytostatic bile acid-cisplatin derivatives cis-diammine-chloro-cholylglycinate-platinum(II) and cis-diammine-bisursodeoxycholate-platinum(II) toward liver cells. *Mol Pharmacol, 61*(4), 853-860. doi:10.1124/mol.61.4.853

Brown, H. K., Schiavone, K., Tazzyman, S., Heymann, D., & Chico, T. J. (2017). Zebrafish xenograft models of cancer and metastasis for drug discovery. *Expert Opin Drug Discov, 12*(4), 379-389. doi:10.1080/17460441.2017.1297416

Bunnell, T. M., Burbach, B. J., Shimizu, Y., & Ervasti, J. M. (2011). β-Actin specifically controls cell growth, migration, and the G-actin pool. *Molecular Biology of the Cell, 22*(21), 4047-4058. doi:10.1091/mbc.e11-06-0582

Burris, H. A., Bakewell, S., Bendell, J. C., Infante, J., Jones, S. F., Spigel, D. R., . . . Von Hoff, D. (2016). Safety and activity of IT-139, a ruthenium-based compound, in patients with advanced solid tumours: a first-in-human, open-label, dose-escalation phase I study with expansion cohort. *ESMO Open, 1*(6), e000154. doi:10.1136/esmoopen-2016-000154

Cabral, H., Nishiyama, N., Okazaki, S., Koyama, H., & Kataoka, K. (2005). Preparation and biological properties of dichloro(1,2-diaminocyclohexane)platinum(II) (DACHPt)-loaded polymeric micelles. *Journal of Controlled Release, 101*(1), 223-232. doi:https://doi.org/10.1016/j.jconrel.2004.08.022

Campbell, E. J., Dachs, G. U., Morrin, H. R., Davey, V. C., Robinson, B. A., & Vissers, M. C. M. (2019). Activation of the hypoxia pathway in breast cancer tissue and patient survival are inversely associated with tumor ascorbate levels. *BMC Cancer, 19*(1), 307. doi:10.1186/s12885-019-5503-x

Chen, L., Shi, Y., Yuan, J., Han, Y., Qin, R., Wu, Q., . . . Jiao, S. (2014). HIF-1 Alpha Overexpression Correlates with Poor Overall Survival and Disease-Free Survival in Gastric Cancer Patients Post-Gastrectomy. *PLOS ONE, 9*(3), e90678. doi:10.1371/journal.pone.0090678

Chen, S., Zhao, X., Chen, J., Chen, J., Kuznetsova, L., Wong, S. S., & Ojima, I. (2010). Mechanism-Based Tumor-Targeting Drug Delivery System. Validation of Efficient Vitamin Receptor-Mediated Endocytosis and Drug Release. *Bioconjugate Chemistry, 21*(5), 979-987. doi:10.1021/bc9005656

Childs, S., Chen, J.-N., Garrity, D. M., & Fishman, M. C. (2002). Patterning of angiogenesis in the zebrafish embryo. *Development, 129*(4), 973. Retrieved from http://dev.biologists.org/content/129/4/973.abstract

Chimote, G., Sreenivasan, J., Pawar, N., Subramanian, J., Sivaramakrishnan, H., & Sharma, S. (2014). Comparison of effects of anti-angiogenic agents in the zebrafish efficacy-toxicity model for translational anti-angiogenic drug discovery. *Drug Des Devel Ther, 8*, 1107-1123. doi:10.2147/dddt.S55621

Chu, T. F., Rupnick, M. A., Kerkela, R., Dallabrida, S. M., Zurakowski, D., Nguyen, L., . . . Chen, M. H. (2007). Cardiotoxicity associated with tyrosine kinase inhibitor sunitinib. *Lancet, 370*(9604), 2011-2019. doi:10.1016/s0140-6736(07)61865-0

Chung, F. S., Santiago, J. S., Jesus, M. F. M. D., Trinidad, C. V., & See, M. F. E. (2016). Disrupting P-glycoprotein function in clinical settings: what can we learn from the fundamental aspects of this transporter? *American journal of cancer research, 6*(8), 1583-1598. Retrieved from https://pubmed.ncbi.nlm.nih.gov/27648351
https://www.ncbi.nlm.nih.gov/pmc/articles/PMC5004065/

Clarke, M. J., Zhu, F., & Frasca, D. R. (1999). Non-Platinum Chemotherapeutic Metallopharmaceuticals. *Chemical Reviews, 99*(9), 2511-2534. doi:10.1021/cr9804238

Cooper, J. A. (1987). Effects of cytochalasin and phalloidin on actin. *J Cell Biol, 105*(4), 1473-1478. doi:10.1083/jcb.105.4.1473

Corte-Real, L., Karas, B., Girio, P., Moreno, A., Avecilla, F., Marques, F., . . . Valente, A. (2019). Unprecedented inhibition of P-gp activity by a novel ruthenium-cyclopentadienyl compound bearing a bipyridine-biotin ligand. *Eur J Med Chem, 163*, 853-863. doi:10.1016/j.ejmech.2018.12.022

Corte-Rodriguez, M., Espina, M., Sierra, L. M., Blanco, E., Ames, T., Montes-Bayon, M., & Sanz-Medel, A. (2015). Quantitative evaluation of cellular

uptake, DNA incorporation and adduct formation in cisplatin sensitive and resistant cell lines: Comparison of different Pt-containing drugs. *Biochem Pharmacol, 98*(1), 69-77. doi:10.1016/j.bcp.2015.08.112

Corte-Rodríguez, M., Espina, M., Sierra, L. M., Blanco, E., Ames, T., Montes-Bayón, M., & Sanz-Medel, A. (2015). Quantitative evaluation of cellular uptake, DNA incorporation and adduct formation in cisplatin sensitive and resistant cell lines: Comparison of different Pt-containing drugs. *Biochemical Pharmacology, 98*(1), 69-77. doi:http://dx.doi.org/10.1016/j.bcp.2015.08.112

Cunha, V., Burkhardt-Medicke, K., Wellner, P., Santos, M. M., Moradas-Ferreira, P., Luckenbach, T., & Ferreira, M. (2017). Effects of pharmaceuticals and personal care products (PPCPs) on multixenobiotic resistance (MXR) related efflux transporter activity in zebrafish (Danio rerio) embryos. *Ecotoxicol Environ Saf, 136*, 14-23. doi:10.1016/j.ecoenv.2016.10.022

Daniels, T. R., Bernabeu, E., Rodríguez, J. A., Patel, S., Kozman, M., Chiappetta, D. A., . . . Penichet, M. L. (2012). Transferrin receptors and the targeted delivery of therapeutic agents against cancer. *Biochimica et biophysica acta, 1820*(3), 291-317. doi:10.1016/j.bbagen.2011.07.016

Davies, M. S., Berners-Price, S. J., & Hambley, T. W. (2000). Slowing of Cisplatin Aquation in the Presence of DNA but Not in the Presence of Phosphate: Improved Understanding of Sequence Selectivity and the Roles of Monoaquated and Diaquated Species in the Binding of Cisplatin to DNA. *Inorganic Chemistry, 39*(25), 5603-5613. doi:10.1021/ic000847w

de Jongh, F. E., van Veen, R. N., Veltman, S. J., de Wit, R., van der Burg, M. E. L., van den Bent, M. J., . . . Verweij, J. (2003). Weekly high-dose cisplatin is a feasible treatment option: analysis on prognostic factors for toxicity in 400 patients. *British journal of cancer, 88*(8), 1199-1206. doi:10.1038/sj.bjc.6600884

Delov, V., Muth-Köhne, E., Schäfers, C., & Fenske, M. (2014). Transgenic fluorescent zebrafish Tg(fli1:EGFP)y1 for the identification of vasotoxicity within the zFET. *Aquatic Toxicology, 150*, 189-200. doi:https://doi.org/10.1016/j.aquatox.2014.03.010

Eastman, A. (1987). The formation, isolation and characterization of DNA adducts produced by anticancer platinum complexes. *Pharmacology & Therapeutics, 34*(2), 155-166. doi:https://doi.org/10.1016/0163-7258(87)90009-X

Egger, A., Arion, V. B., Reisner, E., Cebrián-Losantos, B., Shova, S., Trettenhahn, G., & Keppler, B. K. (2005). Reactions of Potent Antitumor Complex trans-[RuIIICl4(indazole)2]- with a DNA-Relevant Nucleobase and Thioethers: Insight into Biological Action. *Inorganic Chemistry, 44*(1), 122-132. doi:10.1021/ic048967h

Elice, F., Rodeghiero, F., Falanga, A., & Rickles, F. R. (2009). Thrombosis associated with angiogenesis inhibitors. *Best Pract Res Clin Haematol, 22*(1), 115-128. doi:10.1016/j.beha.2009.01.001

Eljack, N. D., Ma, H.-Y. M., Drucker, J., Shen, C., Hambley, T. W., New, E. J., . . . Clarke, R. J. (2014). Mechanisms of cell uptake and toxicity of the

anticancer drug cisplatin. *Metallomics, 6*(11), 2126-2133. doi:10.1039/C4MT00238E

Eming, S. A., Martin, P., & Tomic-Canic, M. (2014). Wound repair and regeneration: mechanisms, signaling, and translation. *Sci Transl Med, 6*(265), 265sr266. doi:10.1126/scitranslmed.3009337

Engeszer, R. E., Patterson, L. B., Rao, A. A., & Parichy, D. M. (2007). Zebrafish in the wild: a review of natural history and new notes from the field. *Zebrafish, 4*(1), 21-40. doi:10.1089/zeb.2006.9997

Fischer, B., Heffeter, P., Kryeziu, K., Gille, L., Meier, S. M., Berger, W., . . . Keppler, B. K. (2014). Poly(lactic acid) nanoparticles of the lead anticancer ruthenium compound KP1019 and its surfactant-mediated activation. *Dalton Trans, 43*(3), 1096-1104. doi:10.1039/c3dt52388h

Fischer, S., Kluver, N., Burkhardt-Medicke, K., Pietsch, M., Schmidt, A. M., Wellner, P., . . . Luckenbach, T. (2013). Abcb4 acts as multixenobiotic transporter and active barrier against chemical uptake in zebrafish (Danio rerio) embryos. *BMC Biol, 11*, 69. doi:10.1186/1741-7007-11-69

Fouquet, B., Weinstein, B. M., Serluca, F. C., & Fishman, M. C. (1997). Vessel Patterning in the Embryo of the Zebrafish: Guidance by Notochord. *Developmental Biology, 183*(1), 37-48. doi:https://doi.org/10.1006/dbio.1996.8495

Frasca, D. R., Gehrig, L. E., & Clarke, M. J. (2001). Cellular effects of transferrin coordinated to [Cl(NH3)5Ru]Cl2 and cis-[Cl2(NH3)4Ru]Cl. *Journal of Inorganic Biochemistry, 83*, 139-149. doi:10.1016/S0162-0134(00)00180-X

G. B. D. (2016). Global, regional, and national life expectancy, all-cause mortality, and cause-specific mortality for 249 causes of death, 1980-2015: a systematic analysis for the Global Burden of Disease Study 2015. *Lancet (London, England), 388*(10053), 1459-1544. doi:10.1016/S0140-6736(16)31012-1

Gagliardi, R., Sava, G., Pacor, S., Mestroni, G., & Alessio, E. (1994). Antimetastatic action and toxicity on healthy tissues of Na[trans-RuCl4(DMSO)Im] in the mouse. *Clin Exp Metastasis, 12*(2), 93-100. doi:10.1007/bf01753975

Gasser, G., Ott, I., & Metzler-Nolte, N. (2011). Organometallic anticancer compounds. *Journal of Medicinal Chemistry, 54*(1), 3-25. doi:10.1021/jm100020w

Gemberling, M., Bailey, T. J., Hyde, D. R., & Poss, K. D. (2013). The zebrafish as a model for complex tissue regeneration. *Trends Genet, 29*(11), 611-620. doi:10.1016/j.tig.2013.07.003

Gianferrara, T., Bratsos, I., & Alessio, E. (2009). A categorization of metal anticancer compounds based on their mode of action. *Dalton transactions (Cambridge, England : 2003)*(37), 7588-7598. doi:10.1039/b905798f

Godwin, A. K., Meister, A., Dwyer, P. J., Huang, C. S., Hamilton, T. C., & Anderson, M. E. (1992). High resistance to cisplatin in human ovarian cancer cell lines is associated with marked increase of glutathione

synthesis. *Proceedings of the National Academy of Sciences, 89*(7), 3070. doi:10.1073/pnas.89.7.3070

Groessl, M., Zava, O., & Dyson, P. J. (2011). Cellular uptake and subcellular distribution of ruthenium-based metallodrugs under clinical investigation versus cisplatin. *Metallomics, 3*(6), 591-599. doi:10.1039/C0MT00101E

Guo, Z., & Sadler, P. J. (1999). Metals in Medicine. *Angewandte Chemie International Edition, 38*(11), 1512-1531. doi:10.1002/(sici)1521-3773(19990601)38:11<1512::Aid-anie1512>3.0.Co;2-y

Hall, M. D., Okabe, M., Shen, D. W., Liang, X. J., & Gottesman, M. M. (2008a). The role of cellular accumulation in determining sensitivity to platinum-based chemotherapy. *Annual Review Of Pharmacology And Toxicology, 48*, 495-535. Retrieved from https://login.proxy.libraries.rutgers.edu/login?url=http://search.ebscohost.com/login.aspx?direct=true&db=edswsc&AN=000253396900018&site=eds-live

Hall, M. D., Okabe, M., Shen, D. W., Liang, X. J., & Gottesman, M. M. (2008b). The role of cellular accumulation in determining sensitivity to platinum-based chemotherapy. *Annu Rev Pharmacol Toxicol, 48*, 495-535. doi:10.1146/annurev.pharmtox.48.080907.180426

Hamaguchi, K., Godwin, A. K., Yakushiji, M., O'Dwyer, P. J., Ozols, R. F., & Hamilton, T. C. (1993). Cross-resistance to diverse drugs is associated with primary cisplatin resistance in ovarian cancer cell lines. *Cancer Res, 53*(21), 5225-5232.

Hambly, T. W. (1997). The influence of structure on the activity and toxicity of Pt anticancer drugs. *Coord. Chem. Rev., 166*, 181-233.

Harrington, C. F., Le Pla, R. C., Jones, G. D., Thomas, A. L., & Farmer, P. B. (2010). Determination of cisplatin 1,2-intrastrand guanine-guanine DNA adducts in human leukocytes by high-performance liquid chromatography coupled to inductively coupled plasma mass spectrometry. *Chem Res Toxicol, 23*(8), 1313-1321. doi:10.1021/tx100023c

Harrington, C. F., & Taylor, A. (2015). Analytical approaches to investigating metal-containing drugs. *Journal of Pharmaceutical and Biomedical Analysis, 106*, 210-217. doi:http://dx.doi.org/10.1016/j.jpba.2014.10.017

Hartinger, C. G., Hann, S., Koellensperger, G., Sulyok, M., Groessl, M., Timerbaev, A. R., . . . Keppler, B. K. (2005). Interactions of a novel ruthenium-based anticancer drug (KP1019 or FFC14a) with serum proteins--significance for the patient. *Int J Clin Pharmacol Ther, 43*(12), 583-585. doi:10.5414/cpp43583

Hartinger, C. G., Jakupec, M. A., Zorbas‐Seifried, S., Groessl, M., Egger, A., Berger, W., . . . Keppler, B. K. (2008). KP1019, A New Redox‐Active Anticancer Agent – Preclinical Development and Results of a Clinical Phase I Study in Tumor Patients. In (Vol. 5, pp. 2140-2155). Zürich: WILEY‐VCH Verlag.

Hartinger, C. G., Zorbas-Seifried, S., Jakupec, M. A., Kynast, B., Zorbas, H., & Keppler, B. K. (2006). From bench to bedside--preclinical and early clinical development of the anticancer agent indazolium trans-[tetrachlorobis(1H-indazole)ruthenate(III)] (KP1019 or FFC14A). *J Inorg Biochem, 100*(5-6), 891-904. doi:10.1016/j.jinorgbio.2006.02.013

Hillegass, J. M., Villano, C. M., Cooper, K. R., & White, L. A. (2007). Matrix metalloproteinase-13 is required for zebra fish (Danio rerio) development and is a target for glucocorticoids. *Toxicol Sci, 100*(1), 168-179. doi:10.1093/toxsci/kfm192

Hillegass, J. M., Villano, C. M., Cooper, K. R., & White, L. A. (2008). Glucocorticoids Alter Craniofacial Development and Increase Expression and Activity of Matrix Metalloproteinases in Developing Zebrafish (Danio rerio). *Toxicological Sciences, 102*(2), 413-424. doi:10.1093/toxsci/kfn010

Holzer, A. K., Samimi, G., Katano, K., Naerdemann, W., Lin, X., Safaei, R., & Howell, S. B. (2004). The copper influx transporter human copper transport protein 1 regulates the uptake of cisplatin in human ovarian carcinoma cells. *Mol Pharmacol, 66*(4), 817-823. doi:10.1124/mol.104.001198

Holzer, A. K., Varki Nm Fau - Le, Q. T., Le Qt Fau - Gibson, M. A., Gibson Ma Fau - Naredi, P., Naredi P Fau - Howell, S. B., & Howell, S. B. (2006). Expression of the human copper influx transporter 1 in normal and malignant human tissues. *J Histochem Cytochem, 54*(9), 1041-1049.

Hoshida, T., Isaka, N., Hagendoorn, J., di Tomaso, E., Chen, Y. L., Pytowski, B., . . . Jain, R. K. (2006). Imaging steps of lymphatic metastasis reveals that vascular endothelial growth factor-C increases metastasis by increasing delivery of cancer cells to lymph nodes: therapeutic implications. *Cancer Res, 66*(16), 8065-8075. doi:10.1158/0008-5472.Can-06-1392

Hotta, K., Matsuo, K., Ueoka, H., Kiura, K., Tabata, M., & Tanimoto, M. (2004). Role of Adjuvant Chemotherapy in Patients With Resected Non–Small-Cell Lung Cancer: Reappraisal With a Meta-Analysis of Randomized Controlled Trials. *Journal of Clinical Oncology, 22*(19), 3860-3867. doi:10.1200/JCO.2004.01.153

Howe, K., Clark, M. D., Torroja, C. F., Torrance, J., Berthelot, C., Muffato, M., . . . Stemple, D. L. (2013). The zebrafish reference genome sequence and its relationship to the human genome. *Nature, 496*(7446), 498-503. doi:10.1038/nature12111

Huang, J., Zhao, Y., Xu, Y., Zhu, Y., Huang, J., Liu, Y., . . . Qi, X. (2016). Comparative effectiveness and safety between oxaliplatin-based and cisplatin-based therapy in advanced gastric cancer: A meta-analysis of randomized controlled trials. *Oncotarget, 7*(23), 34824-34831. doi:10.18632/oncotarget.9189

Ishida, S., Lee, J., Thiele, D. J., & Herskowitz, I. (2002). Uptake of the anticancer drug cisplatin mediated by the copper transporter Ctr1 in yeast and mammals. *Proc Natl Acad Sci U S A, 99*(22), 14298-14302. doi:10.1073/pnas.162491399

Isogai, S., Horiguchi, M., & Weinstein, B. (2001). The Vascular Anatomy of the Developing Zebrafish: An Atlas of Embryonic and Early Larval Development. *Developmental Biology, 230*, 278-301. doi:10.1006/dbio.2000.9995

Jiang, J., Liang, X., Zhou, X., Huang, R., & Chu, Z. (2007). A meta-analysis of randomized controlled trials comparing carboplatin-based to cisplatin-based chemotherapy in advanced non-small cell lung cancer. *Lung Cancer, 57*(3), 348-358. doi:https://doi.org/10.1016/j.lungcan.2007.03.014

Kapitza, S., Jakupec, M. A., Uhl, M., Keppler, B. K., & Marian, B. (2005). The heterocyclic ruthenium(III) complex KP1019 (FFC14A) causes DNA damage and oxidative stress in colorectal tumor cells. *Cancer Lett, 226*(2), 115-121. doi:10.1016/j.canlet.2005.01.002

Karas, B. F., Côrte-Real, L., Doherty, C. L., Valente, A., Cooper, K. R., & Buckley, B. T. (2019). A novel screening method for transition metal-based anticancer compounds using zebrafish embryo-larval assay and inductively coupled plasma-mass spectrometry analysis. *Journal of Applied Toxicology, 39*(8), 1173-1180. doi:10.1002/jat.3802

Karbownik, A., Szalek, E., Urjasz, H., Gleboka, A., Mierzwa, E., & Grzeskowiak, E. (2012). The physical and chemical stability of cisplatin (Teva) in concentrate and diluted in sodium chloride 0.9%. *Contemp Oncol (Pozn), 16*(5), 435-439. doi:10.5114/wo.2012.31775

Katano, K., Kondo, A., Safaei, R., Holzer, A., Samimi, G., Mishima, M., . . . Howell, S. B. (2002). Acquisition of resistance to cisplatin is accompanied by changes in the cellular pharmacology of copper. *Cancer Res, 62*(22), 6559-6565.

Kawakami, A., Fukazawa, T., & Takeda, H. (2004). Early fin primordia of zebrafish larvae regenerate by a similar growth control mechanism with adult regeneration. *Dev Dyn, 231*(4), 693-699. doi:10.1002/dvdy.20181

Kelland, L. R., Barnard, F. J., Evans, I. G., Murrer, B. A., Theobald, B. R. C., Wyer, S. B., . . . Valenti, M. (1995). Synthesis and in Vitro and in Vivo Antitumor Activity of a Series of Trans Platinum Antitumor Complexes. *Journal of Medicinal Chemistry, 38*(16), 3016-3024. doi:10.1021/jm00016a004

Kimmel, C. B., Ballard, W. W., Kimmel, S. R., Ullmann, B., & Schilling, T. F. (1995). Stages of embryonic development of the zebrafish. *Dev Dyn, 203*(3), 253-310. doi:10.1002/aja.1002030302

Kovacs, R., Bakos, K., Urbanyi, B., Kovesi, J., Gazsi, G., Csepeli, A., . . . Horvath, A. (2016). Acute and sub-chronic toxicity of four cytostatic drugs in zebrafish. *Environ Sci Pollut Res Int, 23*(15), 14718-14729. doi:10.1007/s11356-015-5036-z

Kratz, F., Hartmann, M., Keppler, B., & Messori, L. (1994). The binding properties of two antitumor ruthenium(III) complexes to apotransferrin. *Journal of Biological Chemistry, 269*(4), 2581-2588. Retrieved from https://login.proxy.libraries.rutgers.edu/login?url=http://search.ebscohost.com/login.aspx?direct=true&db=edselc&AN=edselc.2-52.0-0027993919&site=eds-live

Küng, A., Pieper, T., Wissiack, R., Rosenberg, E., & Keppler, B. K. (2001). Hydrolysis of the tumor-inhibiting ruthenium(III) complexes HIm trans-[RuCl4(im)2] and HInd trans-[RuCl4(ind)2] investigated by means of HPCE and HPLC-MS. *JBIC Journal of Biological Inorganic Chemistry, 6*(3), 292-299. doi:10.1007/s007750000203

Larson, C. A., Blair Bg Fau - Safaei, R., Safaei R Fau - Howell, S. B., & Howell, S. B. (2009). The role of the mammalian copper transporter 1 in the cellular accumulation of platinum-based drugs. *Mol Pharmacol, 75*(2), 324-330. doi:D - NLM: PMC2684896 EDAT- 2008/11/11 09:00 MHDA- 2009/02/24 09:00 CRDT- 2008/11/11 09:00 AID - mol.108.052381 [pii] AID - 10.1124/mol.108.052381 [doi] PST - ppublish

Lee, S. L., Rouhi, P., Dahl Jensen, L., Zhang, D., Ji, H., Hauptmann, G., . . . Cao, Y. (2009). Hypoxia-induced pathological angiogenesis mediates tumor cell dissemination, invasion, and metastasis in a zebrafish tumor model. *Proc Natl Acad Sci U S A, 106*(46), 19485-19490. doi:10.1073/pnas.0909228106

Leijen, S., Burgers, S. A., Baas, P., Pluim, D., Tibben, M., van Werkhoven, E., . . . Schellens, J. H. (2015). Phase I/II study with ruthenium compound NAMI-A and gemcitabine in patients with non-small cell lung cancer after first line therapy. *Invest New Drugs, 33*(1), 201-214. doi:10.1007/s10637-014-0179-1

Leonard, I. Z., & Randall, T. P. (2005). In vivo drug discovery in the zebrafish. *Nature Reviews Drug Discovery, 4*(1), 35. doi:10.1038/nrd1606

Liang, D., Chang, J., Chin, A., Smith, A., Kelly, C., Weinberg, E., & Ge, R. (2001). The role of vascular endothelial growth factor (VEGF) in vasculogenesis, angiogenesis, and hematopoiesis in zebrafish development. *Mechanisms of development, 108*, 29-43. doi:10.1016/S0925-4773(01)00468-3

Lieberthal, W., Triaca, V., & Levine, J. (1996). Mechanisms of death induced by cisplatin in proximal tubular epithelial cells: apoptosis vs. necrosis. *American Journal of Physiology-Renal Physiology, 270*(4), F700-F708. doi:10.1152/ajprenal.1996.270.4.F700

List, A. F., Kopecky, K. J., Willman, C. L., Head, D. R., Persons, D. L., Slovak, M. L., . . . Appelbaum, F. R. (2001). Benefit of cyclosporine modulation of drug resistance in patients with poor-risk acute myeloid leukemia: a Southwest Oncology Group study. *Blood, 98*(12), 3212-3220. doi:10.1182/blood.V98.12.3212

Litchfield, J. T., Jr., & Wilcoxon, F. (1949). A simplified method of evaluating dose-effect experiments. *J Pharmacol Exp Ther, 96*(2), 99-113.

MacRae, C. A., & Peterson, R. T. (2015). Zebrafish as tools for drug discovery. *Nat Rev Drug Discov, 14*(10), 721-731. doi:10.1038/nrd4627

Maeda, H., Bharate, G. Y., & Daruwalla, J. (2009). Polymeric drugs for efficient tumor-targeted drug delivery based on EPR-effect. *European Journal of Pharmaceutics and Biopharmaceutics, 71*(3), 409-419. doi:https://doi.org/10.1016/j.ejpb.2008.11.010

Maeda, H., Noguchi, Y., Sato, K., & Akaike, T. (1994). Enhanced vascular permeability in solid tumor is mediated by nitric oxide and inhibited by both new nitric oxide scavenger and nitric oxide synthase inhibitor. *Jpn J Cancer Res, 85*(4), 331-334. doi:10.1111/j.1349-7006.1994.tb02362.x

Malina, J., Novakova, O., Keppler, B. K., Alessio, E., & Brabec, V. (2001). Biophysical analysis of natural, double-helical DNA modified by anticancer heterocyclic complexes of ruthenium(III) in cell-free media. *JBIC Journal of Biological Inorganic Chemistry, 6*(4), 435-445. doi:10.1007/s007750100223

Marques, I. J., Weiss, F. U., Vlecken, D. H., Nitsche, C., Bakkers, J., Lagendijk, A. K., . . . Bagowski, C. P. (2009). Metastatic behaviour of primary human tumours in a zebrafish xenotransplantation model. *BMC Cancer, 9*, 128. doi:10.1186/1471-2407-9-128

Medical Letter. (2003). Drugs of choice for cancer. *Treatment Guidelines from the Medical Letter, 1*(7), 41-52.

Meggers, E. (2009). Targeting proteins with metal complexes. *Chemical Communications*(9), 1001-1010. doi:10.1039/B813568A

Melnik, M., & Holloway, C. E. (2006). Stereochemistry of platinum coordination compounds. *Coordination Chemistry Reviews, 250*(17), 2261-2270. doi:https://doi.org/10.1016/j.ccr.2006.02.020

Meyers, J. R. (2018). Zebrafish: Development of a Vertebrate Model Organism. *Current Protocols Essential Laboratory Techniques, 16*(1), e19. doi:10.1002/cpet.19

Michael, G. A., Eugene, H. Y. C., & Nial, J. W. (2015). The state-of-play and future of platinum drugs. *Endocrine-Related Cancer, 22*(4), R219-R233. doi:10.1530/ERC-15-0237

Miller, R. P., Tadagavadi, R. K., Ramesh, G., & Reeves, W. B. (2010). Mechanisms of Cisplatin nephrotoxicity. *Toxins, 2*(11), 2490-2518. doi:10.3390/toxins2112490

Ming, X., Groehler, A. t., Michaelson-Richie, E. D., Villalta, P. W., Campbell, C., & Tretyakova, N. Y. (2017). Mass Spectrometry Based Proteomics Study of Cisplatin-Induced DNA-Protein Cross-Linking in Human Fibrosarcoma (HT1080) Cells. *Chem Res Toxicol, 30*(4), 980-995. doi:10.1021/acs.chemrestox.6b00389

Moreira, T., Francisco, R., Comsa, E., Duban-Deweer, S., Labas, V., Teixeira-Gomes, A.-P., . . . Valente, A. (2019). Polymer “ruthenium-cyclopentadienyl” conjugates - New emerging anti-cancer drugs. *European Journal of Medicinal Chemistry, 168*, 373-384. doi:https://doi.org/10.1016/j.ejmech.2019.02.061

Nakayama, K., Kanzaki, A., Terada, K., Mutoh, M., Ogawa, K., Sugiyama, T., . . . Takebayashi, Y. (2004). Prognostic value of the Cu-transporting ATPase in ovarian carcinoma patients receiving cisplatin-based chemotherapy. *Clin Cancer Res, 10*(8), 2804-2811. doi:10.1158/1078-0432.ccr-03-0454

Nakayama, K., Miyazaki, K., Kanzaki, A., Fukumoto, M., & Takebayashi, Y. (2001). Expression and cisplatin sensitivity of copper-transporting P-type

adenosine triphosphatase (ATP7B) in human solid carcinoma cell lines. *Oncol Rep, 8*(6), 1285-1287. doi:10.3892/or.8.6.1285

National Cancer Institute. (2007). Cisplatin. Retrieved from https://www.cancer.gov/about-cancer/treatment/drugs/cisplatin

National Cancer Institute. (2014). The "Accidental" Cure—Platinum-based Treatment for Cancer: The Discovery of Cisplatin. *Stories of Discovery.* Retrieved from https://www.cancer.gov/research/progress/discovery/cisplatin

National Cancer Institute. (2018, April 27, 2018). Cancer Statistics. *Understanding Cancer.* Retrieved from https://www.cancer.gov/about-cancer/understanding/statistics

Ni Dhubhghaill, O. M., Hagen, W. R., Keppler, B. K., Lipponer, K.-G., & Sadler, P. J. (1994). Aquation of the anticancer complex trans-[RuCl4(Him)2]– (Him = imidazole). *Journal of the Chemical Society, Dalton Transactions*(22), 3305-3310. doi:10.1039/DT9940003305

Nicoli, S., Ribatti, D., Cotelli, F., & Presta, M. (2007). Mammalian Tumor Xenografts Induce Neovascularization in Zebrafish Embryos. *Cancer Research, 67*(7), 2927. doi:10.1158/0008-5472.CAN-06-4268

Noffke, A. L., Habtemariam, A., Pizarro, A. M., & Sadler, P. J. (2012). Designing organometallic compounds for catalysis and therapy. *Chemical Communications, 48*(43), 5219-5246. doi:10.1039/C2CC30678F

Noguchi, Y., Wu, J., Duncan, R., Strohalm, J., Ulbrich, K., Akaike, T., & Maeda, H. (1998). Early phase tumor accumulation of macromolecules: a great difference in clearance rate between tumor and normal tissues. *Jpn J Cancer Res, 89*(3), 307-314. doi:10.1111/j.1349-7006.1998.tb00563.x

North, T. E., Goessling, W., Walkley, C. R., Lengerke, C., Kopani, K. R., Lord, A. M., . . . Zon, L. I. (2007). Prostaglandin E2 regulates vertebrate haematopoietic stem cell homeostasis. *Nature, 447*(7147), 1007-1011. doi:10.1038/nature05883

Novakova, O., Chen, H., Vrana, O., Rodger, A., Sadler, P. J., & Brabec, V. (2003). DNA Interactions of Monofunctional Organometallic Ruthenium(II) Antitumor Complexes in Cell-free Media. *Biochemistry, 42*(39), 11544-11554. doi:10.1021/bi034933u

OECD. (2013). Test No. 236: Fish Embryo Acute Toxicity (FET) Test. *OECD Guidelines for the Testing of Chemicals*. Retrieved from https://www.oecd-ilibrary.org/content/publication/9789264203709-en

Pan, B. F., Sweet, D. H., Pritchard, J. B., Chen, R., & Nelson, J. A. (1999). A transfected cell model for the renal toxin transporter, rOCT2. *Toxicol Sci, 47*(2), 181-186. doi:10.1093/toxsci/47.2.181

Park, M. H., Jung, I. K., Min, W.-K., Choi, J. H., Kim, G. M., Jin, H. K., & Bae, J.-S. (2017). Neuropeptide Y improves cisplatin-induced bone marrow dysfunction without blocking chemotherapeutic efficacy in a cancer mouse model. *BMB reports, 50*(8), 417-422. doi:10.5483/bmbrep.2017.50.8.099

Pfefferli, C., & Jaźwińska, A. (2015). The art of fin regeneration in zebrafish. *Regeneration (Oxford, England), 2*(2), 72-83. doi:10.1002/reg2.33

Pluchino, K. M., Hall, M. D., Goldsborough, A. S., Callaghan, R., & Gottesman, M. M. (2012). Collateral sensitivity as a strategy against cancer multidrug resistance. *Drug Resistance Updates, 15*(1), 98-105. doi:https://doi.org/10.1016/j.drup.2012.03.002

Prior, R., Reifenberger G Fau - Wechsler, W., & Wechsler, W. (1990). Transferrin receptor expression in tumours of the human nervous system: relation to tumour type, grading and tumour growth fraction. *Virchows Arch A Pathol Anat Histopathol, 416*(6), 491-496.

Puckett, C. A., & Barton, J. K. (2007). Methods to Explore Cellular Uptake of Ruthenium Complexes. *Journal of the American Chemical Society, 129*(1), 46-47. doi:10.1021/ja0677564

Ren, W., Han, J., Uhm, S., Jang, Y., Kang, C., Kim, J.-H., & Kim, J. (2015). Recent development of biotin conjugation in biological imaging, sensing, and target delivery. *Chemical Communications, 51*, 10403-10418. doi:10.1039/c5cc03075g.

Rosenberg, B. (1977). Noble metal complexes in cancer chemotherapy. *Advances In Experimental Medicine And Biology, 91*, 129-150. Retrieved from https://login.proxy.libraries.rutgers.edu/login?url=http://search.ebscohost.com/login.aspx?direct=true&db=cmedm&AN=343531&site=eds-live

Rosenberg, B., Van Camp, L., & Krigas, T. (1965). Inhibition of Cell Division in Escherichia coli by Electrolysis Products from a Platinum Electrode. *Nature, 205*(4972), 698-699. doi:10.1038/205698a0

Rosenberg, B., & VanCamp, L. (1970). The Successful Regression of Large Solid Sarcoma 180 Tumors by Platinum Compounds. *Cancer Research, 30*(6), 1799. Retrieved from http://cancerres.aacrjournals.org/content/30/6/1799.abstract

Safaei, R., Katano, K., Samimi, G., Naerdemann, W., Stevenson, J. L., Rochdi, M., & Howell, S. B. (2004). Cross-resistance to cisplatin in cells with acquired resistance to copper. *Cancer Chemotherapy and Pharmacology, 53*(3), 239-246. doi:10.1007/s00280-003-0736-3

Safirstein, R., Miller, P., & Guttenplan, J. B. (1984). Uptake and metabolism of cisplatin by rat kidney. *Kidney International, 25*(5), 753. Retrieved from https://login.proxy.libraries.rutgers.edu/login?url=http://search.ebscohost.com/login.aspx?direct=true&db=edb&AN=15053522&site=eds-live

Sano, K., Inohaya, K., Kawaguchi, M., Yoshizaki, N., Iuchi, I., & Yasumasu, S. (2008). Purification and characterization of zebrafish hatching enzyme – an evolutionary aspect of the mechanism of egg envelope digestion. *The FEBS Journal, 275*(23), 5934-5946. doi:10.1111/j.1742-4658.2008.06722.x

Santoriello, C., & Zon, L. I. (2012). Hooked! Modeling human disease in zebrafish. *The Journal of clinical investigation, 122*(7), 2337-2343. doi:10.1172/JCI60434

Sava, G., Aessio, E., Bergamo, A., & Mestroni, G. (1999a). *Sulfoxide Ruthenium Complexes: Non-Toxic Tools for the Selective Treatment of Solid Tumour Metastases* (Vol. 1). Berlin, Heidelberg: Springer.

Sava, G., Capozzi, I., Clerici, K., Gagliardi, G., Alessio, E., & Mestroni, G. (1998). Pharmacological control of lung metastases of solid tumours by a novel ruthenium complex. *Clin Exp Metastasis, 16*(4), 371-379. doi:10.1023/a:1006521715400

Sava, G., Clerici, K., Capozzi, I., Cocchietto, M., Gagliardi, R., Alessio, E., . . . Perbellini, A. (1999b). Reduction of lung metastasis by ImH[trans-RuCl4(DMSO)Im]: mechanism of the selective action investigated on mouse tumors. *Anticancer Drugs, 10*(1), 129-138. doi:10.1097/00001813-199901000-00016

Sava, G., Frausin, F., Cocchietto, M., Vita, F., Podda, E., Spessotto, P., . . . Zabucchi, G. (2004). Actin-dependent tumour cell adhesion after short-term exposure to the antimetastasis ruthenium complex NAMI-A. *Eur J Cancer, 40*(9), 1383-1396. doi:10.1016/j.ejca.2004.01.034

Sava, G., Pacor, S., Bergamo, A., Cocchietto, M., Mestroni, G., & Alessio, E. (1995). Effects of ruthenium complexes on experimental tumors: irrelevance of cytotoxicity for metastasis inhibition. *Chem Biol Interact, 95*(1-2), 109-126. doi:10.1016/0009-2797(94)03350-1

Schatzschneider, U., Niesel, J., Ott, I., Gust, R., Alborzinia, H., & Wolfl, S. (2008). Cellular uptake, cytotoxicity, and metabolic profiling of human cancer cells treated with ruthenium(II) polypyridyl complexes [Ru(bpy)2(N--N)]Cl2 with N--N=bpy, phen, dpq, dppz, and dppn. *ChemMedChem, 3*(7), 1104-1109. doi:10.1002/cmdc.200800039

Scolaro, C., Bergamo, A., Brescacin, L., Delfino, R., Cocchietto, M., Laurenczy, G., . . . Dyson, P. J. (2005). In Vitro and in Vivo Evaluation of Ruthenium(II)−Arene PTA Complexes. *Journal of Medicinal Chemistry, 48*(12), 4161-4171. doi:10.1021/jm050015d

Seelig, M. H., Berger, M. R., & Keppler, B. K. (1992). Antineoplastic activity of three ruthenium derivatives against chemically induced colorectal carcinoma in rats. *J Cancer Res Clin Oncol, 118*(3), 195-200. doi:10.1007/bf01410134

Serbedzija, G. N., Flynn, E., & Willett, C. E. (1999). Zebrafish angiogenesis: A new model for drug screening. *Angiogenesis, 3*(4), 353-359. doi:10.1023/A:1026598300052

Sewell, G. (2010). Physical and chemical stability of cisplatin infusions in PVC containers. *EJOP, 4*, 11-13.

Seymour, L. W., Miyamoto, Y., Maeda, H., Brereton, M., Strohalm, J., Ulbrich, K., & Duncan, R. (1995). Influence of molecular weight on passive tumour accumulation of a soluble macromolecular drug carrier. *European Journal of Cancer, 31*(5), 766-770. doi:10.1016/0959-8049(94)00514-6

Shaffer, B. C., Gillet, J.-P., Patel, C., Baer, M. R., Bates, S. E., & Gottesman, M. M. (2012). Drug resistance: Still a daunting challenge to the successful treatment of AML. *Drug Resistance Updates, 15*(1), 62-69. doi:https://doi.org/10.1016/j.drup.2012.02.001

Sheth, S., Mukherjea, D., Rybak, L. P., & Ramkumar, V. (2017). Mechanisms of Cisplatin-Induced Ototoxicity and Otoprotection. *Frontiers in cellular neuroscience, 11*, 338-338. doi:10.3389/fncel.2017.00338

Shi, J.-F., Wu, P., Jiang, Z.-H., & Wei, X.-Y. (2014). Synthesis and tumor cell growth inhibitory activity of biotinylated annonaceous acetogenins. *European Journal of Medicinal Chemistry, 71*, 219-228. doi:https://doi.org/10.1016/j.ejmech.2013.11.012

Smith, C. A., Sutherland-Smith, A. J., Kratz, F., Baker, E. N., Keppler, B. H., & Bernhard, K. K. (1996). Binding of ruthenium(III) anti-tumor drugs to human lactoferrin probed by high resolution X-ray crystallographic structure analyses. *JBIC Journal of Biological Inorganic Chemistry, 1*(5), 424-431. doi:10.1007/s007750050074

Stehn, J. R., Haass, N. K., Bonello, T., Desouza, M., Kottyan, G., Treutlein, H., . . . Gunning, P. W. (2013). A Novel Class of Anticancer Compounds Targets the Actin Cytoskeleton in Tumor Cells. *Cancer Research, 73*(16), 5169-5182. doi:10.1158/0008-5472.Can-12-4501

Stordal, B., Hamon, M., McEneaney, V., Roche, S., Gillet, J.-P., O'Leary, J. J., . . . Clynes, M. (2012). Resistance to Paclitaxel in a Cisplatin-Resistant Ovarian Cancer Cell Line Is Mediated by P-Glycoprotein. *PLOS ONE, 7*(7), e40717. doi:10.1371/journal.pone.0040717

Strecker, R., Weigt, S., & Braunbeck, T. (2013). Cartilage and bone malformations in the head of zebrafish (Danio rerio) embryos following exposure to disulfiram and acetic acid hydrazide. *Toxicol Appl Pharmacol, 268*(2), 221-231. doi:10.1016/j.taap.2013.01.023

Tan, J. L., & Zon, L. I. (2011). Chemical screening in zebrafish for novel biological and therapeutic discovery. *Methods Cell Biol, 105*, 493-516. doi:10.1016/b978-0-12-381320-6.00021-7

Tannock, I. F., & Rotin, D. (1989). Acid pH in Tumors and Its Potential for Therapeutic Exploitation. *Cancer Res, 49*(16), 4373-4384. Retrieved from https://login.proxy.libraries.rutgers.edu/login?url=http://search.ebscohost.com/login.aspx?direct=true&db=edselc&AN=edselc.2-52.0-0024379967&site=eds-live

Townsend, D. M., Deng, M., Zhang, L., Lapus, M. G., & Hanigan, M. H. (2003). Metabolism of Cisplatin to a nephrotoxin in proximal tubule cells. *Journal of the American Society of Nephrology : JASN, 14*(1), 1-10. doi:10.1097/01.asn.0000042803.28024.92

Trendowski, M. (2015). Using cytochalasins to improve current chemotherapeutic approaches. *Anti-cancer agents in medicinal chemistry, 15*(3), 327-335. doi:10.2174/1871520614666141016164335

Tripodo, G., Mandracchia, D., Collina, S., Rui, M., & Rossi, D. (2014). New Perspectives in Cancer Therapy: The Biotin-Antitumor Molecule Conjugates. *Medicinal Chemistry 2161-0444, S1*, 1-8. doi:10.4172/2161-0444.S1-004

Union Biometrica. (2016). Large Particle Analysis and Sorting In I. Union Biometrica (Ed.). Holliston, MA: Union Biometrica, Inc.

Vacca, A., Bruno, M., Boccarelli, A., Coluccia, M., Ribatti, D., Bergamo, A., . . . Sava, G. (2002). Inhibition of endothelial cell functions and of angiogenesis by the metastasis inhibitor NAMI-A. *British journal of cancer, 86*(6), 993-998. doi:10.1038/sj.bjc.6600176

Vander Heiden, M. G., Cantley, L. C., & Thompson, C. B. (2009). Understanding the Warburg Effect: The Metabolic Requirements of Cell Proliferation. *Science (New York, N.Y.), 324*(5930), 1029-1033. doi:10.1126/science.1160809

Veinotte, C., Dellaire, G., & Berman, J. (2014). Hooking the big one: The potential of zebrafish xenotransplantation to reform cancer drug screening in the genomic era. *Disease models & mechanisms, 7*, 745-754. doi:10.1242/dmm.015784

Verheul, H. M., & Pinedo, H. M. (2007). Possible molecular mechanisms involved in the toxicity of angiogenesis inhibition. *Nat Rev Cancer, 7*(6), 475-485. doi:10.1038/nrc2152

Walker, M., & Kimmel, C. (2007). A two-color acid-free cartilage and bone stain for zebrafish larvae. *Biotechnic & Histochemistry, 82*(1), 23-28. doi:10.1080/10520290701333558

Wang, F., Chen, H., Parkinson, J. A., Murdoch, P. d. S., & Sadler, P. J. (2002). Reactions of a Ruthenium(II) Arene Antitumor Complex with Cysteine and Methionine. *Inorganic Chemistry, 41*(17), 4509-4523. doi:10.1021/ic025538f

Wang, Y. H., Cheng, C. C., Lee, W. J., Chiou, M. L., Pai, C. W., Wen, C. C., . . . Chen, Y. H. (2009). A novel phenotype-based approach for systematically screening antiproliferation metallodrugs. *Chem Biol Interact, 182*(1), 84-91. doi:10.1016/j.cbi.2009.08.005

Wheate, N. J., Walker, S., Craig, G. E., & Oun, R. (2010). The status of platinum anticancer drugs in the clinic and in clinical trials. *Dalton Transactions, 39*, 8113-8127.

White, R. M., Cech, J., Ratanasirintrawoot, S., Lin, C. Y., Rahl, P. B., Burke, C. J., . . . Zon, L. I. (2011). DHODH modulates transcriptional elongation in the neural crest and melanoma. *Nature, 471*(7339), 518-522. doi:10.1038/nature09882

WHO. (2016). Essential medicines for cancer: WHO recommendations and national priorities. *Bulletin of the World Health Organization, 94*, 735-742.

Wilkinson, R. N., & van Eeden, F. J. (2014). The zebrafish as a model of vascular development and disease. *Prog Mol Biol Transl Sci, 124*, 93-122. doi:10.1016/b978-0-12-386930-2.00005-7

Wu, J., Akaike, T., & Maeda, H. (1998). Modulation of enhanced vascular permeability in tumors by a bradykinin antagonist, a cyclooxygenase inhibitor, and a nitric oxide scavenger. *Cancer Res, 58*(1), 159-165.

Yamasaki, T., Kamba, T., Kanno, T., Inoue, T., Shibasaki, N., Arakaki, R., . . . Nakamura, E. (2012). Tumor microvasculature with endothelial fenestrations in VHL null clear cell renal cell carcinomas as a potent target of anti-angiogenic therapy. *Cancer Sci, 103*(11), 2027-2037. doi:10.1111/j.1349-7006.2012.02412.x

Yang, Y. G., Liu, D., Xia, Y., Zhou, Y. H., Zhong, X. Y., & Liu, J. (2011). Development of NAMI-A-loaded PLGA-mPEG Nanoparticles: Physicochemical Characterization, in vitro Drug Release and in vivo

Antitumor Efficacy. *Chemical Research in Chinese Universities, 27*, 345-349.

Yonezawa, A., Masuda, S., Yokoo, S., Katsura, T., & Inui, K. (2006). Cisplatin and oxaliplatin, but not carboplatin and nedaplatin, are substrates for human organic cation transporters (SLC22A1-3 and multidrug and toxin extrusion family). *J Pharmacol Exp Ther, 319*(2), 879-886. doi:10.1124/jpet.106.110346

Zetter, B. R. (1998). Angiogenesis and tumor metastasis. *Annu Rev Med, 49*, 407-424. doi:10.1146/annurev.med.49.1.407

Zhan, T., Rindtorff, N., & Boutros, M. (2017). Wnt signaling in cancer. *Oncogene, 36*(11), 1461-1473. doi:10.1038/onc.2016.304

Zhang, P., & Sadler, P. J. (2017). Advances in the design of organometallic anticancer complexes. *Journal of Organometallic Chemistry, 839*, 5-14. doi:https://doi.org/10.1016/j.jorganchem.2017.03.038

Zhu, X. Y., Guo, D. W., Lao, Q. C., Xu, Y. Q., Meng, Z. K., Xia, B., . . . Li, P. (2019). Sensitization and synergistic anti-cancer effects of Furanodiene identified in zebrafish models. *Sci Rep, 9*(1), 4541. doi:10.1038/s41598-019-40866-2

Zorzet, S., Bergamo, A., Cocchietto, M., Sorc, A., Gava, B., Alessio, E., . . . Sava, G. (2000). Lack of In vitro cytotoxicity, associated to increased G(2)-M cell fraction and inhibition of matrigel invasion, may predict In vivo-selective antimetastasis activity of ruthenium complexes. *J Pharmacol Exp Ther, 295*(3), 927-933.

Zorzet, S., Sorc, A., Casarsa, C., Cocchietto, M., & Sava, G. (2001). Pharmacological Effects of the Ruthenium Complex NAMI-A Given Orally to CBA Mice With MCa Mammary Carcinoma. *Met Based Drugs, 8*(1), 1-7. doi:10.1155/mbd.2001.1